UNITED NATIONS EDUCATIONAL, SCIENTIFIC AND CULTURAL ORGANIZATION
INTERNATIONAL ATOMIC ENERGY AGENCY
INTERNATIONAL CENTRE FOR THEORETICAL PHYSICS
I.C.T.P., P.O. BOX 586, 34100 TRIESTE, ITALY, CABLE: CENTRATOM TRIESTE

H4.SMR/916 - 11

SEVENTH COLLEGE ON BIOPHYSICS:

Structure and Function of Biopolymers: Experimental and Theoretical Techniques.

4 - 29 March 1996

Protein Crystallography

K.R. ACHARYA
School of Biology and Biochemistry
University of Bath
U.K.

Molecular Biology and Biotechnology

A Comprehensive Desk Reference

Edited by
Robert A. Meyers

X

X-Ray Diffraction of Biomolecules

K. Ravi Acharya and Anthony R. Rees

Key Words

Crystallography Science of crystal structures; the most widely used method to obtain accurate three-dimensional information of biomolecules.

Crystals Three-dimensional array distinguished from an amorphous solid by the regular arrangement of molecules.

Diffraction Specific patterns generated by the scattering of X-rays from molecules that are organized in a continuous arrangement in a crystal.

X-Ray diffraction is one the most commonly used techniques in determining the three-dimensional structures of biomolecules. This contribution considers only the biomolecules that form crystals. The detailed study of such crystals using X-ray diffraction, known as macromolecular crystallography, provides a method by which the three-dimensional architecture of the molecule can be established at or near atomic resolution. The resolution of a study critically affects what we can learn of the biomolecule structure. A protein structure at 2 Å resolution, for example, will provide detailed information about atomic positions, specific atomic interactions (intra- and intermolecular hydrogen bonds, ionic interactions, etc.), solvent accessibility, and some indication of flexibility or mobility of the molecule. It is possible that when the macromolecule under study is governed by the crystal packing forces within the crystal, some changes in the conformation of flexible regions will occur. Comparative structural studies in the crystal (using X-ray crystallography) and in solution (using nuclear magnetic resonance spectroscopy) for the same macromolecule, as well as studies of the same molecule in different crystallization conditions, clearly indicate that this "dynamic" behavior is not obscured in the solid state. Several experiments reported in the literature have also shown that many macromolecules when crystallized remain active, allowing the experimentalist (crystallographer) to perform time resolved structural studies.

Over the last 10 years a considerable increase in the rate of determining the three-dimensional structures of macromolecules has resulted from developments in many aspects of the X-ray crystallographic method, particularly in the areas of diffraction data collection and computer technology. Macromolecular crystallography has gained momentum through significant advances in protein chemistry and molecular biology, which have led to the availability of complex biological systems for structural studies. The method can now be applied successfully to molecules such as small peptides, proteins, and multi-protein complexes through to large biological systems such as viruses.

1 PRINCIPLES

Crystals are three-dimensional arrays with a regular arrangement of molecules. The repeating unit (the unit cell) of a crystal—the basic block from which the whole volume of the crystal is built—may contain multiple copies of the same molecule whose positions are governed by symmetry rules. This format allows compact packing of the molecules within the crystal. In X-ray crystallography, a crystal is bombarded with electromagnetic radiation of a wavelength comparable to the desired resolution (X-rays between 1 and 1.5 Å). The explanation for the diffraction pattern obtained was first described by Bragg and arises mainly because of the scattering of X-rays by the electrons of atoms in the crystal lattice. Since the diffracting power of a single biomolecule is rather weak, three-dimensional crystals that possess billions of molecules are used. The resultant scattered radiation is recombined to form the image of the object, a process that requires the knowledge of "phases" (not directly measurable, hence the "phase problem" in macromolecular crystallography) and the "amplitudes" of the scattered waves (directly measurable) with respect to the others. With reasonable estimates for the phases (through some form of additional information) of all the scattered X-ray beams, it is possible to calculate the "electron density" at any point within the crystal. It is important to remember that diffraction occurs simultaneously from all molecules within the crystal lattice; therefore the final three-dimensional structure will be an average picture of the entire volume of the lattice that was illuminated by the X-rays. Crystallography also provides an infinite number of snapshots of the unit cell, since the frequency of X-rays is far higher than the fastest chemical vibrations within a biomolecule.

The information at a particular point within the biomolecule is "synthesized" from a complete set of diffraction measurements that obeys Bragg's law of X-ray diffraction,

$$2d \sin \theta = \lambda$$

where λ is the wavelength of the radiation, d is the spacing (commonly called resolution in defining the quality of macromolecule structures) within the object being examined, and θ is the half-angle of scattering. The beams that are deflected by only a small angle (low resolution data, quite often due to the solvent scattering contribution surrounding the protein molecules within the crystal lattice) contribute to the broad features of the molecule under study, while the quality and the extent of the fine detail present in the electron density map depend directly on the higher angle diffraction data (high resolution data). The resolution is an important term in defining the quality of the structure of a macromolecule. The main features of a macromolecule that can be traced at different resolutions are as follows.

6 Å resolution	Outline of the molecule, features such as helices can be identified.
3 Å resolution	Course of polypeptide chain can be traced and topology of folding can be established. With the aid of the amino acid sequence, it is possible to place the side chains within the electron density map.
2 Å resolution	Main chain conformation can be established with high accuracy. Details of side chain conformations can be interpreted easily without amino acid sequence data. Bound water molecules can be identified.
1.5 Å resolution	Individual atoms are almost resolved. Clear water structure.
1.2 Å resolution	Hydrogen atoms may become visible.

In practice, only a few macromolecules diffract to 1.2 Å resolution. This is because the structure tends to "smear," obscuring the fine details and making the high resolution data too weak to measure. The smearing may arise from packing defects (spatial) or from thermal motion of atoms (temporal). Direct information about the spatial dynamics can also be obtained, using X-ray diffraction, unlike NMR spectroscopy, which probes the temporal dynamics of a biomolecule.

2 STAGES OF STRUCTURE DETERMINATION

Several excellent reviews describe in detail the various stages involved in structure determination using X-ray crystallography. We shall highlight only the practical aspects involved in such an approach.

At least a few milligram quantities of pure (usually at least 95% pure), homogeneous material are required. A major boost to protein crystallography has been the recent introduction of cloning and expression techniques that enable the production of large amounts of rare proteins. In addition, advances in site-directed mutagenesis have led to novel protein engineering experiments, which enable the crystallographer to introduce changes that improve crystallization or provide specific sites for the binding of heavy atoms (see Section 2.3.1).

2.1 Crystallization

Crystallization is one of the most difficult steps in X-ray crystallography. It is necessary to establish precise conditions under which weak intermolecular forces between biomolecules produce highly ordered crystal packing rather than random aggregation as a precipitate. This procedure depends on achieving supersaturation of the biomolecule in solution, nucleation at a few sites for crystal growth, and sustained growth of single crystals. Despite significant advances in techniques, however, crystallization of a biomolecule is still a black art. One of the most important requirements is that purity and homogeneity be as high as possible.

Standard protocols such as the hanging drop, sitting drop, dialysis, micro and macro seeding, batch, free capillary, and temperature gradient methods are commonly used, depending on the amount of material available. Quite often it is necessary to explore a wide range of conditions, such as sample concentration, pH, concentration of the precipitant (e.g., ammonium sulfate or other salt, polyethylene glycol or other alcohol), added ions or effectors, and their concentrations, temperature, and so on. More recently the use of nonionic detergents has widened the scope of the crystallographic method to include membrane proteins.

2.2 Characterization and Data Collection

Once crystals have been obtained, the next step is to characterize them. If they diffract well, it is necessary to determine the crystallographic and noncrystallographic symmetry they exhibit. Crystallographic symmetry is usually detected uniquely from the diffraction pattern, and in general it should not prevent the determination of the structure. However, the presence of noncrystallographic symmetry is sometimes hard to detect and may make structure determination quite difficult. On the other hand, multiple copies of molecules (e.g., protomer structures of a virus capsid) governed by noncrystallographic symmetry can provide an enormous amount of "phasing power," and the resultant electron density map may be of superior quality to that obtained from a simple packing involving crystallographic symmetry operations alone.

In general the intensities of the diffracted beam are recorded by rotating the crystal within the X-ray beam. These intensities provide the amplitudes of the diffracted beam (structure factors) directly. The crystal is usually mounted in a glass or quartz capillary tube of appropriate diameter. Often, crystallographers face two difficulties: (1) since the crystals usually are sensitive to irradiation, the diffraction pattern fades as the crystal is exposed to the X-ray beam, and (2) the diffraction pattern is weak because the diffracted energy is a very small proportion of the total energy in the incident beam and is spread over a large number of reflections stimulated simultaneously.

Crystals with small unit cells (< 50 Å in each dimension) are often suited for a diffractometer, which records one diffraction spot at a time. Unit cells with lengths of 50–150 Å in crystals of reasonable size often are suited for routine data collection on an electronic area detector able to record several diffraction spots at once. For molecules with large unit cells (such as viruses) or well-ordered crystals with dimensions $0.1 \times 0.1 \times 0.1$ mm^3, the high flux, collimation, and choice of wavelength of synchrotron radiation allows the diffraction spots to be recorded either on a photographic film or on an electronic area detector. Synchrotron radiation has made a major impact by providing an extremely intense and mainly parallel beam of X-rays. Using such intense radiation in combination with electronic area detectors, it is possible to enhance the data collection rate and reduce radiation damage during data collection.

Time-resolved structural studies such as probing enzyme mechanisms require data collection to be fast in comparison to the speed of the reaction. For some systems, standard modes of data collection, possibly aided by using cooling techniques, to lower the working temperature may be sufficiently rapid. Alternatively, very fast data collection using the Laue technique may be employed: here the crystal usually remains stationary, but data are collected using a continuous spectrum of X-ray wavelengths. Depending on the crystal system, if the conditions are favorable it is possible to collect about 70% of the data on one photograph. The potential increase in the rate of data collection with the Laue method is enormous. Most of the recently reported time-resolved experiments using this technique involve data collection in the millisecond time scale.

2.3 Phase Determination

After three-dimensional X-ray intensity data have been collected, it is necessary to address the phase problem to determine the structure of the molecule. Quite often it is possible to derive valuable information on the molecular packing from calculations based on native amplitudes. There are three major methods for obtaining phase information: isomorphic replacement, molecular replacement, and anomalous scattering.

2.3.1 Isomorphous Replacement Method

The classical and generally used method described as "isomorphous replacement" provides indirect experimental estimates of the protein phase angles by observing the interference effects on the intensities of the scattered beams when heavy atoms (at very low concentrations) are added to the protein. If the heavy atom substitution does not affect the surrounding protein structure (isomorphism), and if more than one pattern of heavy atom binding can be produced, it is possible to obtain estimates of the protein phase angles. Certain chemical groups within the protein are good candidates for combining with heavy atoms; these include free sulfhydryls and single or exposed disulfide bridges. Usually it is necessary to screen a wide range of putative heavy atom derivatives at relatively low resolution (e.g., 3.5 Å). A good single isomorphous derivative can be sufficient for a structure determination, but quite often it is necessary to obtain multiple derivatives to derive phase information.

2.3.2 Molecular Replacement Method

The molecular replacement method makes use of a known three-dimensional structure as an approximate starting model to provide phase angles for the observed structure factor amplitudes from the unknown structure. It is applicable only if there is significant (a minimum of 30% but preferably 50% or higher) amino acid sequence identity to a molecule of known three-dimensional structure. When a family of homologous structures is available, it is preferable to calculate an "average structure" for use as a starting model. Quite often, if the relative positions of the copies are not known, the presence of more than one copy of the unknown structure in the asymmetric unit complicates the search. In such cases, phase information must be obtained through the use of an oligomeric search model. Many structural studies now use this technique, either alone or in combination with the method of isomorphous replacement.

2.3.3 Anomalous Scattering

When the biomolecule is rather small, quite often it is rather difficult to prepare isomorphous heavy atom derivatives. In such situations, it is possible to determine the phase angles from the native data. This may be achieved because the scattering properties of atoms change to an absorption edge of the atom. For the usual wavelengths used, this means that quite significant "anomalous scattering" effects occur for atoms such as Fe, Cd, and Se, while the effect is much smaller for S and virtually nonexistent for C, N, O, and H. There are two variations in using this method: Hendrickson's method of resolved anomalous scattering, which requires very accurate intensity measurements at one wavelength, and the multiple-wavelength anomalous dispersion method (mainly used for larger molecules), which requires intensity measurements at several wavelengths. A tunable X-ray source such as synchrotron radiation is ideal for performing such experiments. This method is of obvious use for metalloproteins.

Quite often it is possible to improve the accuracy of the initial set of phases when there is a redundancy of information in the asymmetric unit, either arising as a result of several copies of the molecule (noncrystallographic symmetry), or more generally due to the solvent content of the crystal (usually 30–90%). "Solvent flattening" is a standard technique for crystals with an average solvent content (≥50%). Where the level density in the solvent region is observed, this can be sufficient to resolve the phase ambiguity for a single isomorphous derivative, or in general to improve the quality of the multiple isomorphous replacement phases to yield an interpretable electron density map. If there are multiple copies of the molecule in the asymmetric unit, or more than one type of crystal, "molecular averaging" may also be used to improve the quality of the electron density map.

3 MODEL BUILDING AND REFINEMENT

Based on a good set of phases, it is possible to calculate at 3 Å resolution an electron density map that can be used, with the aid of a known amino acid sequence, to build an atomic model. A computer graphics workstation is now a necessity for model-building work. As mentioned earlier, depending on the resolution and quality of the electron density map, it is possible to construct a three-dimensional structure of the biomolecule. When the initial model is ready, it must be refined against the X-ray observations. Such refinement leads in turn to greatly improved phase information, and the quality of the new, refined map should help in resolving the ambiguities in the structure. Thus it is necessary to interleave model building and refinement until all parts of the molecule are well explained in terms of their electron densities and stereochemistry. Assessment of the quality of the final structure is based on two factors: the reliability index (R-factor) (which should have values between 0.15 and 0.20 for a well-refined structure) and root-mean-square deviation from covalent bond lengths (typically should range between 0.01 and 0.02 Å).

Figure 1 (see color plate 18) highlights the different stages involved in the structure determination of a protein molecule (e.g., toxic shock syndrome toxin-1, a microbial superantigen).

4 PERSPECTIVES

X-Ray crystallography is a vast, highly specialized field, and we have made an attempt to give a bird's-eye view of the technique. Several areas of science are employed, and the technique can be effectively used as a tool to visualize the interactions of biomolecules, an important area in biomedical research. It is absolutely necessary to make a detailed study of molecular structure to reveal clues to how the biomolecule carries out its function. For example, if a protein plays a key role in a particular disease, its three-dimensional structure might enable "rational design" to produce therapeutic drugs that act by modifying the protein function. With the aid of detailed knowledge about the structures of proteins in combination with molecular genetics tools, it is now possible to produce "tailor made" molecules. The rapid increase in the number

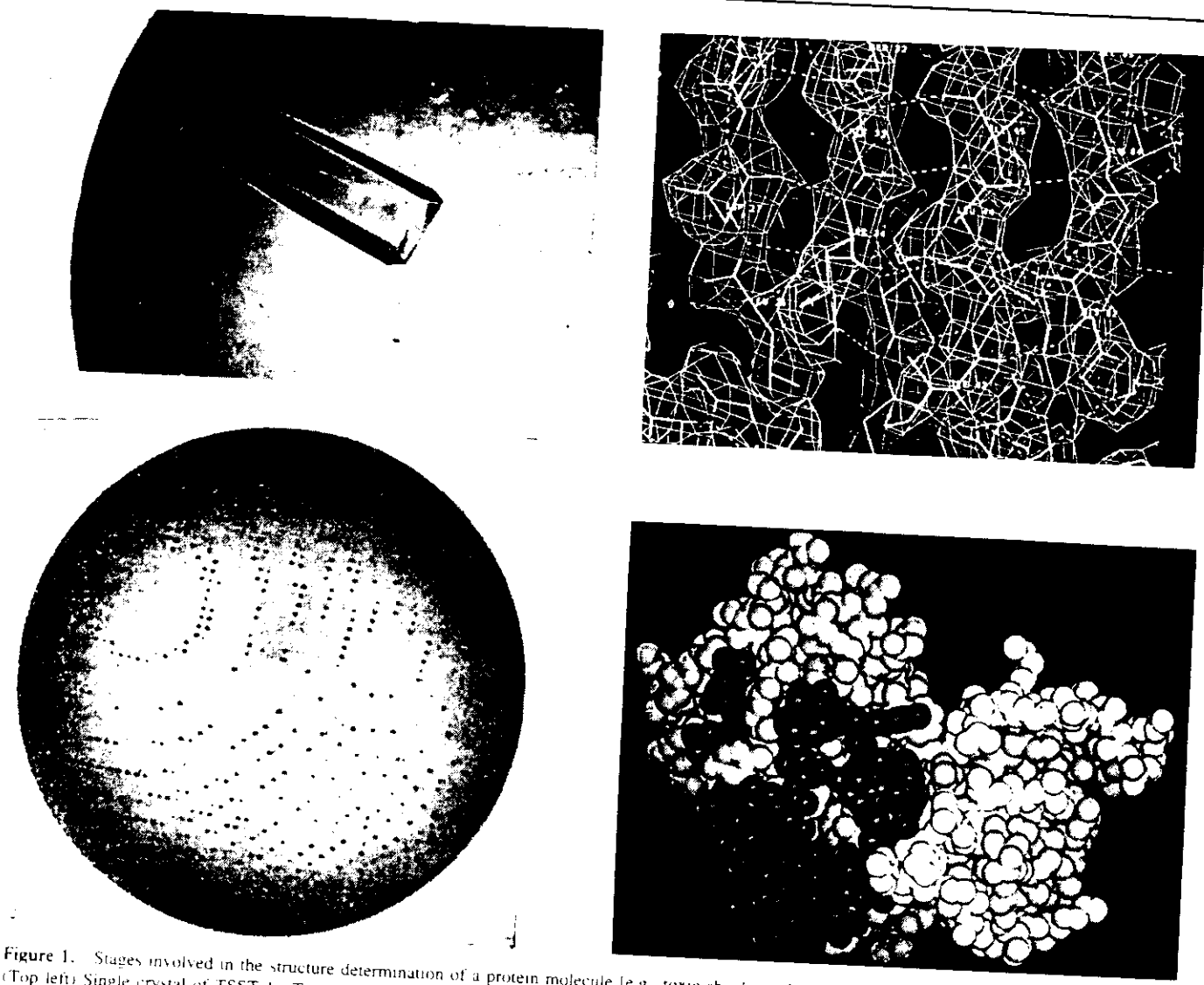

Figure 1. Stages involved in the structure determination of a protein molecule [e.g., toxic shock syndrome toxin 1 (TSST-1), a microbial superantigen]. (Top left) Single crystal of TSST-1. (Top right) Diffraction picture of TSST-1 crystal recorded using MAR Research Imaging Plate system (wavelength 1.5418 Å). The data extend to 2.5 Å resolution. (Bottom left) Part of the 2.5 Å resolution electron density map of TSST-1 with atomic positions superimposed. The region displayed shows four strands of a β-sheet. (Bottom right) Space-filling diagram of TSST-1 (drawn using the 2.5 Å crystal structure). [See color plates 18.]

of structures available in the literature will ultimately provide the information for understanding the "folding properties" of molecules and in time will lead to the design of new molecules. X-Ray crystallography has played and will continue to play a central role in modern biochemistry.

See also PROTEIN ANALYSIS BY X-RAY CRYSTALLOGRAPHY; PROTEIN MODELING; SUPERANTIGENS.

Bibliography

Acharya, K. R., et al. (1994) *Nature*, 367:94–97.

Blundell, T. L., and Johnson, L. N. (1976) *Protein Crystallography*. Academic Press, London.

Bricogne, G. (1976) *Acta Crystallogr.* A32:832–847.

Brunger, A. T., Kurian, J., and Karplus, M. (1987) *Science*, 235:458–460.

Ducruis, A., and Giege, R., Ed. (1992) *Crystallization of Nucleic Acids and Proteins—A Practical Approach*. IRL Press, Oxford.

Gilliland, G. L., and Davies, D. R. (1984) In *Methods in Enzymology*, Vol. 104, W. B. Jacoby, Ed., pp. 370–381. Academic Press, San Diego, CA.

Hendrickson, W. A. (1991) *Science*, 254:51–59.

Jones, E. Y., and Stuart, D. I. (1992) In *Protein Engineering—A Practical Approach*, A. R. Rees, M. J. Sternberg, and R. Wetzel, Eds., pp. 3–32. IRL Press, Oxford.

McPherson, A. (1982) *Preparation and Analysis of Protein Crystals*. Wiley, New York.

McRee, D. E. (1993) *Practical Protein Crystallography*. Academic Press, San Diego, CA.

Michel, H., Ed. (1991) *Crystallization of Membrane Proteins*. CRC Press, Boca Raton, FL.

Rossmann, M. G., Ed. (1972) *The Molecular Replacement Method*. International Science Review, No. 13. Gordon & Breach, New York.

Schlichting, I. et al. *Nature*, 345:309–315.

Wyckoff, H. W., Hirs, C. H. W., and Timasheff, S. N., Eds. (1985) *Methods in Enzymology*, Vols. 114 and 115. Academic Press, San Diego, CA.

PROTEIN CRYSTALLOGRAPHY: MORE SURPRISES AHEAD

DAVID EISENBERG AND CHRISTOPHER P. HILL

As of 1989, over 400 protein structures have been determined, with some 100 solved during the last year. The advances in protein crystallography that have led to this explosion of information are surveyed, and some frontiers of the science are briefly noted.

The surprise of protein crystallography in the 1960s was that protein structures could be determined at all. Each new structure was received with amazement for its complexity, and with fascination for its unexpected new features. In the 1970s the surprise was the variety of structures found, although the majority seemed to cluster into a few general types. In the 1980s the surprise is that protein crystallography has become an indispensible everyday tool of protein chemistry, because of the increased speed of determining structures. This mini-review attempts to summarize the state of protein crystallography as the field moves into the 1990s.

NUMBER OF STRUCTURES

The January 1989 issue of the *Protein Data Bank Newsletter* lists over 400 sets of protein coordinates, about 100 of which were deposited in 1988. Not all of these are distinctly different structures. For example the holdings include some 16 coordinate sets of mutant T4 lysozymes from Brian Matthews' laboratory and 17 coordinate sets for rhinovirus complexed with different antiviral agents from Rossmann's lab. While it is not all that meaningful to define *distinctly different* structures, there seem to be about 120 different protein folds among the 400 deposited structures. There are also a significant number of structures in industrial labs and elsewhere that have been determined but not yet deposited. We hope these will join the other coordinates in the data bank, because the value of the database increases as it grows.

STAGES OF PROTEIN STRUCTURE DETERMINATION

What accounts for the accelerating pace of structure determination? To get some idea of the causes of this explosion of information, we survey the steps in the determination of a protein structure, with emphasis on recent developments.

To determine a protein structure, you must pass through five basic stages (see Fig. 1). Detailed descriptions of these steps are given by dozens of authors in two recent volumes of *Methods of Enzymology*[1], which are strongly recommended. Older reviews are still useful for a broad overview[2,3].

GROWING CRYSTALS

As in other aspects of life, the first step may be the hardest: in this

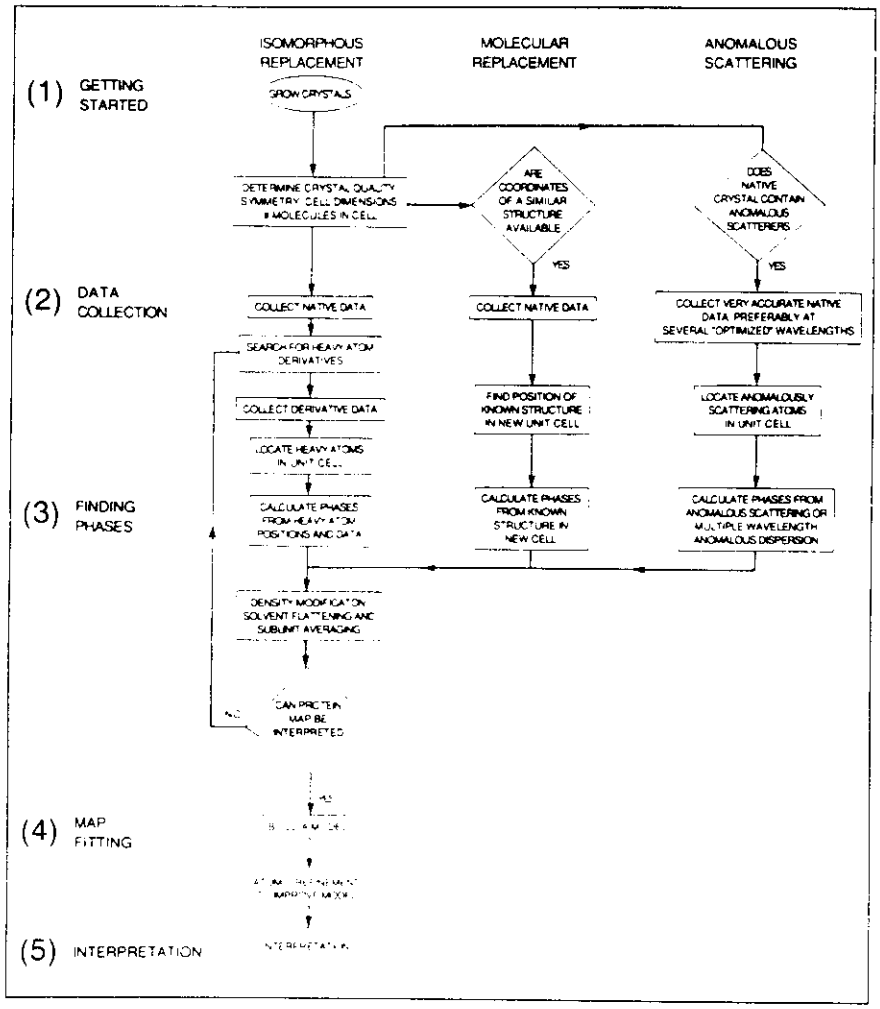

FIGURE 1

The five basic stages in the determination of a protein structure. (1) Growing and characterizing the crystals. (2) Collecting the X-ray data that is, the intensities of the diffraction spots. (3) Getting over the phase problem, the annoyance that intensities are only half the quantities needed to calculate the electron density, the picture of the protein. Missing are the phases, one for each diffraction spot, which cannot yet be measured directly. (4) Building a model of the protein into the electron density using computer graphics. Then, improving the model by atomic refinement, in which atomic positions are adjusted to minimize the discrepancy between observed intensities and those calculated from the model. (5) Interpreting the final model.

case, you must grow X-ray grade crystals. These must be several tenths of a millimetre in each dimension, and need to be well enough ordered to give good X-ray diffraction spots. The basic difficulty is that good crystals grow from protein solutions under a narrow range of conditions. Many variables must be sampled to find these conditions, among them: protein concentration, pH, concentration of precipitant (usually ammonium sulfate or some other salt, polyethylene glycol, or an alcohol), added ions or effectors and their concentrations, temperature, and the method and kinetics of variation of concentrations or temperature. In short, you must sample a multidimensional space starting with an amount of protein that is often too small for a comprehensive search. Suggestions for approaching this problem have been put forward[4,5].

Some crystallization methods are depicted in Fig. 2. The hanging drop is the most widely used, because many conditions can be sampled with relatively little protein (some 50–200 crystallizing conditions can be sampled with 5 mg of protein). Both hanging and sitting drop methods can be automated[6,7], and it seems likely that such automated crystal searches will account for the next increase in speed of protein structure determination.

Whatever the method chosen, your chances of growing good crystals depends more on the purity and homogeneity of the protein than any other factor. If another protein is present, it may precipitate first, forming thousands of heterogeneous nuclei for your protein to grow on when its solubility is reduced, thus producing microscopic crystals. The same result will be obtained if your protein is partially denatured or in multiple forms,

METHOD		COMMENT	ADVANTAGES	DRAWBACKS
Hanging Drop	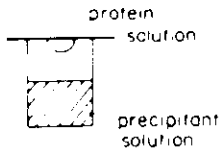	As drop and reservoir equilibrate by vapor diffusion, concentration of precipitant and protein increase in drop.	Small quantities of protein are required. (5 x mg for 50-200 drops). Rapid survey of possible conditions	Crystals often small. Not as repeatable as other methods.
Sitting Drop		Used for drops of greater than 20μl volume	Larger crystals possible.	Requires more protein.
Dialysis	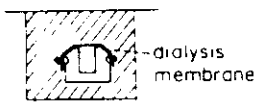	Precipitant diffuses across membrane into protein solution	Large crystals possible.	Requires more protein and dexterity than hanging drops.
Seeding	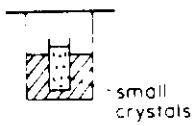	Small or microscopic crystal introduced into protein solution. Can be used with any of the above techniques. figure shows a sitting drop	Used for enlarging crystals.	Need a small crystal to start with.
Batch		Precipitant is mixed with protein solution and left to stand	Numerous large crystals possible.	Requires lots of protein
Free Capillary Diffusion		Protein solution is layered on the precipitant solution. Capillary sealed with wax or by melting glass.	Excellent repeatability. Can be the best method if nucleation requires much higher protein concentration than growth	Curvature of capillary makes it difficult to recognize microcrystals.
Temperature Gradient	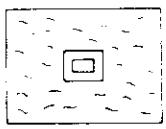	Protein solution slowly cools in a dewar flask packed in a box full of insulation material	Can work if protein solubility varies with temperature	Requires lots of protein. Takes time to set up

FIGURE 2

Some of the methods used for the crystallization of a protein.

because it can itself provide many nuclei. Since the process of crystallization involves placing small protein samples in contact with surfaces, there are many opportunities for denaturation of the protein as you are searching for crystals. Addition of a mild detergent[8] may help to avoid some surface denaturation. If, on the other hand, your protein does not form nuclei easily, larger crystals may be obtained by introducing very small crystals into fresh crystallizing solutions as seeds for further growth[9].

TABLE I
Data collection

Method	Comment	Advantages	Drawbacks
Film:			
Precession	Crystal and film move. A screen allows only certain reflections to be recorded.	Gives an undistorted view of the reciprocal lattice. Good for finding space group, unit cell dimensions and screening for heavy atom derivatives.	No longer used for full data collection because it takes too many crystals and too much time.
Rotation	With the film stationary the crystal is rotated in small (0.5–3.0°) increments.	Efficient because many spots are recorded on each film. Film has high spatial resolution.	Film has high intrinsic noise; it must be developed and densitometered.
Laue	Polychromatic X rays with stationary crystal.	Most of the data collected from one crystal very quickly.	In developmental stage; requires a synchrotron.
Counter methods:			
Diffractometer	Crystal and detector move; one diffraction spot is recorded at a time.	Very accurate data possible, good for measuring anomalous differences.	Inefficient for large unit cells, including all but the smallest proteins.
Area detector	Commercial models use either multiwire proportional counter or television technology.	Combines efficiency of rotation geometry with accuracy of an electronic detector. Usually the method of choice.	Limited spatial resolution is a problem for very large unit cells.

CHARACTERIZATION AND DATA COLLECTION

Assuming that you have been skilful and lucky enough to grow large crystals, your next step is to characterize the diffraction pattern of the crystal. This will tell you the resolution of the electron density that you can hope to determine, as well as the size and symmetry of the unit cell of the crystal. This information is necessary to select the method of data collection (Table I). Small unit cells (i.e. < 5 nm on each edge) are often best suited for a diffractometer. Unit cells with lengths 5–20 nm are often best suited for collection on an area detector, because there are many more diffraction spots than for the small unit cell, and many can be collected at once on the area detector. For even larger unit cells, such as some viruses, the high flux and collimation of synchrotron radiation may be desirable, using film as the detector because of its greater ability to separate the closely spaced diffraction spots. The availability of synchrotron X-ray sources and of commercial area detectors have greatly speeded X-ray data collection. Developments in hardware and software are continuing and within the next decade we can hope for a new generation of detectors which will combine high speed with increased spatial resolution and lower background.

PHASE DETERMINATION

Having collected the X-ray intensities, you still have to defeat the phase problem (Table II). Max Perutz' discovery in the 1950s that heavy atoms bound within protein crystals can supply the phases[10] remains the main route to solving new structures. But this *isomorphous replace-*

ment method is increasingly supplemented by other techniques. The development of new methods is another of the main reasons that structure determination is faster than it used to be, because they avoid the tedious search for the heavy atom adducts needed for isomorphous replacement.

When a similar protein structure is already known, *molecular replacement* techniques can often locate the molecule in the new unit cell and thus lead to the phases for the new structure[11]. Or, if the structure contains a heavier atom, phases may be estimated from *anomalous scattering*. This method requires especially accurate measurement of the small differences in intensity (typically 1–8%) between diffracted X rays which have been reflected from the front and the back of the same set of Bragg planes. There are two variations: Hendrickson's method[16] of resolved anomalous scattering requires very accurate intensity measurements at one wavelength; the MAD method[17] requires intensity measurements at several wavelengths. Synchrotrons yield high intensity X rays of variable wavelength. Thus as synchrotron X-ray diffraction becomes increasingly available, the phase problem may be effectively defeated by anomalous scattering measurements.

Table II
Methods of determining phases

Method	Requirements	Comment	Refs
Multiple isomorphous replacement (MIR)	At least two heavy atom derivatives.	The most general method.	10
Single isomorphous replacement (SIR)	One very good heavy atom derivative.	Requires additional phase information, e.g. from solvent flattening, subunit averaging or anomalous scattering.	11, 12
Molecular replacement	A known similar structure, whose coordinates are used to position molecule in unit cell and to calculate phases.	Eliminates need for heavy atom derivatives.	13
Non-crystallographic symmetry averaging	Several copies of protein molecule in asymmetric unit.	Yields excellent phases when many subunits can be averaged, as in some viruses.	14, 15
Resolved anomalous scattering	Very accurate data. An anomalously scattering group in native crystal.	Requires additional phase information, e.g. from model-building or density modification.	16
Multiple-wavelength anomalous dispersion (MAD)	An anomalously scattering group in native crystal. A tunable X-ray source (i.e. a synchrotron).	Could become the standard method for metalloproteins.	17

Initial phases from isomorphous replacement and the other methods are often poor. These give degraded electron density that is sometimes too blurred even to trace the polypeptide chain. To improve the phases, a variety of methods have been devised. Some, involving general chemical assumptions, are collected under the term *density modification*. *Solvent flattening*[12] means applying the reasonable assumption that the large solvent regions around the protein have a uniform electron density. *Subunit averaging*[14,15] means applying the assumption that chemically equivalent subunits have the same structure. Both of these assumptions can improve the initial phases to the point that you can trace the polypeptide chain in the electron density and can identify the side chains. Subunit averaging increases in power as the number of identical protein chains increases.

Atomic refinement

Once a polypeptide model has been built with the aid of computer graphics[18,19], the phases can again be improved by refining the model to fit the measured intensities of diffraction, or to fit some combination of the measured intensities and a potential energy function. It is during

Table III

Some frontiers of protein crystallography

	Requirements	Potential	Comments	Refs
Time-resolved crystallography	Sub-second data collection, possible only with Laue method using polychromatic synchrotron X rays.	Direct observation of intermediates on a reaction pathway or conformational change.	All molecules in the crystal must change together. Triggering of such concerted changes is a difficult problem.	23, 24
Membrane proteins	Crystal growth remains the major limitation.	Structures are needed to illuminate such events as transport, signaling and energy transduction.	Importance of work in this area was recognized by the 1988 Nobel prize for chemistry, awarded to Deisenhofer, Huber and Michel for the light reaction center structure.	25
Large assemblies	Heterogeneity can make crystals hard to grow. Synchrotron data collection is almost essential. Phase determination may be difficult, except in cases of high non-crystallographic symmetry.	Learning new types of biological organization.	Results to date include the spectacular successes with viruses and heroic efforts with ribosomes.	26
Drug design	Structure of target enzyme should be determined at high resolution with as many inhibitors as possible.	A major practical pay-off of crystallography.	Offers possibility for collaboration of crystallographers with chemists and theorists.	27
Designed peptides	Crystals can be difficult to grow. Tight packing can make isomorphous replacement difficult.	Tests of rules for protein folding and elucidation of small folding motifs.	The peptide may be a fragment of a naturally occurring protein or the result of *de novo* design.	28, 29
Directed mutagenesis, biochemistry and structure	Good collaboration between crystallographers and biochemists. Rapid data collection is useful, because in general many crystals will be studied.	Assessing the role of specific side-chains in structure, catalysis, recognition and stability.	This approach is widely used already and is certain to grow.	
Combined methods	NMR or computational models to aid X-ray structure, and vice versa.	A deeper interplay of methods, yielding energetic and dynamic information as well as structural.	As distinctions among X-ray, NMR and computational models are blurred, care must be taken to catalog what is model and what is known structure.	30

this process of *atomic refinement* that much of the valuable biochemical information is established. During the 1980s refinement methods grew far more powerful, with the introduction of restrained least squares methods[20] and combined X-ray and molecular dynamics techniques[21]. These methods permit more detailed information to be extracted from electron density maps. For example, Smith *et al.*[22] found that in four high resolution structures, 6–13% of the side chains are in multiple, discrete conformations.

FRONTIERS OF PROTEIN CRYSTALLOGRAPHY

Each new protein structure allows us to correlate kinetic, spectroscopic and other observations on that system. Moreover, every new structure also contributes to our understanding of two of the central problems of current biochemistry. One is the protein folding problem; by careful examination of an accurate structure, new information is gained on the relationship of amino acid sequence to three-dimensional structure. Similarly, most protein structures contribute to our understanding of molecular recognition, and the stability of biological complexes, another of the important, general questions of current biochemistry.

These problems are at the frontier of protein crystallography, but there are many other problems being addressed by this technique. A few are listed in Table III. Some involve efforts to use crystallography to get time-dependent pictures of proteins[23,24]. Another area is the study of protein complexes with other cellular components, particularly lipids and nucleic acids. Still other problems of much current research are protein-targeted drug design, designed peptides, directed mutagenesis, and combinations of X-ray crystallography with NMR, computational, and spectroscopic analysis. The next decade is certain to see advances in all of these areas, with protein crystallography playing a central role, increasingly as an everyday tool of the protein laboratory.

Has the excitement gone out of protein crystallography? The first three months of this year (1989) have seen the publication of four new protein folds[31–34] and the first crystal structure of a protein from the AIDS (HIV) virus[35]. These structures suggest there are many surprises ahead.

ACKNOWLEDGEMENTS

The authors gratefully acknowledge support from NIH research grants GM31299 and GM 39558.

REFERENCES

1 Wyckoff, H. W., Hirs, C. H. W. and Timasheff, S. N. (eds) (1985) *Methods Enzymol.* 114–115
2 Blundell, T. L. and Johnson, L. N. (1976) *Protein Crystallography*, Academic Press
3 McPherson, A. (1982) *The Preparation and Analysis of Protein Crystals*, John Wiley & Sons
4 Carter, C. W., Jr and Carter, C. W. (1979) *J. Biol. Chem.* 254, 12219–12223
5 Cox, M. J. and Weber, P. C. (1988) *J. Cryst. Growth* 90, 318–324
6 Kelders, H. A., Kalk, K. H., Gros, P. and Hol, W. G. J. (1987) *Protein Engineering* 1, 301–303
7 Cox, M. J. and Weber, P. C. (1987) *J. Appl. Crystallogr.* 20, 366–373
8 McPherson, A., Koszelak, S., Axelrod, H., Day, J., Williams, R., Robinson, L., McGrath, M. and Cascio, D. (1986) *J. Biol. Chem.* 261, 1969–1975

9 Thaller, C., Eichele, G., Weaver, L. H., Wilson, E., Karlsson, R. and Jansonius, J. N. (1985) *Methods Enzymol.* 114, 132–135
10 Green, D. W., Ingram, V. M. and Perutz, M. F. (1954) *Proc. R. Soc. London Ser. A* 255, 287–307
11 Blow, D. M. and Rossmann, M. G. (1961) *Acta Crystallogr.* 14, 1195–1202
12 Wang, B-C. (1985) *Methods Enzymol.* 115, 90–112
13 Rossmann, M. G. (ed.) (1972) *The Molecular Replacement Method* Gordon & Breach
14 Bricogne, G. (1976) *Acta Crystallogr.* A32, 832–847
15 Rossmann, M. G., Arnold, E., Erickson, J. W., Frankenberger, E. A., Griffith, J. P., Hecht, H-J., Johnson, J. E., Kamer, G., Luo, M., Mosser, A. G., Rueckert, R. R., Sherry, B. and Vriend, G. (1985) *Nature* 317, 145–153
16 Hendrickson, W. A., Smith, J. L. and Sheriff, S. (1985) *Methods Enzymol.* 115, 41–55
17 Guss, J. M., Merritt, E. A., Phizackerley, R. P., Hedman, B., Murata, M., Hodgson, K. O. and Freeman, H. C. (1988) *Science* 241, 806–811
18 Jones, T. A. (1985) *Methods Enzymol.* 115, 157–171
19 Richardson, J. S. and Richardson, D. C. (1985) *Methods Enzymol.* 115, 189–206
20 Hendrickson, W. A. (1985) *Methods Enzymol.* 115, 252–270
21 Brünger, A. T., Kuriyan, J. and Karplus, M. (1987) *Science* 235, 458–460
22 Smith, J. L., Hendrickson, W. A., Honzatko, R. B. and Sheriff, S. (1986) *Biochemistry* 25, 5018–5027
23 Moffat, K., Szebenyi, D. and Bilderback, D. (1984) *Science* 223, 1423–1425
24 Hajdu, J., Machin, P. A., Campbell, J. W., Greenhough, T. J., Clifton, I. J., Zurek, S., Gover, S., Johnson, L. N. and Elder, M. (1987) *Nature* 329, 178–181
25 Deisenhofer, J., Epp, O., Miki, K., Huber, R. and Michel, H. (1985) *Nature* 318, 618–624
26 Harrison, S. C. (1984) *Trends Biochem. Sci.* 9, 345–351
27 Hol, W. G. J. (1986) *Angewandte Chemie* 25, 767–778
28 Landschulz, W. H., Johnson, P. F. and McKnight, S. L. (1988) *Science* 240, 1759–1764
29 Eisenberg, D., Wilcox, W., Eshita, S. M., Pryciak, P. M., Ho, S. P. and DeGrado, W. F. (1986) *Proteins: Structure, Function, Genetics* 1, 16–22
30 Braun, W., Epp, O., Wüthrick, K. and Huber, R. (1989) *J. Mol. Biol.* 206, 669–676
31 Parker, M. W., Pattus, F., Tucker, A. D. and Tsernoglou, D. (1989) *Nature* 337, 93–96
32 Weber, P. C., Ohlendorf, D. H., Wendoloski, J. J. and Salemme, F. R. (1989) *Science* 243, 85–88
33 Ke, H., Thorpe, C. M., Seaton, B. A., Marcus, F. and Lipscomb, W. N. (1989) *Proc. Natl Acad. Sci. USA* 86, 1475–1479
34 Hough, E., Hansen, L. K., Birknes, B., Jynge, K., Hansen, S., Hordvik, A., Little, C., Dodson, E. and Derewenda, Z. (1989) *Nature* 338, 357–360
35 Navia, M. A., Fitzgerald, P. M. D., McKeever, V. M., Leu, C-T., Heimbach, J.C., Herber, W. K., Sigal, I. S., Darke, P. L. and Springer, J. P. (1989) *Nature* 337, 615–620

D. Eisenberg and C. P. Hill are at the Molecular Biology Institute and the Department of Chemistry and Biochemistry, University of California, Los Angeles, CA 90024, USA.

Cryocrystallography

Structure 15 December 1994, **2**:1135–1140

Crystallographic studies are being extended to increasingly challenging systems: ever larger molecules, more complex viruses, membrane proteins, and assemblies. The crystals are often radiation-sensitive and scatter X-rays weakly, in many cases posing severe data collection problems. Synchrotron sources, high-performance area detectors and enhanced computational power have made it possible to tackle more difficult crystals and have greatly improved and simplified collection in general. Another tool, data collection at cryogenic temperatures, addresses more directly some of the problems associated with macromolecular crystals. Low-temperature techniques are coming into widespread use, and have become the routine method of data collection in a few laboratories. Cryogenic collection can make possible otherwise intractable projects, helping to expand the range of applications of crystallography to include some of the most exciting problems in biology. It is now clear that low-temperature techniques also offer real advantages with more conventional crystals, so that they should be considered for all macromolecular X-ray studies.

The primary benefit of data collection at cryogenic temperatures is a reduction in the rate of radiation damage, which often substantially extends crystal lifetime. Frequently, an entire data set can be collected from a single crystal when many would otherwise be required. But cryocrystallography offers other advantages that can contribute to the ultimate success of a data-collection effort. In many cases, the highest resolution to which accurate data can be recorded increases, either because of a reduction in thermal disorder or simply as a result of longer exposure times and a more stable crystal. The mounting techniques used are gentler and lead to less background scatter than conventional methods, and long-term storage and re-use of crystals are also possible. Finally, low-temperature techniques can be used to stabilize transient states, such as catalytic intermediates, that are too short-lived for study at higher temperatures. What are the disadvantages? Initially, of course, the complexity and cost associated with data collection increase, although with experience the techniques prove straightforward and the greater productivity more than offsets the additional expense. A more serious problem is that some crystals prove difficult to cool without unacceptable lattice distortion or increase in mosaic spread. In most cases, however, conditions can be defined which minimize the detrimental effects.

Flash-cooling

The principal challenge of cryogenic data collection is to cool the crystal without damaging it. At minimum, this requires the prevention of crystalline ice formation in the internal and external aqueous solution. Various strategies have been used (see [1–4] for descriptions), but the technique that has proven most effective and generally applicable is flash-cooling [5–7]. Here, the temperature of a sample is rapidly lowered (to ~100 K), so that ice nucleation does not occur before the viscosity of the solution is high enough (below the glass transition temperature) to prevent ice lattice formation (see [8,9]). The result is a rigid glass that encases the crystal lattice. Even with the fastest cooling rates, however, ice will form in most harvest solutions and severely damage the crystal. One approach is to remove nearly all the external liquid from the crystal by transferring it to a hydrocarbon oil [1,10]. In a number of cases (see [3]), samples can then be flash-cooled satisfactorily. Many crystals (particularly the more challenging ones) are damaged with this technique, either by handling, incompatibility with the oil, or subsequent flash-cooling. A more general method is to prevent ice formation during flash-cooling by adding cryoprotectants [5,10,11]. Combined with the crystal-mounting technique described below, this approach has proven successful for a broad range of samples, and it is now the most widely used method for cooling to cryogenic temperatures (see [12] for a detailed description).

Cryoprotectants

Added cryoprotectants are not intended to maintain the harvest solution in a liquid state. They simply slow nucleation so that a rigid glass is formed before ice formation occurs. (Added solute also affects the viscosity of the solution as it cools, raising the glass transition temperature (see [9]), so that less time is available for ice nucleation during flash-cooling.) The effectiveness of compounds as cryoprotectants, or more precisely as glass-forming agents, varies considerably [13]. Even closely related compounds can have widely different cryoprotective abilities. For example, (2*R*,3*R*)-(–)butane-2,3-diol is a particularly effective cryoprotectant, but mixtures containing the *meso* isomer can be much poorer glass-forming agents [13]. Fortunately, fairly high cooling rates (see below) can be attained with samples the size of macromolecular crystals. This allows one to consider a number of compounds when searching for one compatible with the crystals at a concentration that insures glass formation. A list of cryoprotectants that have been used successfully is given in Table 1. Glycerol is often tried first, and it was used most frequently among the studies surveyed in producing Table 1. Ethylene glycol, low-molecular-mass polyethylene glycol, and 2-methyl-2,4-pentanediol (MPD) are also popular. For the most part, the remainder have been used when these cryoprotectants did not give satisfactory results.

Table 1. List of cryoprotectants used successfully in flash-cooling macromolecular crystals.

Type	Concentration (%)
Glycerol	13–30 (v/v)
Ethylene glycol	11–30 (v/v)
Polyethylene glycol 400	25–35 (v/v)
Xylitol	22 (w/v)
(2*R*,3*R*)-(−)-butane-2,3-diol	8 (v/v)
Erythritol	11 (w/v)
Glucose	25 (w/v)
2-methyl-2,4-pentanediol (MPD)	20–30 (v/v)

The list was compiled from unpublished observations in the laboratories of Stephen Harrison and Don Wiley at Harvard University and a survey of structures and reports in six journals for the years 1993 and 1994. Forty different crystals are represented. The range of reported concentrations for each cryoprotectant is also given.

Obtaining good cryoprotectant conditions is straightforward in most cases. The simplest approach is to begin by including candidate cryoprotectants in the harvest solution. The minimum concentration needed will depend on the additive and the other components of the harvest mix. To avoid damaging the crystal, it is usually necessary to introduce the cryoprotectant slowly, either by dialysis or by serial transfer, and if possible, the crystal should be allowed to equilibrate fully before flash-cooling. Permitting full equilibration generally eliminates problems associated with non-isomorphism. In a number of cases, however, exposing the crystal to the cryoprotectant for a brief period has given good results. This method is particularly useful when the crystal is not stable for long periods in cryoprotectant solutions. Other methods of achieving satisfactory cryoprotection have been reported. It is possible, for example, to transfer some crystals from the normal mother liquor to unrelated solutions that contain cryoprotectant [14–16]. Another convenient approach is to grow the crystals in the presence of cryoprotectant, eliminating the need for a potentially damaging transfer to harvest buffer.

Even when ice formation is prevented, some crystals will still be damaged by flash-cooling. This can be the most troublesome aspect of the technique. The damage is evident as a broadening of the rocking curve, sometimes coupled with a significant decrease in the diffraction limit. It may result from stress induced by thermal contraction (possibly differential contraction of the crystal and solvent) or changes in solution parameters (for example dielectric) as the sample cools. If resolution is not lost, relative to crystals at ambient temperature, the increase in rocking-curve width can often be tolerated. An effort should be made to minimize any significant damage, however, by varying solution parameters. Changing the type or increasing the concentration of the cryoprotectant can be helpful. Alterations in other solution parameters such as ionic strength, pH and buffer system should also be considered, either for their initial effect on the strength of the lattice, or to compensate fo changes during cooling. Usually, some combination o parameters that eliminates the damage or reduces it t acceptable levels can be found.

Mounting, cooling and storage

Cryocrystallography is becoming more widely used i part because simple, effective methods for cooling an maintaining the crystals at low temperature are nov available. A major advance was the introduction by Teng [17] of a novel crystal-mounting technique intended pri marily for flash-cooling. The crystal is held in a thin film of cryoprotectant-containing solution formed within a small loop (Fig. 1). The method places little mechanica stress on the crystals, so it is excellent for fragile samples (In fact, it can be used for crystals at ambient temperatures by sealing the loop and a reservoir of harvest solution within a large-diameter X-ray capillary.) This technique also exposes a large surface area, which is important for achieving high cooling rates. Originally, thin metal wire was used to form the loop, but the X-ray opaque wire creates blind regions where data can not be measured. Loops are now made from very fine (~10 μm diameter) fibers of nylon or glass wool [12]. Error from absorption by these loops is small, particularly if excess solution is minimized by making the loop just large enough to accommodate the crystal (see Fig. 1). With this mounting technique, background scatter and absorption are much reduced compared with crystals placed in standard glass capillary tubes [17].

Two methods are commonly used to rapidly cool the crystals once they are mounted in a loop. Placing the crystal directly in the stream of cold nitrogen gas from a cryostat is probably the most common flash-cooling technique (see [2,12]). (The principles of cryostat operation have been described [2,18], and several excellent commercial cryostats are now available.) The procedure is simple, and because it is usually performed on an X-ray camera, the crystal is already in position for analysis. However, it probably does not afford maximum cooling rates (H Hope, LJ Walker, PO Moreno, abstract PE01, American Crystallographic Association Meeting, Atlanta, 1994), requires the availability of a cryostat, and is not efficient when cooling and storing a large number of crystals (see below). Alternatively, the crystal and loop can be plunged directly into a cryogenic liquid [5–7]. Higher cooling rates can be achieved using this technique, and a cryostat need not be available when preparing samples. Using standard cryogens (ethane, propane, and some types of freon) is, however, more difficult and potentially more dangerous (because of flammability) than flash-cooling in a gas stream. Liquid nitrogen, although employed successfully in an early study [5], has been considered unsuitable for this technique because it was thought to form an insulating layer of gas around the sample, slowing heat transfer [9]. But recent measurements suggest that the cooling rates with liquid nitrogen and standard cryogens are more comparable than expected (H Hope, LJ Walker, PO Moreno, abstract

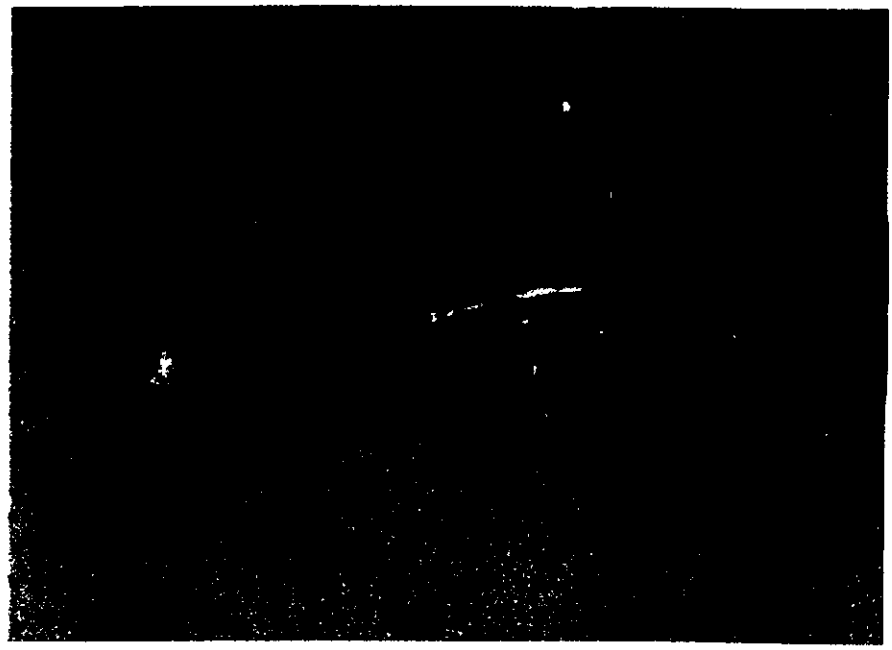

Fig. 1. Photograph of a flash-cooled crystal mounted in a fiber loop. The crystal was picked up with the loop (left side of the figure) from a drop of harvest buffer and flash-cooled in the nitrogen gas stream from a commercial cryostat. The loop was made by forming it around a wire support and twisting the free ends to form a long stem, which was then coated with glue to both stiffen it and prevent unraveling. The stem was cemented to a wire support (visible on the right-hand side of the figure), which was attached to a steel base (not shown). The loop diameter is ~0.25 mm.

PE01, American Crystallographic Association Meeting, Atlanta, 1994). Although additional information on cooling rates is needed, we have had success flash-cooling directly into liquid nitrogen. Avoiding the other cryogens greatly simplifies the technique, and many samples can be prepared in a short time.

Both methods of flash-cooling require a rapid, trouble-free mechanism for transferring the sample to the X-ray camera. When cooling in the gas stream, evaporation from the loop-mounted sample is rapid because of the large surface area, and it must be handled very quickly (often within only a few seconds) to prevent drying. When flash-cooling directly in liquid cryogen, the sample must be transferred to the cryostat gas stream without warming. A magnetic system has been developed [12] to permit rapid attachment of the loop to a goniometer on the X-ray camera. A magnetic strip is attached to the top of a goniometer, and the loop assembly, which has a steel base, can then be placed on and off quickly. A locating pin on the goniometer guarantees that the loop is positioned accurately in the cold stream of the cryostat. This magnetic holder is also the basis of a system for storing crystals in liquid nitrogen using standard cryogenic dewars. Storage of the crystals allows flash-cooling to be done in any convenient location, such as a cold room for example. The crystals can then be transferred to the X-ray camera when needed. This system is particularly useful when preparing samples for data collection at synchrotron radiation sources, allowing more productive use of the limited time available at these facilities. Crystals can be prepared under standardized conditions, prescreened and catalogued in the laboratory, and transported in liquid nitrogen to the synchrotron source. Some crystals degrade in growth and harvest solutions, and liquid nitrogen storage is an excellent way of stabilizing crystals for long periods. It also allows crystals to be re-used if, for example, additional data are required.

Comments and examples

Many of the results and experiences with flash-cooling have been presented in earlier reviews [2,3], and a comprehensive treatment will not be attempted here. The recent structure determination [19,20] of the low-pH form of soluble influenza virus hemagglutinin fragment (TBHA2) illustrates the usefulness of flash-cooling techniques. Crystals were grown from 55%–65% ammonium sulfate in space group $C222_1$, with unit cell dimensions of a=174.7 Å, b=231.8 Å and c=54.5 Å, and with one trimer of 57 kDa molecular mass per asymmetric unit (70% solvent content). At room temperature, they were highly radiation-sensitive and only a small portion of a data set could be obtained from a single crystal. Accurate data could be collected to only ~4.0 Å using a rotating anode X-ray source, and it was difficult to construct a complete set by merging data from a number of crystals. In addition, the protein supply was limited, and derivatives were required. Fortunately, it was easy to find good cryoprotectant conditions. Crystals were transferred through a series of harvest solutions containing increasing concentrations of glycerol (5% to 20% (v/v) by 5% steps at room temperature), with at least 30 min equilibration at each step. They were then flash-cooled in the nitrogen gas stream at ~110K. The full width of the rocking curve increased only slightly, from ~0.4° at room temperature to ~0.5° at low temperature, and the cell constants decreased to a=168.7 Å, b=231.7 Å and c=53.8 Å. With flash-cooled TBHA2, a complete data set could be collected from a single crystal without radiation decay. The quality of these data were somewhat better than partial data sets from room temperature crystals (Fig. 2a). Subsequently, higher-resolution native data were collected at a synchrotron source from one crystal, and the structure was determined using two derivatives collected (using a rotating anode) from single crystals at low temperature.

An increase in mosaic spread during flash-cooling was not a serious problem with TBHA2 (although the rocking-curve width at room temperature was already high). Recent experience with rocking-curve changes is not in general well documented, but at Harvard University a survey of 19 different crystal systems found eight crystals with little or no increase in rocking-curve width, three crystals with an increase of 50% or less, and eight crystals with an increase of around 100% (for example 0.2° increasing to 0.4°). These results appear to be consistent with those from other laboratories using similar techniques. Although a broadening of the rocking curve must have some adverse effect on data quality, it is usually more than counterbalanced by the positive effects of cryogenic collection. Current detectors and software help to minimize the effects of a broader rocking curve. Every effort should be made to reduce or eliminate any increase, but even when broadening of the rocking curve is still substantial, cryogenic collection can often be the best route to completion of the project.

The TBHA2 unit cell decreased in volume by ~4.7% on flash cooling. This volume change is typical [4,21–24], although values can vary and larger changes occasionally occur (possibly when cryoprotectant is introduced). The differences between room-temperature and cryogenic structures of the same proteins have been analyzed in a number of cases [21–26]. Thermal expansion is not uniform, but results from movements of secondary and tertiary elements, with predominantly α-helical regions having slightly higher expansion coefficients than mainly β-sheet domains. However, these effects only cause small differences in the relative positions of secondary structure elements (up to a few tenths of an Angstrom), and they are not a concern in most studies. Cooling to cryogenic temperatures can reduce refined atomic B-factor values, particularly for more ordered crystals. Side chains may become better ordered, and occasionally they adopt significantly different conformations. Also, a larger number of ordered solvent molecules are usually found at cryogenic temperatures. Where lower atomic B-factor values have been reported, the resolution limit of diffraction may increase [2,4,27]. Even when this effect is not significant (i.e. for crystals with greater static disorder), the advantages of data collection at cryogenic temperatures (single crystal, longer exposure times, low background and absorption) usually result in significantly improved data statistics and an effective increase in resolution.

Previous reports have emphasized the apparent lack of radiation damage with flash-cooled crystals using rotating anode X-ray generators [2,3] and synchrotron sources [27]. Although the improvements in stability under these conditions are dramatic, radiation damage does still occur and has recently been characterized [28]. As in room-temperature data collection, the effects of the damage are a decrease in the intensity of reflections, progressing from high to low resolution, and a broadening of the rocking-curve width (Fig. 2b). The useful lifetime of a crystal is roughly 5×10^{15} photons mm^{-2}, close to the estimate of

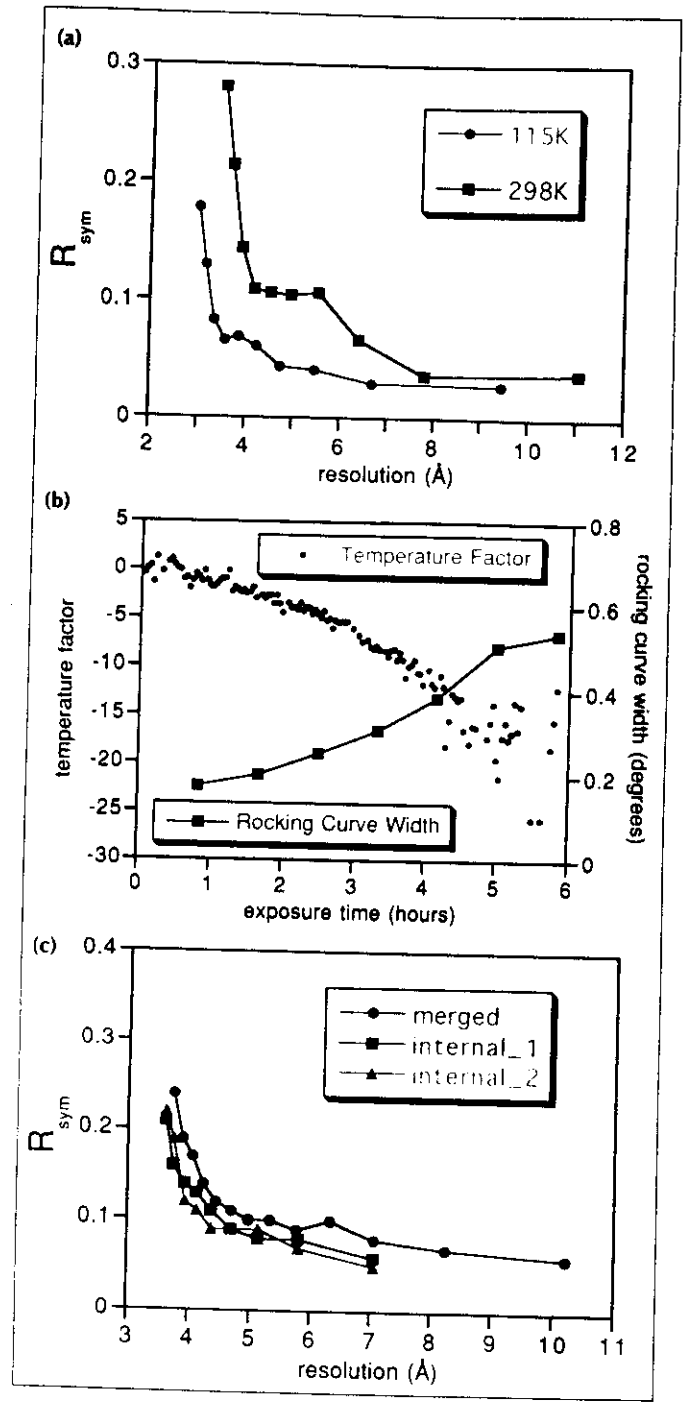

Fig. 2. Results with flash-cooled crystals. **(a)** Plot of merging statistics for single TBHA2 crystals [19,20]. $R_{sym}=\Sigma_{ij}|I_{ij}-\langle I_i\rangle|/\Sigma_{ij}|I_{ij}|$, where I_{ij} is the intensity of an individual measurement and $\langle I_i\rangle$ is the mean value for all measurements of each independent reflection. The data collected at 298 K are a partial set and the data from the crystal at 115 K are a complete set. **(b)** Crystal decay at cryogenic temperature. The scaling temperature factors for successive data frames and refined rocking curve width are plotted against exposure time. The data were collected from one crystal of influenza virus hemagglutinin (HA) [28]. The scaling temperature factor is given by $I_{scaled}=k_i I_{obs}\exp(-B_i\sin^2\Theta/\lambda^2)$ where k_i and B_i are the scale factor and temperature factor respectively for the ith batch. The rocking curve estimate is for full peak width. **(c)** Merging of data from a number of flash-cooled crystals. Statistics are plotted for two single crystals and a combined data set from a number of crystals of the reverse transcriptase from HIV-1 [30].

Henderson [29] based on experience with electron irradiation. As proposed by Henderson, the rigid glass encasing the crystal at cryogenic temperatures may prevent movement of radiolytic fragments and damage to one molecule from propagating to nearby portions of the lattice. This mechanical support would then be the mechanism responsible for the increase in crystal lifetime. The decay that does occur would result simply from the damage to individual molecules, and it should therefore be relatively independent of crystal type. Indeed, different crystals do show similar rates of decay at cryogenic temperatures. For the mosaic spread to increase, however, larger distortions of the crystal lattice must still occur to some extent. At the observed rate of decay, crystals are effectively free of damage when irradiated by rotating-anode sources, and lifetime considerations may be ignored when setting exposure times. At high-intensity synchrotron sources, however, trade-off between crystal decay and exposure time is still required for weakly scattering crystals. In most cases, as with TBHA2, selection of exposure times so that a complete data set can be collected from one crystal will give an acceptable resolution limit. When the data quality achieved using this approach is not adequate, longer exposure times will be necessary and multiple crystals must be used to construct the data set. The structure determination of the unliganded form of reverse transcriptase from the human immunodeficiency virus is an extreme example of the need for multiple crystals [30]. Small crystals (0.15 mm×0.40 mm ×0.02 mm) grow in space group C2 with a large unit cell (a=168.7 Å, b=162.8 Å, c=331.8 Å) and four molecules of 117 kDa molecular mass each per asymmetric unit. With the small crystal size and large cell dimensions, long exposure times at a synchrotron source are required to record any diffraction to higher resolution than 3.5 Å. Only ~5° of data could be collected from a single crystal at low temperature, and 34 crystals were used to construct the final data set. As shown in Fig. 2c, the merging statistics for data from individual crystals agree well with data combined from a number of crystals, indicating that they are acceptably isomorphous.

Outlook

Routine cryogenic data collection from macromolecular crystals is now possible, and the technique will continue to gain in popularity as more difficult problems are attempted. Recently, for example, two types of virus crystals have been successfully flash-cooled: rotavirus (BRS Temple, BA Harris and SC Harrison, personal communication) and cowpea mosaic virus/rhinovirus 14 chimera (C Momany, T Lin and JE Johnson, personal communication). In addition, the combination of cryogenic methods and phasing by multi-wavelength anomalous diffraction (MAD) is particularly powerful, simplifying data collection and extending the MAD technique to radiation-sensitive crystals. A number of structures have now been determined in this way: human chorionic gonadotropin [31], lacR core fragment (AM Friedman, TO Fischmann and TA Steitz, personal communication), phage T4 gene32–ssDNA complex (Y Shamoo, AM Friedman, MR Parsons, WH Koenigsburg and TA Steitz, personal communication) and NFκB p50 homodimer (C Mueller, *et al.*, personal communication). Finally, one of the most exciting applications of flash-cooling is the study of transient or intermediate states in enzymology, and several examples have already been reported (X Ding, BF Rasmussen, GA Petsko and D Ringe, abstract E02, American Crystallographic Association Meeting, Atlanta, 1994) [26,32]. It is clear that, in many ways, the flash-cooling method is becoming an essential tool for the macromolecular crystallographer.

Acknowledgements: I thank members of the Harrison and Wiley research groups and other colleagues for sharing unpublished data; Barbara Harris, Sanjoy Ray, Steve Gamblin, Per Bullough, Fred Hughson, Stan Watowich, Rick Walter and Karin Reinisch for discussions; and Stephen Harrison for support.

References

1. Hope, H. (1988). Cryocrystallography of biological macromolecules: a generally applicable method. *Acta Crystallogr. B* **44**, 22–26.
2. Hope, H. (1990). Crystallography of biological macromolecules at ultra-low temperature. *Annu. Rev. Biophys. Biophys. Chem.* **19**, 107–26.
3. Watenpaugh, K.D. (1991). Macromolecular crystallography at cryogenic temperatures. *Curr. Opin. Struct. Biol.* **1**, 1012–1015.
4. Earnest, T., Fauman, E., Craik, C.S. & Stroud, R. (1991). 1.59 Å structure of trypsin at 120K: Comparison of low temperature and room temperature structures. *Proteins* **10**, 171–187.
5. Haas, D.J. & Rossmann, M. (1970). Crystallographic studies on lactate dehydrogenase at −75°C. *Acta Crystallogr. B* **26**, 998–1004.
6. Parak, F., Frolov, E.N., Mossbauer, R.L. & Goldanskii, V.I. (1981). Dynamics of metmyoglobin crystals investigated by nuclear gamma resonance absorption. *J. Mol. Biol.* **145**, 825–833.
7. Hartmann, H., Parak, F., Steigemann, W., Petsko, G.A., Ringe Ponzi, D. & Frauenfelder, H. (1982). Conformational substates in a protein: Structure and dynamics of metmyoglobin at 80 K. *Proc. Natl. Acad. Sci. USA* **79**, 4967–4971.
8. Mayer, E. (1985). Vitrification of pure liquid water. *J. Microsc.* **140**, 3–15.
9. Dubochet, J., *et al.*, & Schultz, P. (1988). Cryo-electron microscopy of vitrified specimens. *Q. Rev. Biophys.* **21**, 129–228.
10. Hope, H., *et al.* & Yonath, A. (1989). Cryocrystallography of ribosomal particles. *Acta Crystallogr. B* **45**, 190–199.
11. Dewan, J.C. & Tilton, R.F. (1987). Greatly reduced radiation damage in ribonuclease crystals mounted on glass fibers. *J. Appl. Crystallogr.* **20**, 130–132.
12. Rodgers, D.W. (1995). Practical cryocrystallography. *Methods Enzymol.*, in press.
13. Sutton, R.L. (1991). Critical cooling rates to avoid ice crystallization in solutions of cryoprotective agents. *J. Chem. Soc. Faraday Trans.* **87**, 101–105.
14. Petsko, G.A. (1975). Protein crystallography at sub-zero temperatures: cryo-protective mother liquors for protein crystals. *J. Mol. Biol.* **96**, 381–392.
15. Ray, W.J. Jr., Bolin, J.T., Puvathingal, J.M., Minor, W., Liu, U. & Muchmore, S.W. (1991). Removal of salt from a salt-induced protein crystal without cross-linking. Preliminary examination of desalted crystals of phosphoglucomutase by X-ray crystallography at low temperature. *Biochemistry* **30**, 6866–6875.
16. Wierenga, R.K., Zeelen, J.Ph. & Nobel, M.E.M. (1992). Crystal transfer experiments carried out with crystals of trypanosomal triosephosphate isomerase (TIM). *J. Cryst. Growth* **122**, 231–234.
17. Teng, T.Y. (1990). Mounting of crystals for macromolecular crystallography in a free-standing thin film. *J. Appl. Crystallogr.* **23**, 387–391.
18. Rudman, R. (1976). *Low-Temperature X-ray Diffraction*. Plenum Press, New York.
19. Bullough, P.A., Hughson, F.M., Treharne, A.C., Ruigrok, R.W.H., Skehel, J.J. & Wiley, D.C. (1994). Crystals of a fragment of influenza hemagglutinin in the low pH induced conformation. *J. Mol. Biol.* **236**, 1262–1265.
20. Bullough, P.A., Hughson, F.M., Skehel, J.J. & Wiley, D.C. (1994). Structure of influenza hemagglutinin at the pH of membrane fusion. *Nature* **371**, 37–43.

21. Teeter, M.M. & Hope, H. (1986). Progress in the water structure of the protein crambin by X-ray diffraction at 140 K. *Ann. N. Y. Acad. Sci.* **482**, 163–165.
22. Frauenfelder, H., *et al.*, Max, N. (1987). Thermal expansion of a protein. *Biochemistry* **26**, 254–261.
23. Tilton, R.F., Jr., Dewan, J.C. & Petsko, G.A. (1992). Effects of temperature on protein structure and dynamics: X-ray crystallographic studies of the protein ribonuclease-A at nine different temperatures from 98–320 K. *Biochemistry* **31**, 2469–2481.
24. Young, A.C.M., Tilton, R.F. & Dewan, J.C. (1994). Thermal expansion of hen egg-white lysozyme. *J. Mol. Biol.* **235**, 302–317.
25. Walter, J., Stegemann, W., Singh, T.P., Bartunik, H., Bode, W. & Huber, R. (1982). On the disordered activation domain in trypsinogen: chemical labeling and low temperature crystallography. *Acta Crystallogr. B* **38**, 1462–1472.
26. Watt, W., Tulinsky, A., Swenson, R.P. & Watenpaugh, K.D. (1991). Comparison of the crystal structures of a flavodoxin in its three oxidation states at cryogenic temperatures. *J. Mol. Biol.* **218**, 195–208.
27. Young, A.C.M., Dewan, J.C.,Thompson, A.W. & Nave, C. (1990). Enhancement in solution and lack of radiation damage in a rapidly frozen lysozyme crystal subjected to high-intensity synchrotron radiation. *J. Appl. Crystallogr.* **23**, 215–218.
28. Watowich, S.J., Skehel, J.J. & Wiley, D.C. (1994). Cryocrystallography of influenza virus hemagglutinin crystals. *Acta. Crystallogr. D*, in press.
29. Henderson, R. (1993). Cryo-protection of protein crystals against radiation damage in electron and X-ray diffraction. *Proc. R. Soc. Lond. B* **241**, 6–8.
30. Rodgers, D.W., *et al.*, & Harrison, S.C. (1995). The structure of unliganded reverse transcriptase from the human immunodeficiency virus type 1. *Proc. Natl. Acad. Sci. USA*, in press.
31. Wu, H., Lustbader, J.W., Liu, Y., Canfield, R.E. & Hendrickson, W.A. (1994). Structure of human chorionic gonadotropin at 2.6 Å resolution from MAD analysis of the selenomethionyl protein. *Structure* **2**, 545–558.
32. Chen, C.C.H. & Herzberg, O. (1992). Inhibition of β-lactamase by clavulanate: trapped intermediates in cryocrystallographic studies. *J. Mol. Biol.* **224**,1103–1113.

David W Rodgers, Department of Molecular and Cellular Biology, Harvard University, Cambridge MA 02138, USA.

As MAD as can be

Randy J Read

With the recent demonstration that multiwavelength anomalous dispersion (MAD) can provide accurate experimental phases at high resolution, crystallographers have gained a tool with which to study solvation and flexibility in proteins, and a test-bed for the development of crystallographic methods.

Address: Department of Medical Microbiology and Immunology, University of Alberta, Edmonton, Alberta T6G 2H7, Canada.

Structure 15 January 1996, 4:11–14

 ISSN 0969-2126

Burling, Weis, Flaherty and Brünger [1] have recently described what is probably the most accurate and complete experimental determination of phases for a protein crystal structure to date. They used multiwavelength anomalous dispersion (MAD) phasing to determine accurate phases to 1.8 Å resolution for a dimeric fragment of rat mannose binding protein (MBP). This experiment provides a resounding affirmation of the MAD technique, the promise of which has been championed for some time by Hendrickson [2]. By circumventing many of the usual sources of uncertainty, such an experiment gives us confidence in structural details that are at the limit of the abilities of X-ray crystallography.

Background

To understand the significance of this work, we must start from an appreciation of the phase problem and the limitations of the methods used to deal with it. The diffracted X-rays measured from a protein crystal are the Fourier transform of the atomic structure (actually, of the density of electrons in space). Because the Fourier transform can be reversed, we can build up a picture of the electron density from the diffracted waves. But this is where the phase problem rears its head: what we measure is only the intensity of a diffracted wave, and this tells us its amplitude but not its phase angle. It is the phase angle that determines where the peaks and troughs go in the electron density reconstruction, and is, therefore, more important to the appearance of the electron density map than the measured amplitudes! Because they cannot be measured directly, the phases must be deduced in some way.

The traditional method of phase determination is multiple isomorphous replacement (MIR) [3]. In this method, heavy metal compounds are bound to the protein in the crystal. They perturb the diffraction pattern significantly, in a way that gives information about the possible values of the phase angle. In an ideal experiment, the data would be measured without error and the native and derivative crystals would be isomorphous, that is, they would differ only in whether or not they contained heavy atoms. Two derivative crystals would then be sufficient to determine the phases unambiguously. But experiments are never ideal. The bound heavy atoms usually cause small changes in protein conformation or mobility, or they change the packing in the crystal. On top of this, the systematic errors of data measurement vary from one crystal to another. The consequences of the errors become more serious in the higher resolution diffraction terms that define the fine details, so MIR electron density maps are almost always limited to providing a relatively fuzzy picture of the protein.

The MAD phasing method can overcome most of these difficulties, both in theory (see Hendrickson [2] for a review and a more complete explanation) and, as now demonstrated by Burling *et al.* [1], in practice. In this method, a single crystal containing anomalous scatterers (the inner-shell electrons of which have transitions close in energy to the X-ray energy) is used to collect diffraction data sets at a number of carefully chosen X-ray wavelengths. As the X-ray wavelength is changed in the vicinity of the absorption edge, the contribution to the diffraction pattern from the anomalous scatterers changes rapidly, both in its magnitude and in its phase. The change in magnitude has an effect equivalent to the addition of a heavy atom in isomorphous replacement. The phase change in the contribution from the anomalous scatterers leads to a reduction of symmetry in the diffraction pattern, so that intensity differences appear between Bijvoet pairs of reflections. Each wavelength thus provides two observations that cast light on each phase, through effects analogous to isomorphous replacement. In contrast to isomorphous replacement, the systematic errors can nearly be made to cancel (because the measurements are made close in time from the same crystal in the same orientation), and there is perfect isomorphism because the measurements are all made on the same crystal. With perfect isomorphism, the potential phase accuracy does not fall off with resolution. In fact, the anomalous scattering effects, which arise from the tightly bound inner-shell electrons, fall off much less with resolution than the normal scattering from the bulk of electrons, so that the relative size of the anomalous scattering signal can even increase with resolution.

MAD phasing has moved from being a theoretical possibility to an almost routine method for solving crystal structures, largely through the work of Hendrickson and his colleagues who were responsible for devising solutions to

many of the practical and theoretical problems. A quick literature search shows that in 1995 alone at least six structures were solved with the help of MAD phasing. But the recent MAD phasing experiment on MBP [1] comes closer than previous studies to achieving the full promise of the method.

The MBP MAD experiment

The essential differences in this experiment were not so much in methodology as in the way that experimental conditions were carefully optimized. The Yb^{3+}-substituted MBP crystal was chosen for the experiment for three reasons: it diffracts to high resolution, ytterbium has a strong anomalous scattering effect, and the sites where Yb^{3+} replaces the normal Ca^{2+} ligands are well ordered [4]. In addition, there is a dimer in the asymmetric unit of the crystal, so that molecules in different packing environments can be compared. Data were collected at four wavelengths chosen to optimize the phase information, whereas often only three wavelengths are used. But the most important factor in the success of this experiment is probably the precision and completeness of the measurements. More than 99% of the possible diffraction data to 1.8 Å resolution were measured at each wavelength, most to good precision, ensuring that experimental phases were determined from eight observations for almost every diffraction term. The refinement of the structure of the anomalous scatterers and the determination of the phase probability curves were carried out by maximum likelihood methods similar to those recently introduced for MIR [5].

Perhaps we should not expect to see an abundance of experimental phase sets at this level of accuracy, at least not in the near future. Not all crystals are equally amenable, and the method requires a generous amount of beam time on a synchrotron that is well-equipped for the precise control of wavelength. These factors have generally limited previous investigations. As more synchrotron beam lines are constructed with MAD phasing in mind, and more crystallographers become aware of its potential, such experiments will be seen more often.

Conclusions from the MBP experiment

Escape from model bias

Experimental phases are normally poorly determined at the limit of resolution, so in order to fit the diffraction data and supply more accurate estimates of the phases crystallographers rely on the refinement of atomic models. This works, but at a price: the maps computed from model phases, especially after refinement, have a bias to reproduce the model [6]. The problem is the paucity of data. For optimization methods to work well, there should be a much larger number of observations than adjustable parameters. At the modest but common resolution of 2.8 Å, a protein structure has about the same number of observations as parameters. With too many adjustable parameters it is possible to over-fit the data; errors in one part of the structure can be compensated, in part, by small adjustments in the rest of the structure. Electron density will tend to appear where there are atoms in the model, even if there is nothing in the true structure. The situation improves with resolution, but few structures diffract to a resolution that is high enough to avoid any over-fitting.

Model bias can be reduced, but not eliminated, by using appropriate coefficients to compute the electron density maps [7]. For the rare protein crystals that diffract to better than atomic resolution (e.g. crambin [8] and rubredoxin [9]), there are sufficient observations to make refinement behave, and refinement bias ceases to be a problem. The MAD phases determined in the MBP experiment may be no more accurate than those obtained from a model at the end of careful refinement, but they are completely uncontaminated by model bias. Safer conclusions about mobility and solvent structure can therefore be drawn.

Protein mobility

Protein crystal structures are usually modeled as a set of atoms at defined positions. To account for thermal motion and disorder around these positions, the atoms are also assigned B values. This model of motion is based on the assumption that the atoms vibrate harmonically and isotropically about their positions, an assumption that we know from theory and experiment to be false [10]. But realistic models of mobility require more parameters and, as discussed above, protein structures already tend to have a distressing number of parameters.

Mobility can been modeled in various ways, each method involving a different number of parameters. The general features can, in fact, be modeled with fewer parameters than the traditional B factors, using normal modes [11]. At a more detailed level, discrete disorder can be modeled for a small number of side chains [10], or multiple models of the whole structure can be refined simultaneously [12]. In the ultimate treatment of mobility, the protein model that is refined is the ensemble average of conformations generated in a molecular dynamics simulation [13]. Accurate MAD phases provide a direct picture that can be used to validate such models [1].

Solvent structure

In a typical protein crystal, half of the volume is occupied by disordered solvent. This disordered solvent has an almost uniform density level, a feature that is exploited in solvent-flattening techniques. Nonetheless, one would not expect all positions near a protein surface to be equally favourable for a solvent molecule, a conclusion that is supported by results from computer simulations of proteins in an isolated box of water [14,15] or in a crystal lattice [16].

It has been difficult to compare these computer simulations with the results of crystal structure determinations. As attempts to model details of the solvent distribution in a crystal [17] require the addition of even more parameters, they could easily be subject to artefacts of over-fitting. On the other hand, if the solvent distribution is not modeled, it is implicitly assumed to be flat, so model bias will lead to maps that have flatter solvent regions than they ought to.

The MAD phases for MBP give us an independent picture of solvent in a protein crystal, and the density distribution indeed is seen to be non-uniform. Two observations support the overall validity of the picture: the radial distribution of solvent electron density surrounding various atom types agrees with our expectations of hydrogen bonding; also, as expected, there is diffuse solvent density at van der Waals distance from hydrophobic groups (which do not provide favoured solvent binding sites).

Because the features in the solvent electron density are much weaker than those in the protein density, it will be essential to explore the influence of possible sources of error before interpreting the finer details. Even small errors in the experimental phases will inevitably add noise to difference maps. As well, because the crystals diffract beyond 1.8 Å, the truncation of the data at this limit will introduce diffraction ripples, which may be particularly evident at the boundary between well-ordered protein and poorly ordered solvent.

A test-bed for methods

Those who derive new methods for protein crystallography constantly run into the problem of what to test them on. Some tests are done on simulated data with various sources of simulated error, so that success can be gauged objectively. Unfortunately, reality may differ from simulations in ways that interfere with a method. For instance, the solvent distribution is generally assumed to be flat; depending on how badly this assumption is violated in real crystals, simulations may overestimate the power of solvent flattening. Also, it is difficult to carry out realistic simulations of anisotropic and anharmonic motions, so the use of simulated data provides a poor test of how well we can deal with the effect of these complicated motions.

Instead of simulating data, we can combine observed amplitudes with either MIR or model phases. The disadvantage is that MIR phases suffer from large experimental errors, and model phases suffer from model bias (unless they come from one of those rare crystals that diffract to atomic resolution). Phases from accurate MAD experiments will be a great improvement.

Structure refinement is one area that could benefit from improved test data as there is good reason to hope that dramatic improvements could yet be made in refinement methods. It is commonly found that low resolution structure factors come to agree much better with a model after it has been refined against high resolution data, no matter how much care was taken in the earlier refinement at low resolution. This is true even if the number of parameters is not increased. In other words, it seems to be possible to distinguish between better and worse models using only the lower resolution data, but current refinement methods fail to find the way.

Tests of refinement methods need a benchmark of how well it is possible to represent the true structure using a model constructed of atoms with coordinates and B values. This could be obtained by carrying out a refinement of MBP using the experimental phases as restraints. Refinements performed only against the amplitudes that are normally available could then be judged by how well they approached this ideal. We, and others, have been working to implement maximum likelihood methods of structure refinement [18,19]. Tests at intermediate stages of refinement show that maximum likelihood works much better than the traditional least-squares methods (NS Pannu and RJ Read, unpublished data), but a test for whether it gets further at the end of refinement has been lacking.

Similarly, accurate experimental MAD phases could be used to judge the success of phase improvement methods such as density modification, or the accuracy of models of mobility or solvent distribution. In addition to giving direct answers in selected cases, MAD phases could provide well-defined targets for crystallographic methods, thereby accelerating their development considerably.

References

1. Burling, F.T., Weis, W.I., Flaherty, K.M. & Brünger, A.T. (1995). Direct observation of protein solvation and discrete disorder using experimental crystallographic phases. *Science* (in press).
2. Hendrickson, W.A. (1991). Determination of macromolecular structures from anomalous diffraction of synchrotron radiation. *Science* **254**, 51–58.
3. Blow, D.M. & Crick, F.H.C. (1959). The treatment of errors in the isomorphous replacement method. *Acta Cryst.* **12**, 794–802.
4. Weis, W.I., Kahn, R., Fourme, R., Drickamer, K. & Hendrickson, W.A. (1991). Structure of the calcium-dependent lectin domain from a rat mannose-binding protein determined by MAD phasing. *Science* **254**, 1608–1615.
5. Otwinowski, Z. (1991). Maximum likelihood refinement of heavy atom parameters in isomorphous replacement and anomalous scattering. In *Proceedings of the CCP4 Study Weekend.* (Wolf, W., Evans, P.R. & Leslie, A.G.W., eds), pp. 80–86, SERC Daresbury Laboratory, Warrington, UK.
6. Hodel, A., Kim, S.-H. & Brünger, A.T. (1992). Model bias in macromolecular crystal structures. *Acta Cryst. A* **48**, 851–858.
7. Read, R.J. (1986). Improved Fourier coefficients for maps using phases from partial structures with errors. *Acta Cryst. A* **42**, 140–149.
8. Teeter, M.M., Roe, S.M. & Heo, N.H. (1993). Atomic resolution (0.83-Ångstrom) crystal structure of the hydrophobic protein crambin at 130 K. *J. Mol. Biol.* **230**, 292–311.
9. Dauter, Z., Sieker, L.C. & Wilson, K.S. (1992). Refinement of rubredoxin from *Desulfovibrio vulgaris* at 1.0 Å with and without restraints. *Acta Cryst. B* **48**, 42–59.
10. Smith, J.L., Hendrickson, W.A., Honzatko, R.B. & Sheriff, S. (1986). Structural heterogeneity in protein crystals. *Biochemistry* **25**, 5018–5027.

11. Diamond, R. (1990). On the use of normal modes in thermal parameter refinement: theory and application to the bovine pancreatic trypsin inhibitor. *Acta Cryst. A* **46**, 425–435.
12. Kuriyan, J., Osapay, K., Burley, S.K., Brünger, A.T., Hendrickson, W.A. & Karplus, M. (1991). Exploration of disorder in protein structures by X-ray restrained molecular dynamics. *Proteins* **10**, 340–358.
13. Gros, P., van Gunsteren, W.F. & Hol, W.G.J. (1990). Inclusion of thermal motion in crystallographic structures by restrained molecular dynamics. *Science* **249**, 1149–1152.
14. Komeiji, Y., Uebayasi, M., Someya, J. & Yamato, I. (1993). A molecular dynamics study of solvent behavior around a protein. *Proteins* **16**, 268–277.
15. Steinbach, P.J. & Brooks, B.R. (1993). Protein hydration elucidated by molecular dynamics simulation. *Proc. Natl. Acad. Sci. USA* **90**, 9135–9139.
16. Kitson, D.H., *et al.*, & Hagler, A.T. (1993). On achieving better than 1-Ångstrom accuracy in a simulation of a large protein – *Streptomyces griseus* protease A. *Proc. Natl. Acad. Sci. USA* **90**, 8920–8924.
17. Badger, J. & Caspar, D.L.D. (1991). Water structure in cubic insulin crystals. *Proc. Natl. Acad. Sci. USA* **88**, 622–626.
18. Read, R.J. (1990). Structure-factor probabilities for related structures. *Acta Cryst. A* **46**, 900–912.
19. Bricogne, G. (1991). A multisolution method of phase determination by combined maximization of entropy and likelihood. III. Extension to powder diffraction data. *Acta Cryst. A* **47**, 803–829.

versity of Western Australia and the Western Australia Department of Agriculture (Perth, Western Australia, in December 1993 and January 1994) and weighed with a Mettler AE50 balance that was accurate to 0.1 mg.

14. Male spiders copulate with paired structures (emboli) that are inserted through separate coiled ducts into the paired sperm storage organs (spermathecae) of the female. In *Latrodectus*, the tip of the male's embolus always breaks off during insertion and remains inside the spermathecae or coiled ducts (*19*). By counting broken emboli inside 23 nonvirgin females (collected near Perth, Western Australia, in January 1994), I determined that 30.4% (7/23) had received only one palpal insertion, 52.2% (12/23) had received two palpal insertions and so had mated with one or two males, and 17.4% (4/23) had received three palpal insertions and so had mated with at least two and possibly three males.
15. G. A. Parker, *Biol. Rev.* **45**, 525 (1970); B. Sillen-Tullberg, *Behav. Ecol. Sociobiol.* **9**, 283 (1981). The proportion of eggs fertilized by the N male (x) was $x = (a - c)/(b - c)$ where a is the proportion hatched in the NI or IN group, b is the proportion hatched in the NN group, and c is the proportion hatched in the II group. P_2 in the IN group equaled x, and P_2 in the NI group equaled $1 - x$.
16. When the spermathecae of field-collected females (n = 23) were dissected (*14*), a total of 43 emboli were discovered. Of these, the majority (40/43) were located inside the female spermathecae rather than in the coiled ducts, suggesting that most males ejaculate directly into the sperm storage organ. Ejaculates of second males might then mix randomly with sperm already in the spermatheca, which suggests that increased sperm transfer is the mechanism by which longer copulation durations result in increased paternity.
17. Female rejection behavior is distinct and readily observable. In interactions that led to a successful copulation, the female remained quiescent in the web during most of the male's courtship. In comparison, rejection behavior consisted of a female repeatedly hitting at a courting male with her front legs, causing the male to drop from the web on a dragline. The male usually returned to the web and resumed courtship after the first few displacements, but nonreceptive females continued this behavior until the male eventually ceased courtship completely and moved to the substrate below the web.
18. T. E. Christenson and K. C. Goist Jr., *Behav. Ecol. Sociobiol.* **5**, 87 (1979); F. Vollrath and G. A. Parker, *Nature* **360**, 156 (1992).
19. R. G. Breene and M. H. Sweet, *J. Arachnol.* **13**, 331 (1985); B. J. Kaston, *Trans. San Diego Soc. Nat. Hist.* **16**, 33 (1970); J. W. Abalos and E. C. Baez, *Psyche* **70**, 197 (1963); R. D. S. Bhatnagar and J. G. Rempel, *Can. J. Zool.* **40**, 465 (1962).
20. L. M. Forster, in *Commerce and the Spread of Pests and Disease Vectors*, M. Laird, Ed. (Praeger, New York, 1984), pp. 273–289.
21. J. Kavale, thesis, University of Otago, Dunedin, New Zealand (1986).
22. K. Ross and R. L. Smith, *J. Arachnol.* **7**, 69 (1979).
23. S. K. Sakaluk, *Science* **223**, 609 (1984); *Evolution* **40**, 584 (1986); N. Wedell, *ibid.* **45**, 1975 (1991); *ibid.* **47**, 1203 (1993); D. T. Gwynne, in *Arthropod Social Systems*, J. Choe and B. Crespi, Eds. (Princeton Univ. Press, Princeton, NJ, in press).

24. I thank my supervisor, D. T. Gwynne, for considerable discussion and comments on this work and manuscript; W. J. Andersen, S. T. Emlen, L. M. Forster, P. D. Lorch, A. C. Mason, and P. W. Sherman for comments on the project or earlier versions of the manuscript; an anonymous reviewer for valuable suggestions; and W. J. Bailey, I. Dadour, C. Thomas, B. York Main, the University of Western Australia, and the Western Australia Department of Agriculture for facilitating my fieldwork. Supported by Natural Sciences and Engineering Research Council of Canada (operating grant to D. T. Gwynne and a 1967 Science and Technology scholarship to M.C.B.A.).

14 August 1995; accepted 2 November 1995

Direct Observation of Protein Solvation and Discrete Disorder with Experimental Crystallographic Phases

F. Temple Burling, William I. Weis,* Kevin M. Flaherty, Axel T. Brünger*

A complete and accurate set of experimental crystallographic phases to a resolution of 1.8 angstroms was obtained for a 230-residue dimeric fragment of rat mannose-binding protein A with the use of multiwavelength anomalous dispersion (MAD) phasing. An accurate image of the crystal structure could thus be obtained without resort to phases calculated from a model. Partially reduced disulfide bonds, local disorder, and differences in the mobility of chemically equivalent molecules are apparent in the experimental electron density map. A solvation layer is visible that includes well-ordered sites of hydration around polar and charged protein atoms, as well as diffuse, partially disordered solvent shells around exposed hydrophobic groups. Because the experimental phases and the resulting electron density map are free from the influence of a model, they provide a stringent test of theoretical models of macromolecular solvation, motion, and conformational heterogeneity.

Solvation and motion play key roles in protein folding, stability, and function. Water molecules are integral components of folded proteins, and the differential preference of amino acids for the aqueous environment is the basis of the hydrophobic effect, which is thought to be an important driving force in protein folding (*1*). Hydration of residues that participate in protein-ligand interactions and macromolecular association is important in determining the thermodynamics of binding. Molecular motion and flexibility are also essential aspects of macromolecular function, particularly in the induced fit, flexible-to-rigid transitions and large-scale conformational changes that occur in many proteins (*2*).

X-ray diffraction data result from temporal and spatial averaging over a large number of molecules in the crystal lattice and therefore provide an averaged view of solvation and flexibility. At the resolution limits typical of macromolecular crystals, the structure is usually modeled by a single conformer together with discrete sites of hydration. Thermal fluctuations are approximated by isotropic, harmonic motions. These models provide an incomplete description of the crystal structure. For example, solvent molecules constitute a large volume of macromolecular crystals (*3*), but only a small fraction of the solvent, consisting of fully occupied hydration sites ("bound" or "ordered" water molecules), is modeled. The remaining solvent is disordered but not completely featureless (*4*, *5*). It is particularly difficult to describe regions containing disordered solvent, portions of the molecule that display large thermal fluctuations [likely anisotropic and possibly anharmonic (*6*)], and conformational variability, all of which appear at relatively low electron density levels because of averaging over the copies in the crystal.

The interpretation of low electron density levels is made difficult by the presence of model bias that arises when inaccurate or incomplete experimental phases are substituted or augmented by phases derived from a model. When a feature is included in the model used to calculate phases for electron density maps, it often appears in the maps whether or not it is correct (*7*). In addition to causing model bias, inclusion of incorrect features in refinement can produce a relatively low conventional R value [$R = \Sigma_h ||F_{obs}(h)| - |F_{calc}(h)|| / \Sigma_h |F_{obs}(h)|$], which measures the agreement between structure factor amplitudes ($|F_{calc}|$) calculated from the refined model and the observed amplitudes ($|F_{obs}|$) over all reflections h. Misinterpretation or overinterpretation of the diffraction data can be reduced by monitoring the cross-validated or free R value (*8*); reduction of the free R value indicates a meaningful improvement of the model, whereas changes in the model that increase the free R value are likely fitting noise in the data.

The final R and free R values of macromolecular models are much larger than would be predicted from the statistical error in the observed amplitudes, presumably because current refinement models do not provide adequate descriptions of solvation

F. T. Burling and A. T. Brünger, Howard Hughes Medical Institute and Department of Molecular Biophysics and Biochemistry, Yale University, New Haven, CT 06520, USA.
W. I. Weis and K. M. Flaherty, Department of Structural Biology, Stanford University, Stanford, CA 94305, USA.
*To whom correspondence should be addressed.

Table 1. Data statistics. The space group is $P2_12_12_1$, with unit-cell parameters a = 65.51 Å, b = 72.22 Å, and c = 45.04 Å. Bijvoet mates were measured an average of 3.6 times. Statistics are given for diffraction data between 50 and 1.8 Å resolution. Values in parentheses are for data in the range 1.84 to 1.80 Å.

Wavelength (Å)	Number of reflections	Completeness (%)	Signal* (%)	R_{sym}† (%)
λ_1 1.3860 (edge)	37,989	99.2 (97.0)	87.5 (64.3)	8.0 (15.8)
λ_2 1.3854 (peak)	38,055	99.3 (97.3)	87.9 (64.6)	8.0 (15.5)
λ_3 1.3849 (inflection)	38,051	99.3 (97.1)	89.4 (69.4)	7.9 (14.2)
λ_4 1.3565 (remote)	38,059	99.3 (98.1)	89.8 (71.0)	7.7 (13.6)

*Percentage of reflections with $I > 3\sigma(I)$. †$R_{sym} = \Sigma_h \Sigma_i |I_i(h) - \langle I(h)\rangle| / \Sigma_h \Sigma_i I_i(h)$, where $I(h)$ is the ith measurement and $\langle I(h)\rangle$ is the weighted mean of all measurements of $I(h)$.

and thermal motion (5, 9). It is therefore desirable to obtain accurate experimental phases at high resolution that can be used to produce electron density maps free of model bias. Models can then be improved and validated by comparison with the experimental phases. The standard method of experimental phase determination, multiple isomorphous replacement (MIR), is inappropriate for this purpose because nonisomorphism between native and derivative crystals limits the accuracy of the phases to resolutions well short of the diffraction limit of the crystal. In contrast, the multiwavelength anomalous dispersion (MAD) phasing method permits accurate phasing to the measurable diffraction limit, because phases are obtained from the variation in anomalous scattering at different wavelengths from a single crystalline species (*10*).

We have obtained an accurate set of MAD phases for a crystal of the dimeric Yb^{3+}-substituted subtilisin fragment of mannose-binding protein A (sub–MBP-A) (*11*, *12*). A complete set of MAD data was measured to 1.8 Å resolution (*13*) (Tables 1 and 2). Two approaches were used to extract phases from these data. First, phases were obtained by the least-squares method (*10*, *14*) implemented in the MADLSQ program (*10*, *15*) (Tables 2 and 3). A limitation of the MADLSQ procedure is that it does not produce reliable figure-of-merit estimates for the phases (*16*). Therefore, a second, "probabilistic" approach was used to analyze the MAD data, which consists of computing phase probability distributions derived from lack-of-closure relations between the observed reflections at different wavelengths (Table 4) (*17*). The advantage of the probabilistic treatment is that the phase probability distributions and corresponding figures of merit incorporate the predicted errors of the anomalous scatterer model as well as those of the observed intensities (Table 5). Figure-of-merit weighted electron density maps obtained from the probabilistic treatment should therefore be a more accurate representation of the actual electron density distribution, although the phase centroids obtained from both methods are the same to within the estimated error ($\Delta(\Delta\phi)$) (Tables 3 and 5).

The resulting experimental electron density map is of exceptional quality (Fig. 1), as expected from the phasing statistics and the high figure of merit (Table 4). The map was used to correct the model of Ho^{3+}-substituted sub–MBP-A (*18*) for subsequent refinement against the observed structure factor amplitudes (*19*) (Table 6). Water molecules were placed in the experimental MAD electron density map with conservative criteria (*19*) for peak height, shape, and hydrogen-bonding distance (Fig. 1A). The high quality of the experimental phases is demonstrated by the low average phase difference with the model phases and the high correlation coefficient between experimental and calculated protein electron density (Table 6).

The experimental electron density map shows that one of the two disulfide bonds in sub–MBP-A (Cys^{128}–Cys^{217}) exists as a roughly equal mixture of oxidized and reduced states in both protomers (Fig. 1B). The decreased occupancy in the oxidized state of Cys^{217} is indicated by its lower electron density level compared with that of the Cys^{128} thiol group. In the reduced state, the Cys^{217} sulfhydryl group is capable of forming hydrogen bonds to one of two carbonyl oxygens, and the Cys^{128} sulfhydryl group can form a hydrogen bond to a third carbonyl oxygen (Fig. 1B). This feature has not been observed in previous high-resolution structures of MBP-A (*18*, *20*) and may be unique to this particular sample.

Although most regions of the molecule can be modeled well with conventional refinement methods (Fig. 1, A and B), other

Table 3. MAD phasing statistics: least-squares method [MADLSQ (*10*, *15*)]. The least-squares phasing and statistics were obtained with the MADSYS suite of programs (*29*).

	50 to 1.80 Å	1.88 to 1.80 Å
$R_{sym}(\lvert {}^{o}F_T \rvert)$*	0.069	0.126
$R_{sym}(\lvert {}^{o}F_A \rvert)$*	0.239	0.470
$\langle\Delta(\Delta\phi)\rangle$*	20.7°	35.2°
$\langle m_{LSQ}\rangle$†	0.94	0.89

*$R_{sym}(|F|) = \Sigma_h \Sigma_i |F_i(h)| - \langle|F(h)|\rangle| / \Sigma_h \Sigma_i \langle|F(h)|\rangle$, where $F_i(h)$ is the amplitude of the ith determination and $\langle|F(h)|\rangle$ is the weighted mean of all determinations of $|F(h)|$, ${}^{o}F_T$ is the structure factor due to normal scattering from all the atoms, ${}^{o}F_A$ is the structure factor due to normal scattering from Yb^{3+} only, $\Delta\phi$ is the phase difference between ${}^{o}F_T$ and ${}^{o}F_A$, and $\langle\Delta(\Delta\phi)\rangle$ is the mean difference between independent determinations of $\Delta\phi(h)$. Quantities do not include reflections with $m = 0$, where m is the figure of merit. †$\langle m_{LSQ}\rangle$ is the mean figure of merit, and here includes 88 reflections with $m = 0$.

Table 2. MAD phasing statistics: anomalous diffraction ratios and refined scattering factors. Values for the observed anomalous diffraction ratios are $\langle \Delta F_i^2 \rangle^{1/2} / \langle F_i^2 \rangle^{1/2}$, where ΔF_i is the Bijvoet difference at one wavelength (diagonal elements) or the dispersive difference at the two wavelengths intersecting at an off-diagonal element. The differences between Bijvoet mates at each wavelength for centric reflections, which would be 0.00 for perfect data, are shown in parentheses and serve as an estimate of the noise in the anomalous signals. Scattering factors $\Delta f'$ and $\Delta f''$ were held fixed at their theoretical values (*28*) at the remote wavelength to provide an absolute reference scale. Scattering factors at the other wavelengths were refined. Shown are the values obtained by MADLSQ (*10*, *18*); the values obtained from X-PLOR (*17*) are equal to within 10%.

Wavelength	Observed diffraction ratios				Scattering factors (e)	
	Edge (λ_1)	Peak (λ_2)	Inflection (λ_3)	Remote (λ_4)	$\Delta f'$	$\Delta f''$
λ_1	0.132 (0.056)	0.072	0.105	0.098	−25.4	10.7
λ_2		0.249 (0.056)	0.078	0.080	−19.7	23.2
λ_3			0.188 (0.054)	0.057	−9.4	17.5
λ_4				0.116 (0.053)	−10.3	10.1

Table 4. MAD phasing statistics: probabilistic method [X-PLOR (*17*, *27*)].

	50 to 1.80 Å	1.88 to 1.80 Å
Phasing power*		
$\lambda_4 \rightarrow \lambda_1$	4.3	2.9
$\lambda_4 \rightarrow \lambda_{-1}$	7.7	5.3
$\lambda_4 \rightarrow \lambda_2$	4.7	3.3
$\lambda_4 \rightarrow \lambda_{-2}$	10.8	7.8
$\lambda_4 \rightarrow \lambda_3$	2.7	1.6
$\lambda_4 \rightarrow \lambda_{-3}$	8.8	6.1
$\lambda_4 \rightarrow \lambda_{-4}$	7.9	6.1
$\langle m_{probl}\rangle$†	0.91	0.80

*Phasing power $[\lvert F_{h_4} - F_{h_i}\rvert^2] / \int_4 P_{\lambda_4 \rightarrow \lambda_i}(\phi)[\lvert F_{\lambda_4}\rvert e^{i\phi} + F_{h_i} - F_{\lambda_i}\rvert - \lvert F_{\lambda_i}\rvert]^2 d\phi]^{1/2}$ computed for individual lack-of-closure expressions between the reflections of the reference wavelength λ_4, its Friedel mate, and the Bijvoet pairs measured at the other wavelengths (*17*). †$\langle m_{probl}\rangle$ is the mean figure of merit.

portions of the structure show varying degrees of conformational variability and disorder. Multiconformer refinement (*21*) was used to model this variability. Motion of certain side chains is observed (Fig. 1C), whereas complete disorder is inferred from large variations of the members of the multiconformer ensemble and from the lack of electron density for the first two residues of protomer B and for several surface side chains. The conformational variability is more pronounced for the second protomer: It has higher temperature factors when refined as a single conformer, as well as larger root-mean-square differences among members of the multiconformer ensemble (Table 6). This variability may be attributable to the different number of crystal packing interactions made by the two protomers (44 residues of protomer A participate in lattice contacts, compared with 30 in protomer B). The introduction of multiconformer refinement slightly improved both R values and the phase accuracy of the model (Table 6). However, the resulting R values are still significantly larger than the predicted error of the observed amplitudes ($R \gg R_{cryst}/2$) (Table 1).

Most of the difference between observed and calculated electron density (*22*) occurs in the solvent regions, whereas little difference is apparent within the protein (Fig. 2A). Thus, incomplete treatment of solvent appears to be a significant component of the error in the model. The difference electron density map is very similar to the experimental electron density map in the solvent regions (Fig. 2B). Moreover, the experimental electron density in the bulk solvent regions is virtually independent of the reference wavelength used for the lack-of-closure expressions and the map calculation (*17*). The similarity among these electron density maps in the bulk solvent regions suggests that the observed features are a consequence of the actual solvent distribution and are not caused by noise in the data. They represent a time-averaged image of the solvent distribution around the protein. Thus, our results provide evidence for the existence of a nonuniform solvent distribution around proteins, as proposed by Badger, Caspar, and colleagues (*4*) on the basis of similar features in potentially noisy (*22*) or model-based ($|F_{obs}| - |F_{calc}|$) $\exp(i\phi_{calc})$ difference electron density maps.

Site-specific radial distribution functions of solvent electron density (*5*) were computed from the experimental electron density map. They indicate a well-defined solvation shell around hydrophilic and hydrophobic groups (Fig. 2, C to E). Specific sites of hydration were apparent around polar and charged groups at hydrogen-bonding distance (compare with Fig. 1A). A diffuse electron density layer was apparent at approximately van der Waals distance around hydrophobic groups. A marked example is a ringlike feature near the methyl groups of Leu^{203} in protomer A (Fig. 2B). The electron density around Leu^{203} in protomer A suggests a network of four to five partially disordered water molecules (*23*). The disorder is presumably attributable to the many possible placements of water molecules around hydrophobic groups, which undergo rapid motion as indicated by nuclear magnetic resonance experiments on proteins (*24*).

The experimental electron density map described here was computed without resort to model phases. The partially disordered solvent, multiple conformations,

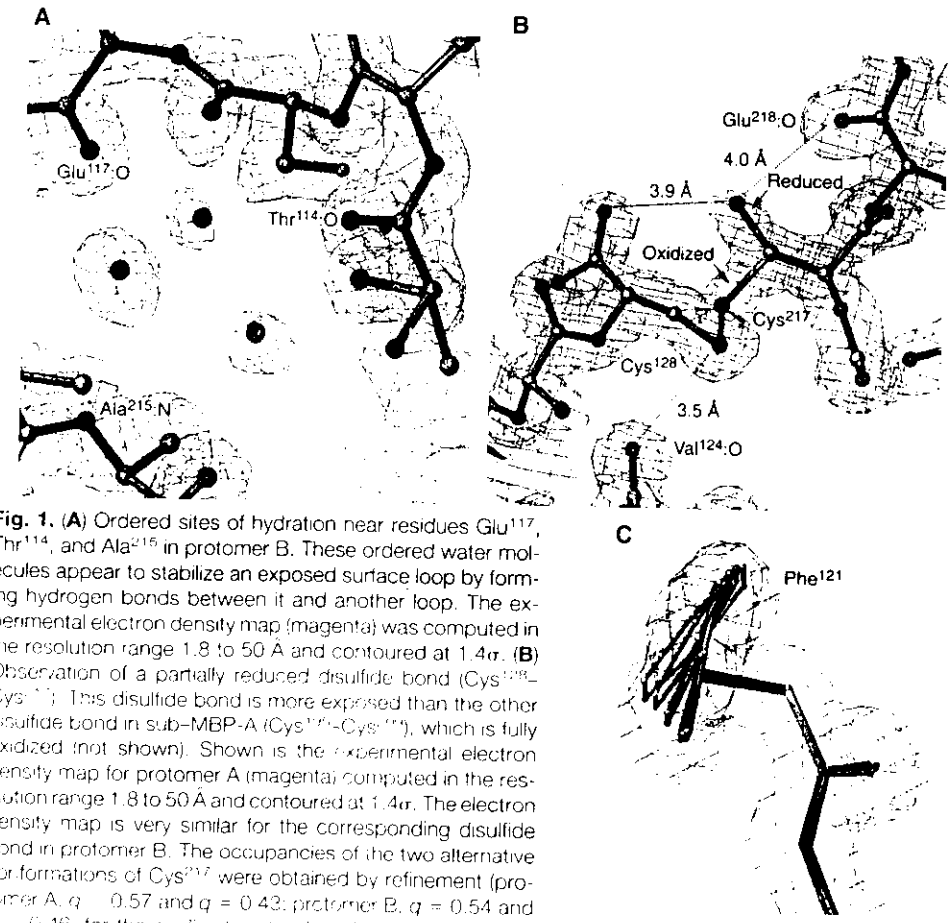

Fig. 1. (**A**) Ordered sites of hydration near residues Glu^{117}, Thr^{114}, and Ala^{215} in protomer B. These ordered water molecules appear to stabilize an exposed surface loop by forming hydrogen bonds between it and another loop. The experimental electron density map (magenta) was computed in the resolution range 1.8 to 50 Å and contoured at 1.4σ. (**B**) Observation of a partially reduced disulfide bond (Cys^{128}–Cys^{217}). This disulfide bond is more exposed than the other disulfide bond in sub-MBP-A (Cys^{74}–Cys^{77}), which is fully oxidized (not shown). Shown is the experimental electron density map for protomer A (magenta) computed in the resolution range 1.8 to 50 Å and contoured at 1.4σ. The electron density map is very similar for the corresponding disulfide bond in protomer B. The occupancies of the two alternative conformations of Cys^{217} were obtained by refinement (protomer A, q = 0.57 and q = 0.43; protomer B, q = 0.54 and q = 0.46, for the oxidized and reduced states, respectively). The sulfhydryl group of the alternative conformation of Cys^{217} can form hydrogen bonds with the carbonyl group of Glu^{218} or that of Cys^{128} (sulfur oxygen distances are 4.0 and 3.9 Å for protomer A and 3.5 and 4.3 Å for protomer B, respectively). The sulfhydryl group of the reduced form of Cys^{128} can form a hydrogen bond with the carbonyl group of Val^{124} (distance is 3.5 Å in both protomers). The observed distances are within the range of observed cysteine-carbonyl hydrogen bonds (*30*). (**C**) Example of local conformational variability: wagging motion of Phe^{121} in protomer A. Multiconformer refinement (*21*) produces a family of conformers with considerable side-chain dihedral angle variability ($-172° < \chi_1 < -165°$, $54° < \chi_2 < 82°$) that fits the electron density better than does a refined single conformer ($\chi_1 = -168°$, $\chi_2 = 74°$). The experimental electron density map (magenta) is computed in the resolution range 1.8 to 50 Å and contoured at 1.4σ. Bonds and atoms are colored according to atom type (blue, N; red, O; tan, C; and green, S).

Table 5. MAD phasing statistics: comparison between least-squares and probabilistic methods.

	$\langle\phi_{LS} - \phi_{prob}\rangle$*	$\langle\cos^{-1}(m_{LS})\rangle$	$\langle\cos^{-1}(m_{prob})\rangle$
Strong anomalous data†	10.5°	5.1°	8.3°
Weak anomalous data‡	21.9°	11.4°	20.3°
All data	18.2°	9.3°	16.4°

*Mean phase difference between phases obtained from the least-squares method (ϕ_{LS}) and the centroid phase obtained from the probabilistic method (ϕ_{prob}), corrected for the contribution of the anomalous scatterer model. †The portion (32%) of the data with the strongest anomalous signal ($|\Delta F| = ||F^+| - |F^-|| > 2\sigma_{|\Delta F|}$ and $|F| > 2\sigma_F$). ‡Remaining 68% of the data.

and partially reduced disulfide bonds apparent in the map are therefore real features of the crystal structure and not an artifact of the refinement process. The experimental electron density map and the resulting solvent radial distribution functions thus serve as a stringent test of theoretical computer simulations of solvated proteins in a crystalline environment (*25*). Comparison of simulated solvent radial distribution functions around proteins (*25*) with those derived from the experimental map (Fig. 2, C to E) shows reasonable agreement around polar groups, but a somewhat broader distribution around hydrophobic groups is apparent in the experimental radial distribution function. The theoretical computer simulations may be improved by investigating this and other discrepancies between the simulations and the observed data, some of which may be attributable to crystallization conditions. Improved models of thermal motion, discrete disorder, and solvation for crystallographic refinement could be obtained by directly incorporating the experimental phase information into the refinement process to increase the observable-to-parameter ratio (*26*). Ultimately, these models could be used to obtain information about solvation, conformational variability, and motion in instances in which high-resolution experimental phase information is unavailable.

Table 6. Conventional (*19*) and multiconformer (*21*) refinement statistics. Statistics are for the resolution range of 10 to 1.8 Å.

	Conventional	Multiconformer
R value (%)	19.1	16.7
Free *R* value (*8*, *19*) (%)	21.7	20.3
Bond length deviation (Å)	0.009	0.005
Bond angle deviation (degrees)	1.4	1.1
Improper angle deviation (degrees)	1.4	1.1
Residues in disallowed phi-psi regions (%)	0.5	0.6
Non-hydrogen protein atoms	1778	14,224
Water molecules ($B \leq 60$ Å^2)	159	159
NCS protomer A vs. B RMSD (residues 118 to 220) (Å)*	1.1 (0.56)	0.92 (0.48)
$\langle B \rangle$ for protomer A (Å^2)	13.3	8.1
$\langle B \rangle$ for protomer B (Å^2)	17.7	9.2
RMSD for protomer A (Å)†		0.58 (0.33)
RMSD for protomer B (Å)†		0.81 (0.58)
Mean phase difference (calc vs. exp) (degrees)‡	27.3	26.2
Map correlation coefficient for protomer A (calc vs. exp)§	0.92	0.93
Map correlation coefficient for protomer B (calc vs. exp)§	0.89	0.91

*Root-mean-square difference (RMSD) between corresponding atoms of the two protomers. Residues 109 to 117 were not included because the conformation differs markedly between the two protomers (*18*). Values in parentheses are for backbone atoms (N, C, C_α). †Average RMSD between each member of the multiconformer refinement (*21*) and the mean structure. Values in parentheses are for backbone atoms. ‡$\langle|\phi_{exp} - \phi_{calc}|\rangle$, where ϕ_{exp} is the centroid phase of the experimental phase probability distribution and ϕ_{calc} is the phase of the calculated structure factor F_{calc}. §$\langle\rho_{exp}\rho_{calc}\rangle/\sqrt{\langle\rho^2_{exp}\rangle\langle\rho^2_{calc}\rangle}$, where ρ_{exp} is the experimental electron density, ρ_{calc} is the calculated electron density, and the averages are taken over the volume of the indicated protomer.

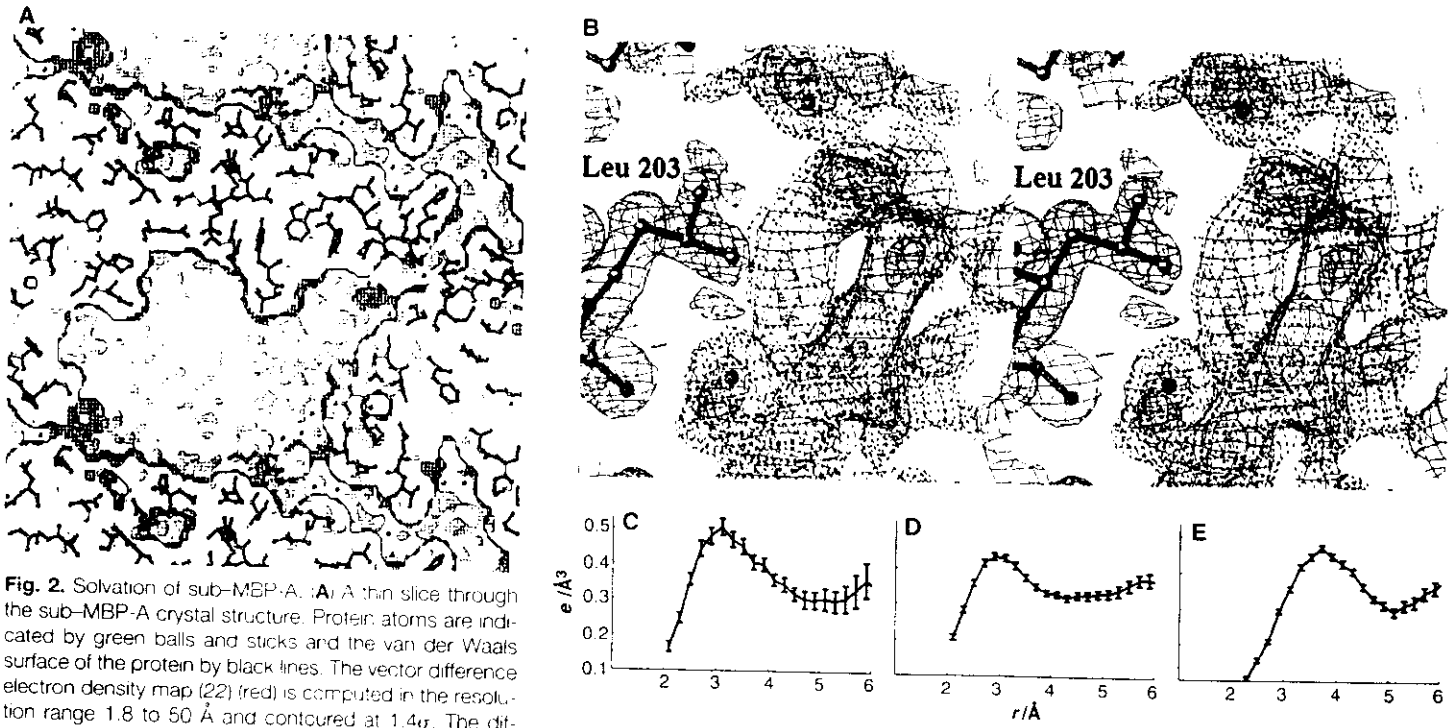

Fig. 2. Solvation of sub–MBP-A. (**A**) A thin slice through the sub–MBP-A crystal structure. Protein atoms are indicated by green balls and sticks and the van der Waals surface of the protein by black lines. The vector difference electron density map (*22*) (red) is computed in the resolution range 1.8 to 50 Å and contoured at 1.4σ. The diffraction data are virtually complete below 10 Å, and thus the observed features cannot be caused by truncation errors. (**B**) Stereo view of the solvent density around Leu^{203} in protomer A. The vector difference electron density map (*22*) is shown at 1.4σ (red), and the experimental electron density map at 1.4σ (magenta) and at 0.7σ (dashed black, with the density around the protein masked out for clarity). All maps are computed in the resolution range 1.8 to 50 Å. The difference map is very similar to the experimental map [the correlation coefficient (Table 6) between the two maps is 0.62 in the solvent regions and 0.02 in the protein regions]. The experimental map is largely independent of the reference wavelength used (the map correlation coefficients in the bulk solvent regions are ~0.9 between the experimental map computed with the reference wavelength λ_1 and those computed with wavelengths λ_2, λ_3, and λ_4). These high correlation coefficients preclude effects of uncorrelated noise in the observed amplitudes, but they do not exclude effects attributable to correlated (wavelength-independent) noise. However, correlated noise would produce erroneous difference electron density throughout the whole unit cell, including the protein, where little difference electron density is observed. (**C** to **E**) Radial distribution functions computed from the experimental map as described previously (*5*) in the resolution range 1.8 to 50 Å around ordered nitrogen (C), oxygen (D), and carbon (E) surface protein atoms; *r* is the distance between the averaged solvent electron density and the particular surface protein atoms. The radial distribution functions were placed on an approximate e/Å^3 scale by scaling the F_{obs} structure factor according to Wilson statistics and by adjusting the *F*(000) term such that the average electron density in the bulk solvent regions is equal to 0.333e/Å^3.

REFERENCES AND NOTES

1. M. Levitt and B. H. Park, *Structure* **1**, 223 (1993); E. Westhof, *Water and Biological Macromolecules* (CRC Press, Boca Raton, FL, 1993); B. T. Nall and K. A. Dill, *Conformations and Forces in Protein Folding* (American Association for the Advancement of Science, Washington, DC, 1991).
2. W. S. Bennett and R. Huber, *Crit. Rev. Biochem.* **15**, 291 (1985); G. E. Schulz, *Curr. Opin. Struct. Biol.* **1**, 883 (1991); M. Gerstein, A. Lesk, C. Chothia, *Biochemistry* **33**, 6739 (1994).
3. B. W. Matthews, *J. Mol. Biol.* **33**, 491 (1968).
4. J. Badger and D. L. D. Caspar, *Proc. Natl. Acad. Sci. U.S.A.* **88**, 622 (1991); J. Badger *et al.*, *Nature Struct. Biol.* **2**, 77 (1995).
5. J.-S. Jiang and A. T. Brünger, *J. Mol. Biol.* **243**, 100 (1994).
6. J. Kuriyan *et al.*, *ibid.* **190**, 227 (1986); T. Ichiye and M. Karplus, *Proteins Struct. Funct. Genet.* **2**, 236 (1987); *Biochemistry* **27**, 3487 (1988); W. Doster *et al.*, *Nature* **337**, 754 (1989); T. D. Romo *et al.*, *Proteins Struct. Funct. Genet.* **22**, 311 (1995).
7. A. Hodel, S.-H. Kim, A. T. Brünger, *Acta Crystallogr.* **A48**, 851 (1992).
8. A. T. Brünger, *Nature* **355**, 472 (1992).
9. F. T. Burling and A. T. Brünger, *Isr. J. Chem.* **34**, 165 (1994).
10. W. A. Hendrickson, *Science* **254**, 51 (1991).
11. W. I. Weis *et al.*, *J. Biol. Chem.* **266**, 20678 (1991).
12. The sub–MBP-A system was chosen for several reasons: (i) Crystals of lanthanide substituted sub–MBP-A diffract well past 1.8 Å resolution (*11*). (ii) As shown by the original structure determination at 2.3 Å resolution with Ho^{3+}-substituted protein (*18*), the experimental phases were expected to be highly accurate because of the large contribution of two well-ordered Yb^{3+} per 115-residue protomer to the total scattering and the large anomalous scattering effects present at the lanthanide L_{III} edge. (iii) The dimer forms the asymmetric unit of the crystal (*11*, *18*), providing two independent views of the protein in the crystal lattice.
13. Preparation of sub-MBP-A cocrystallization with $YbCl_3$, and characterization of heavy-atom binding sites were performed as described (*11*). Data were measured at beamline X4A at the National Synchrotron Light Source (Brookhaven, NY). A single crystal (0.35 mm by 0.1 mm by 0.1 mm) was serially transferred through solutions containing 15% polyethylene glycol 3350, 100 mM tris HCl (pH 8.0), 10 mM NaCl, 2 mM $YbCl_3$, and 0, 5, 7.5, 10, and 15% 2-methyl-2,4-pentanediol as a cryoprotectant. The crystal was flash-cooled and maintained at 110 K during data collection. An x-ray fluorescence scan of the crystal was taken after each fill of the synchrotron beam (total of four fills) and the monochromator was recalibrated to the absorption peak. Diffraction data were measured at four wavelengths chosen to optimize both Bijvoet and dispersive differences: λ_1, the absorption edge, corresponding to a minimum of the real part ($\Delta f'$) of the anomalous scattering factor for Yb^{3+}; λ_2, the absorption peak, corresponding to a maximum of the imaginary part ($\Delta f''$) of the anomalous scattering factor for Yb^{3+}; λ_3, the downward inflection of the L_{III} edge white line, corresponding to a minimum in $\Delta f'$; and λ_4, a high-energy remote wavelength, corresponding to a near maximal value of $\Delta f'$. Complete diffraction data were obtained from a single orientation by offsetting a major axis of the crystal from the spindle (to avoid a blind region) and collecting 65 consecutive 1.5° oscillation images. Each 1.5° sector of reciprocal space was measured at spindle settings ϕ and ϕ + 180°, to collect Bijvoet mates, at one wavelength, and repeated for each wavelength so that eight images from each region were measured successively. Thus, one region of reciprocal space was measured at different wavelengths during the same fill on the synchrotron ring to avoid potential systematic errors due to recalibration of the monochromator. Full imaging plates were scanned on a Fuji BAS2000 scanner. Profile fit, Lorentz polarization–corrected intensities were obtained with the use of DENZO and SCALEPACK [Z. Otwinowski, *Proceedings of the CCP4 Study Weekend. Data Collection and Processing*, Warrington, UK, 29 and 30 January 1993, L. Sawyer, N. Isaacs, S. Bailey, Eds. (SERC Daresbury Laboratory, Warrington, UK, 1993), pp. 56–62]. Bijvoet mates were treated as independent observations for scaling and merging. Diffraction data for the four wavelengths were placed on a quasi-absolute scale, and the four data sets were scaled to one another with the CCP4 programs TRUNCATE and RSTATS [Collaborative Computing Project 4, *The CCP4 Suite: Programs for Protein Crystallography* (SERC Daresbury Laboratory, Warrington, UK, 1994)] for the MADLSQ calculations, and with X-PLOR (*27*) for the probabilistic calculations.
14. J. Karle, *Int. J. Quantum Chem. Symp.* **7**, 356 (1980).
15. Anisotropic scale factors were applied to the unmerged diffraction data to reduce noise in the Bijvoet and dispersive differences. The MADLSQ procedure was applied to the scaled and unmerged diffraction data. Redundantly determined amplitudes and phases were merged after the MADLSQ procedure (*10*).
16. A. Pähler, J. L. Smith, W. A. Hendrickson, *Acta Crystallogr.* **A46**, 537 (1990).
17. In contrast to the least-squares approach (*15*), the diffraction data were both scaled and merged before phasing, with Bijvoet mates treated as independent reflections. The high-energy remote wavelength λ_4 was chosen as the reference wavelength for phasing and for crystallographic refinement because it is the most complete set and has the lowest R_{sym} (Table 1). Observations of both Bijvoet mates at the four wavelengths are assumed to be statistically uncorrelated. The phase probability distribution $P_{\lambda_4}(\phi)$ for a particular reflection at wavelength λ_4 is thus given by a product of phase probability distributions,

$$P_{\lambda_4}(\phi) = P_{\lambda_4 - \lambda_1}(\phi) P_{\lambda_4 - \lambda_2}(\phi) P_{\lambda_4 - \lambda_3}(\phi) \ldots \quad (1)$$

[J. C. Phillips and K. O. Hodgson, *Acta Crystallogr.* **A36**, 856 (1980)]. The phase probability distributions $P_{\lambda_4 - \lambda_1}(\phi)$ are obtained from lack-of-closure expressions,

$$P_{\lambda_4 - \lambda_1}(\phi) = \exp\left[- \frac{(|F_{\lambda_4} e^{i\phi} + F_{-\lambda_1}| - |F_{\lambda_1}|)^2}{2\epsilon\sigma_{\lambda_4}^2 + 2\epsilon\sigma_{\lambda_1}^2 + \epsilon E_r^2} \right] \quad (2)$$

[T. C. Terwilliger and D. Eisenberg, *Acta Crystallogr.* **A43**, 6 (1987)], where F_{λ_4} is the amplitude of the observed structure factor at wavelength λ_4, σ_{λ_4} is the standard deviation of the amplitude at wavelength λ_4, ϵ is a statistical weight, F_{r_1} is the wavelength-dependent component (dispersive and anomalous) to the structure factor of the anomalous scatterer centers at wavelength λ_1, and E_r is related to the error of the anomalous scatterer model. A negative sign in front of the wavelength number (λ_{-1}) indicates the Bijvoet mate of the particular reflection at wavelength λ_1. F_{r_1} can be estimated from the iterative relation

$$F_{r_1} = 2\left\langle \int_\phi P_{\lambda_4 - \lambda_1}(\phi) |F_{\lambda_4} e^{i\phi} + F_{-\lambda_1}| F_{\lambda_1} \right.$$
$$\left. \times P_{\lambda_4}(\phi) d\phi \Big/ \epsilon\sigma_{\lambda_4}^2 + \epsilon\sigma_{\lambda_1}^2 \right\rangle \quad (3)$$

where $P_{\lambda_4 - \lambda_1}(\phi)$ is given by Eq. 2 and the angular brackets denote an averaging over reflections in equal-volume resolution bins. The sharpness of the phase probability distribution $P_{\lambda_4 - \lambda_1}(\phi)$ is related to the magnitude of the F_{r_1} vector; that is, the lack-of-closure expression depends simultaneously on both dispersive and anomalous differences, making the phase probability distributions less dependent on the choice of the reference wavelength than those obtained from a standard MIR approach [V. Ramakrishnan, J. T. Finch, V. Graziano, P. L. Lee, R. M. Sweet, *Nature* **362**, 219 (1993)]. Furthermore, the large anomalous signals present in the data (Table 2) result in a breakdown of the approximation in standard MIR treatments, so that the mean of the structure factor amplitudes of a Bijvoet pair does not equal the amplitude for the nonanomalous ("native") structure factor [$F_{native} \neq (|F^+| + |F^-|)/2$]. Use of separate lack-of-closure expressions for each Bijvoet mate between a reference wavelength and the others avoids this approximation. Detailed comparisons of the various methods will be presented elsewhere (A. T. Brünger, K. M. Flaherty, F. T. Burling, W. I. Weis, in preparation). Parameters of a model of the anomalous scatterer centers (positions, thermal factors, occupancies, and real and imaginary anomalous scattering factors of F_{r_1}) were refined by conjugate-gradient minimization against a maximum likelihood function,

$$R_{ML} = \sum_r 1/N \int_\phi P_{\lambda_4}(\phi)(|F_{\lambda_4} e^{i\phi}$$
$$- F_{r_1} - F_{r_2}| - |F_{\lambda_1}|)^2 d\phi \quad (4)$$

[G. Bricogne, *Acta Crystallogr.* **A40**, 410 (1984); Z. Otwinowski, *Proceedings of the CCP4 Study Weekend*, Warrington, UK, 25 and 26 January 1991, W. Wolf, P. R. Evans, A. G. W. Leslie, Eds. (SERC Daresbury Laboratory, Warrington, UK, 1991, pp. 80–85]. This method is similar to the generation of phase probability distributions from the MADLSQ-derived wavelength-independent structure factors by the MADABCD procedure (*16*), in that Bijvoet and dispersive differences contribute to a lack-of-closure expression for each measured data point. It differs in two respects: (i) Phase probability distributions are obtained for structure factors at a reference wavelength, instead of the wavelength-independent structure factors derived from MADLSQ. (ii) The parameters of the anomalous scatterer model are refined in an iterative fashion with the maximum likelihood function R_{ML}, which makes the refinement more robust and the figures of merit more realistic. The experimental electron density map was computed with figure-of-merit weighted amplitudes at the reference wavelength λ_4 and centroid phases obtained from $P_{\lambda_4}(\phi)$ (Eq. 1). Centroid phases of $P_{\lambda_4}(\phi)$ were also used for phase difference calculations.
18. W. I. Weis, R. Kahn, R. Fourme, K. Drickamer, W. A. Hendrickson, *Science* **254**, 1608 (1991).
19. The previously determined Ho^{3+}-substituted sub-MBP-A structure refined at 2.3 Å resolution (*18*) served as an initial model for rigid-body refinement with X-PLOR (*27*). The program O [T. A. Jones, J. Y. Zou, S. W. Cowan, M. Kjeldgaard, *Acta Crystallogr.* **A47**, 110 (1991)] was used to make relatively minor corrections. One hundred fifty-nine ordered water positions were identified by selecting well-separated and approximately spherical peaks at 1.5σ above the average density of the experimental map with the protein masked out and within hydrogen-bonding distance to polar or charged atoms. Refinement made use of resolution-dependent weighting $1/[1 - B_w(1/2d) - 1.6]^2$ similar to that used in PROLSQ [W. A. Hendrickson, *Methods Enzymol.* **11**, 252 (1985)], where d denotes the Bragg spacing, and B_w = 5.4 was obtained by linear fit to the structure factor amplitudes versus d (W. I. Weis, unpublished data). This weighting scheme allows inclusion of low-angle reflections, which contain most of the information about solvent but which would otherwise dominate the refinement of the protein model. Overall B factor refinement, overall anisotropic B factor refinement, conjugate-gradient positional refinement, and a slow-cooling simulated annealing cycle [A. T. Brünger, A. Krukowski, J. Erickson, *Acta Crystallogr.* **A46**, 585 (1990)] were performed. The Yb^{3+} were held fixed during simulated annealing (to avoid excessive movements resulting from the large mass), which was followed by conjugate-gradient positional refinement, individual restrained B factor refinement, and refinement of the real ($\Delta f'$) and imaginary ($\Delta f''$) parts of the anomalous scattering factor of the Yb^{3+} chemical type. Geometric restraints used parameters previously described [R. A. Engh and R. Huber, *Acta Crystallogr.* **A47**, 392 (1991)]. The free R value was monitored with a test set containing a random selection of 6% of the diffraction data (the test set is defined such that both Friedel mates of a given reflection are included in the set). Noncrystallographic symmetry constraints or restraints were not imposed at any point in the refinement. The Cys^{317} sulfhydryl group was refined with two alternative conformations (Fig. 1B). A

refinements were performed with X-PLOR (27).
20. W. I. Weis, K. Drickamer, W. A. Hendrickson, *Nature* **360**, 127 (1992); W. I. Weis and K. Drickamer, *Structure* **2**, 1227 (1994).
21. Multiple conformers [J. Kuriyan *et al.*, *Proteins* **10**, 340 (1991)] (9) of the sub–MBP-A protein molecules were generated starting with the model that was obtained after single-conformer refinement (19). The water molecules and Yb^{3+} were restrained to their initial positions. Conformers of the protein were rendered invisible to each other in terms of chemical interactions. Each conformer in the ensemble contributed equally to the calculated structure factor with the occupancy set to the reciprocal of the number of conformers. Evaluation of the free *R* value as a function of the number of conformers produced a shallow minimum for eight conformers, which were used for subsequent analysis.
22. Vector difference electron density maps were computed by taking the vector difference between complex structure factors [$F_{c,i} \exp(i\phi_{c,i}) - F_{c,ref} \exp(i\phi_{c,ref})$], the experimental structure factor with centroid phases obtained from P_1 (*6*) (*17*) minus that computed from the refined single-conformer model. A conventional (model-phased) difference electron density map consisting of a Fourier synthesis of ($|F_{o,i}| - |F_{c,ref}|$) $\exp(i\phi_{c,ref})$ is an approximation of the vector difference map [J. Drenth, *Principles of Protein X-ray Crystallography* (Springer-Verlag, New York, 1994), pp. 150–152]. As a consequence, vector difference maps of sub–MBP-A were observed to have less noise than conventional difference maps.
23. M. M. Teeter, *Proc. Natl. Acad. Sci. U.S.A.* **81**, 6014 (1984).
24. G. M. Clore *et al.*, *Structure* **2**, 89 (1994).
25. M. Levitt and R. Sharon, *Proc. Natl. Acad. Sci. U.S.A.* **85**, 7557 (1988); Y. Komeiji *et al.*, *Proteins* **16**, 268 (1993); M. Karplus and G. A. Petsko, *Nature* **347**, 631 (1990); P. J. Steinbach and B. R. Brooks, *Proc. Natl. Acad. Sci. U.S.A.* **90**, 9135 (1993); V. Lounnas *et al.*, *Biophys. J.* **66**, 601 (1994).
26. D. C. Rees and M. Lewis, *Acta Crystallogr.* **A39**, 94 (1983); E. Arnold and M. G. Rossmann, *ibid.* **A44**, 270 (1988); L. M. Rice and A. T. Brunger, *Proteins Struct. Funct. Genet.* **19**, 277 (1994).
27. A. T. Brunger, *X-PLOR, Version 3.1: A System for X-ray Crystallography and NMR* (Yale Univ. Press, New Haven, CT, 1992); developmental version of X-PLOR, available on request.
28. D. T. Cromer, *J. Appl. Crystallogr.* **16**, 437 (1983); ——— and D. L. Liberman, *J. Chem. Phys.* **53**, 1891 (1970).
29. W. A. Hendrickson and W. I. Weis, unpublished data.
30. L. M. Gregoret, S. D. Rader, R. J. Fletterick, F. E. Cohen, *Proteins Struct. Funct. Genet.* **9**, 99 (1991).
31. We thank P. Gros for assistance in designing the X-PLOR crystallographic language for phasing; V. Agniwal, S. Shah, and M. Willis for help with data collection; C. Ogata for beamline support; and P. Adams, M. Gerstein, M. Levitt, and L. Rice for critical reading of the manuscript. The coordinates and the diffraction data have been deposited with the Brookhaven Data Bank (accession number 1YTT). Supported by the Howard Hughes Medical Institute (A.T.B.), NSF (DIR9021975, A.T.B.), and NIH (GM50565, W.I.W.). W.I.W. is a Pew Scholar in the Biomedical Sciences.

8 September 1995; accepted 1 November 1995

Temporal Processing Deficits of Language-Learning Impaired Children Ameliorated by Training

Michael M. Merzenich,* William M. Jenkins, Paul Johnston, Christoph Schreiner, Steven L. Miller, Paula Tallal

Children with language-based learning impairments (LLIs) have major deficits in their recognition of some rapidly successive phonetic elements and nonspeech sound stimuli. In the current study, LLI children were engaged in adaptive training exercises mounted as computer "games" designed to drive improvements in their "temporal processing" skills. With 8 to 16 hours of training during a 20-day period, LLI children improved markedly in their abilities to recognize brief and fast sequences of nonspeech and speech stimuli.

Experiments conducted in human (*1*) and monkey (*2*) neurological models of perceptual learning have demonstrated that the capacity for segmentation of successive events in sensory input streams can be sharpened, apparently throughout life, by practice. Electrophysiological studies of learning-induced plasticity conducted in the neocortices of monkeys have provided a growing body of evidence about the neural processes that underlie practice-based improvements in both temporal segmentation and spectral (spatial) discrimination performances (*3*–*5*). These studies have shown that the ability of an adult animal to make fine distinctions about the temporal or spectral features of complex inputs can be sharply improved, or degraded, by a period of intensive behavioral training (*2*–*4*, *6*).

In parallel with animal and human models of temporal sequence learning, earlier studies of the receptive deficits of LLI children (*7*) had shown that they have a "temporal processing deficit" expressed by limited abilities at identifying some brief phonetic elements presented in specific speech contexts and by poor performances at identifying or sequencing short-duration acoustic stimuli presented in rapid succession (*8*). Consistent with a temporal processing deficit hypothesis, LLI children can distinguish these brief speech features and can correctly reconstruct stimulus input sequences if stimuli are presented in slower forms or at slower event rates (*8*).

Taken together, these experimental findings led us to hypothesize that the deficits underlying the phonetic reception limitations of a LLI child might arise in early life as a consequence of abnormal perceptual learning that then contributes to abnormal language learning (*3*, *4*). For example, a child might simply make more-limited-than-normal use of temporal information as he or she learns to make distinctions about speech inputs as a learning alternative, or a child might generate a representation of phonetic information under early childhood conditions (for example, in the presence of middle ear disease) under which acoustic inputs are consistently muffled. Cortical plasticity studies indicate that temporal processing deficits like those that emerge in LLI children would be expected from these learning scenarios, if they were to be undertaken in a training regime applied in a monkey model (*3*, *4*).

Visual psychophysical studies have already shown that very great improvements in the recognition of brief, successively presented stimuli can be achieved with practice in adult humans (*1*). In this study, we asked: Can we substantially alter the deficient temporal processing capacities of young, school-age LLI children by similar acoustic practice?

For training tools, we produced two audiovisual (AV) "games" designed around a circus theme to engage 5- to 10-year-old children at high levels of attention and enthusiasm within highly repetitive learning tasks. The first AV game (Circus Sequence) was a perceptual identification task in which a correct response in the exercise was a faithful reproduction of the order of two-stimuli sound sequences by touch-screen button-press sequences (*9*). The nonverbal stimuli applied in training were 16 octave-per-second upward- or downward-gliding (U and D, respectively) frequency-modulated (FM) tonal pairs (U-U, U-D, D-U, or D-D). Stimuli in each FM pair swept across the same frequency range. These stimuli were in the range of sweep frequencies and speeds that apply for the formant transitions of English consonants that LLI children have difficulty recognizing (*7*, *8*). The interstimulus intervals (ISIs) and FM frequencies were adaptive parameters.

The second game was a phonetic element recognition exercise implemented as a two-alternative forced-choice task in which the child was presented two consonant-

M. M. Merzenich, W. M. Jenkins, P. Johnston, C. Schreiner, W. M. Keck Center for Integrative Neurosciences and Coleman Laboratory, University of California, San Francisco, CA 94143–0732, USA.
S. L. Miller and P. Tallal, Center for Molecular and Behavioral Neuroscience, Rutgers University, 197 University Avenue, Newark, NJ 07102, USA.
* To whom correspondence should be addressed.

CATALYSIS IN ENZYME CRYSTALS

J. HAJDU, K. R. ACHARYA, D. I. STUART, D. BARFORD AND L. N. JOHNSON

New developments in X-ray crystallography may produce three-dimensional movies of catalysis and structural changes.

Twenty years ago studies on lysozyme[1] (the first enzyme structure to be solved) and its inhibitor complexes led immediately to a proposal for the catalytic mechanism of the enzyme. Today more than 50 different enzyme structures are known. Crystallographic studies, however, have been confined either to unliganded enzymes or to stable enzyme–ligand complexes. Direct observation of conversion of substrate to product (or other transient events) in the crystal has, until recently, remained an unfulfilled dream, largely because data collection times with conventional X-ray techniques are long (days to months) while molecular events relevant to biological processes happen on the picosecond to kilosecond time scale. This problem may be circumvented to some degree by working at very low temperatures in order to freeze out intermediates and match the timescale of the experiment with the timescale of the data collection[2–4]. However, suitable cryoprotectants are not always available and cooling may change the mechanism of the reaction, limiting the application of this approach. The recent development of new techniques at synchrotron radiation sources, particularly the white beam Laue method, allows a dramatic reduction in the time needed for data collection. Transient phenomena (e.g. structural changes, catalysis or phase transitions) down to the millisecond time scale and below may now be investigated by X-ray crystallography in certain cases.

An enzyme crystal is a highly ordered three-dimensional arrangement of protein molecules with a number of well defined and stable contacts. The lattice contacts are similar to, but less extensive than, contacts between subunits in oligomeric proteins and may have a similar effect on protein function in the crystal as subunit–subunit contacts have on oligomeric proteins in solution. The lattice allows for some flexibility and protein molecules may undergo limited conformational changes. Protein crystals contain 20–80% water representing a somewhat more dense environment than the cytosol (70–80% w/w water). Many enzymes retain their activity in the crystal[5]. A three-dimensional network of channels (Fig. 1) provides access for diffusing substrates. The restriction imposed by the lattice on the motion of the protein (or of the substrate in the crystal) may result in reduction or even absence of activity in some cases. A few enzymes are believed to be more active in the crystal than in solution (e.g. papain[5]).

In an X-ray experiment, the resulting image is both a spatial average of all the molecules in the crystal volume irradiated, and a time average of the structures existing during the period of data collection. Consider an

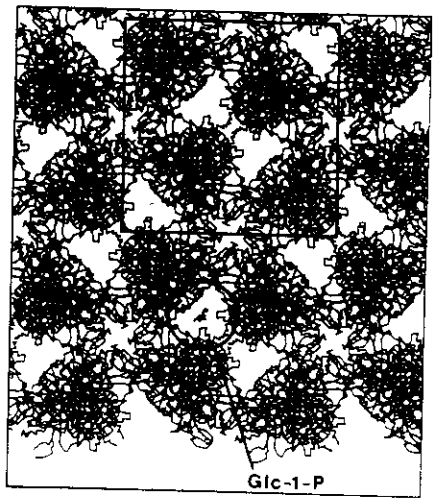

FIGURE 1

The crystal lattice of tetragonal phosphorylase b crystals viewed down the c axis. The protein is shown as an α-carbon trace. A unit cell is marked in the centre of the figure. Glucose 1-phosphate (Glc-1-P), a substrate of the enzyme, is drawn in one of the solvent filled channels which run the whole length of the crystal. *Adapted from a drawing by P. J. McLaughlin.*

enzyme which catalyses a three-step reaction in the crystal. For the sake of simplicity, it is assumed that the reaction is irreversible and that all components bind with the same binding constant to the enzyme in the crystal. The distribution of the various components in the crystal as a function of time is shown in Fig. 2. The ratio of the rate constants k_1, k_2 and k_3 determines the shape of the curves whereas the absolute value of these constants determines the time scale of the reaction. If, as in Fig. 2b, reaction 2 is much slower than the others, then the intermediate produced in the preceding step (compound B) will accumulate transiently and dominate the crystal for some time. With fast data collection, it may be possible to dissect this reaction and obtain a set of structures representing various stages along the reaction coordinate. In favourable cases (e.g. points marked with cross-hatching in Fig. 2) a single dominant structure may emerge. In other regions mixtures of structural states will be observed and it will be necessary to develop techniques that allow deconvolution of the average structure into its components. In certain cases it may be possible to achieve favourable volume averaging by inducing a transient population inversion in the crystal so that almost all molecules adopt the same structural state. Magnetic reorientation (depending on the symmetry of the crystal), lasing, optical pumping, pH jump, temperature jump and photodissociation are some of the possibilities. With enzymatic reactions, varying the temperature is often the easiest way of creating a population inversion since the steps governing the formation and breakdown of intermediates have different activation energies and enthalpies.

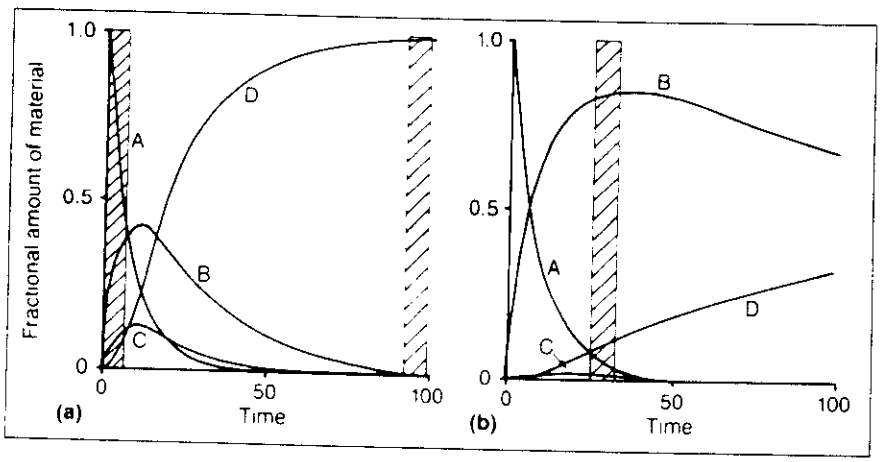

FIGURE 2

Transient accumulation of intermediates in a set of three consecutive reactions:

$$\mathbf{A} \xrightarrow{k_1} \mathbf{B} \xrightarrow{k_2} \mathbf{C} \xrightarrow{k_3} \mathbf{D}$$

(**a**) when $k_1 = k_2 = k_3$, and (***b***) when $k_2 < k_1 = k_3$ (specifically, $k_1 = k_3 = 20\,k_2$)

Hatched areas show times when volume averaging is more or less favourable in the crystal (see text).

THE SYNCHROTRON RADIATION SOURCE

Particle accelerators were originally built for high-energy research into the sub-atomic structure of matter. Around 1970 it was recognized that the electromagnetic radiation produced during the acceleration of charged particles (the so called synchrotron radiation) could be used for biological and material science research. In a given accelerating field, the effect is greater with particles of low mass/charge ratio. The first dedicated synchrotron radiation source (the SRS at Daresbury, UK, 1981) uses electrons. The radiation is confined to a narrow cone around the instantaneous direction of the flight (it is tangential to the curved electron orbit). At the SRS the main storage

ring (96 m in circumference) accelerates electrons to 2 GeV energy with a circulating electron current of several hundred milliamperes. Electrons are held in a closed orbit by 16 bending magnets providing an intense and continuous radiation from X rays to radio frequencies. Below about 1 Å wavelength, radiation emission from the main bending magnets falls rapidly. It is possible to introduce much tighter bending on short sections of high field. These more complicated particle orbits are produced by special magnets known as wigglers[6] and undulators[7]. The result is an altered spectral profile shifted into the region of interest for crystallography (0.2–2.5 Å). The radiation is intense, pulsed, well collimated, polarized and tuneable over a wide energy range. It has had a significant impact on research in protein crystallography (see for example, Ref. 8). The advent of high-intensity synchrotron radiation sources had made the real time study of structural changes possible[9]. Larly results include the kinetic study of muscle[10,11], of microtubule polymerization[12] and real time studies of phase transitions in phosphatidylethanolamine[13]. Application of time resolved studies to three-dimensional structures is now underway. Data may be recorded in two different ways: one method uses a single wavelength (monochromatic techniques) and the other a much broader spectral range (Laue or white X-radiation techniques).

Monochromatic data collection

Monochromatic data collection is the most widely used method in protein crystallography (Fig. 3a). With monochromatic X-rays, only a small proportion of the lattice planes diffract at any particular orientation of the crystal and the crystal has to be rocked through a small angle (1–2 degrees) in order to record the full reflections (Fig. 4a). To bring other planes into the diffracting position, the crystal has to be rotated to a new setting and the procedure repeated with a new film. A full data set to a given resolution is one containing reflections from all possible arrangements of the lattice planes with interplanar spacing greater than or equal to the 'resolution' of the data set. In the case of glycogen phosphorylase b, for example, every structure shown in

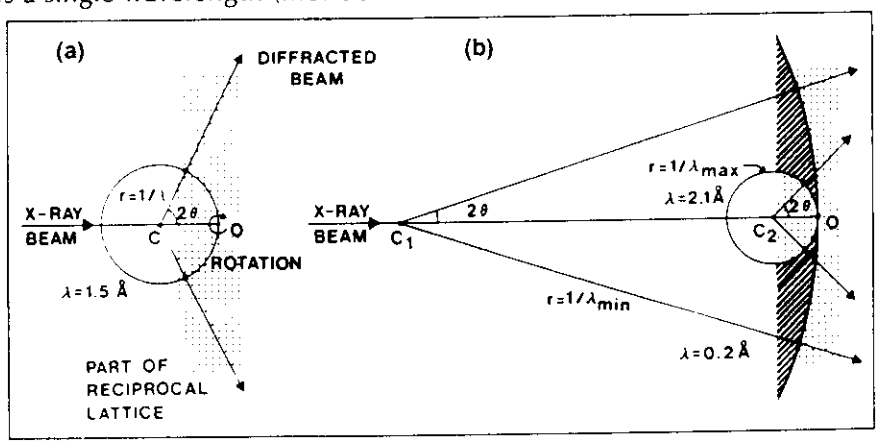

Figure 3

Diffraction geometry for monochromatic and Laue methods. The diagram shows the Ewald construction, a simple geometric construction which encompasses Bragg's law and which is a useful aid in the description of diffraction (see Ref. 31). A sphere is drawn with centre C and a radius equivalent to the reciprocal of the wavelength. The reciprocal lattice is placed with origin O at the point where the straight through the beam cuts the sphere. Diffraction occurs whenever a reciprocal lattice point cuts the sphere. (a) **Monochromatic method:** With a single wavelength (e.g. 1.5 Å) only a few reciprocal lattice points cut the sphere and there are only a few diffracted rays recorded on the film. The reciprocal lattice must be rotated (achieved by rotating the crystal) in order to bring other spots into the diffracting position. (b) **Laue method:** The reciprocal lattice is illuminated with a spectrum of X rays with wavelengths varying from 0.2 Å to 2.1 Å. All reciprocal lattice points between these limits (shaded region in the diagram) will lie on an appropriate sphere and will diffract. The unit cell size in the figure corresponds to 12.5 Å. Typical unit cell sizes are 100 Å in a protein crystal. The reciprocal lattice points are very much closer together and consequently a very much larger number of reflections will be recorded than can be illustrated in the figure.

Fig. 5 required 32 exposures, each with 1.5 degree oscillation (Fig. 4a) to produce a data set to 2.7 Å resolution. The use of a high-intensity synchrotron source sped up data collection from one week on our standard laboratory equipment to 25 minutes for our fastest monochromatic data set at the SRS. This meant an overall data rate of 50 reflections/second, due solely to the high intensity of the X-ray beam.

Case study: catalysis in crystals of glycogen phosphorylase b

Phosphorylase is active in the crystal[14–15]. Activity is not confined to the surface molecules but is a property of the whole crystal. Using a sequence of monochromatic data sets to record the diffraction images, we have been able to monitor the interconversion of substrates into products in the crystal[15–16].

In muscle, phosphorylase (EC 2.4.1.1) catalyses the phosphorylytic breakdown of glycogen to produce glucose 1-phosphate (for a recent

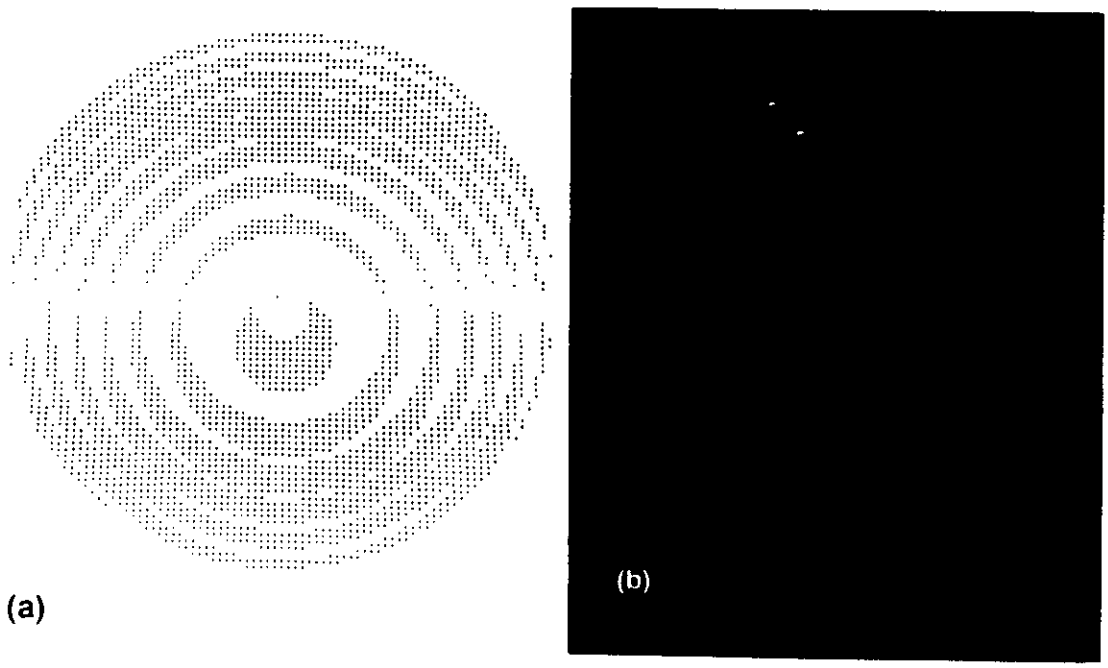

FIGURE 4

Computer generated images of (a) monochromatic and (b) Laue diffraction patterns. (**a**) Simulated oscillation photograph using monochromatic X rays (wavelength: 0.88 Å, crystal to film distance: 174 mm, oscillation range: 0–1.5 degree) of a phosphorylase b crystal ($P4_32_12$, a=b=128.8 Å, c=116.2 Å) for one of the 32 oscillation photographs used to calculate the map shown in Fig. 6. (**b**) Computer-generated Laue diffraction pattern of phosphorylase with the crystal rotated to 22.5 degrees from the position with a* anti-parallel to the beam and c* coinciding with the spindle of an oscillation camera. (a* and c* = reciprocal cell axes.) Crystal to film distance=133.8 mm. Film radius=59 mm. Effective wavelength range contributing to reflections: 0.2–2.1 Å. Each spot on the photograph has been given a colour code to indicate the wavelength of the contributing X-ray beam (blue:0.2 Å; red:2.1 Å). With overlapping reflections, the colour corresponding to the longest component is shown. *(Programmes by Dr I. J. Clifton, SERC Daresbury Laboratory.)*

review see Ref. 17). The enzyme is also capable of slowly transforming the glycosylic substrate analogue, heptenitol (2,6-anhydro-1-deoxy-D-gluco hept-1-enitol) into heptulose 2-phosphate (Fig. 6) (Ref. 18–20). What makes these reactions so promising for time resolved analysis is the fact that the rate-limiting step is the interconversion of the respective ternary enzyme–substrate complexes to products. This means that the active enzyme–substrate complex will transiently accumulate in the crystal similarly to compound B of Fig. 2b. Hence, providing that data collection is fast compared to the half-life of the complex, it may be possible to observe the ternary enzyme–substrate complex before it is converted into products. During the reaction, some active sites will be occupied by substrates, and some will be occupied by products. The relative amount of these species will vary with time.

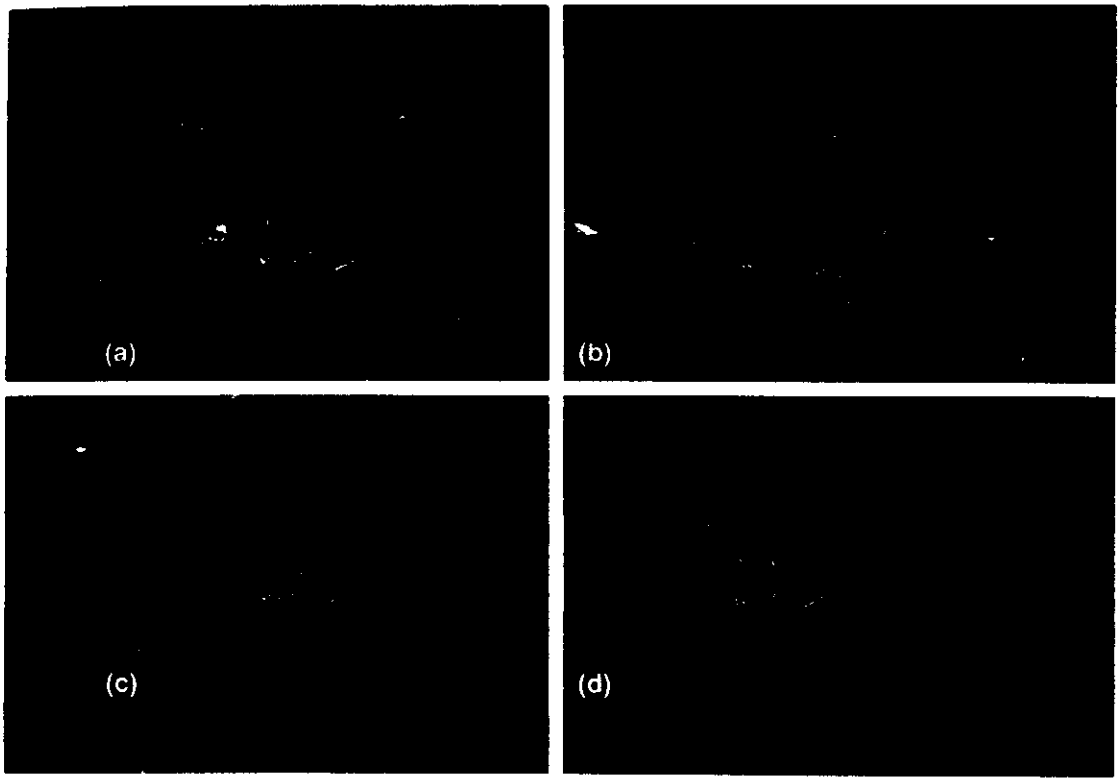

FIGURE 5

Four snapshots of the heptenitol + P_i to heptulose 2-phosphate reaction in crystals of glycogen phosphorylase b: the active site and its vicinity is shown. A single contour level is displayed at a third of the maximal peak height. Residues are shown as they appear in the unliganded native enzyme. Water molecules in the native structure are represented as crosses. A new crystal was used for each data set. (**a**) 100 mM heptenitol (no reaction). (**b**) 100 mM heptenitol + 50 mM phosphate. 10 min soak followed by rapid data collection (60 min) at 13°C. (**c**) 100 mM heptenitol + 50 mM P_i + 50 mM maltoheptaose, 15 min soak followed by rapid data collection (45 min) at 20°C. (**d**) 50 h soak in 100 mM heptenitol + 50 mM P_i + 50 mM maltoheptaose followed by 2.5 h of data collection. All solutions contained 2.5 mM AMP, 10 mM *N,N*-bis(2-hydroxyethyl)-2-aminoethane sulfonic acid and 10 mM magnesium acetate. The pH was set to 6.7 (20°C).

In the phosphorylase b experiments the crystal was mounted in a flow cell[21,22] and the reaction was initiated by flowing substrate over the crystal. Diffusion and saturation binding was over in about 10 min. Data collection took place either immediately after this or after various resting times to allow the reaction to proceed. Fig. 5 shows snapshots of the

$$\text{heptenitol} + P_i \rightarrow \text{heptulose 2-phosphate}$$

reaction depicting the formation and transformation of the enzyme–substrate complex into the product, heptulose 2-phosphate (Fig. 5d).

An obvious drawback to the time resolved studies with monochromatic X-rays is that a new crystal is required for each experiment and that the current time resolution is relatively coarse (~ 0.5–1 h). All of the crystal is needed for each data set and radiation damage renders the exposed crystal useless for further work.

THE LAUE METHOD

This method was used by Friedrich, Knipping and von Laue to record the first X-ray diffraction from a crystal of copper sulphate in 1912 (Fig. 3a). The method, which utilizes the complete white spectrum of the radiation, fell into disuse because conventional X-ray sources did not give a satisfactory spectrum and because of difficulties in unravelling the complicated diffraction patterns. Synchrotron sources, modern computers and developments in computing software have resolved these problems. With the Laue method (see for example, Refs 23 and 24) it is possible to record almost all of the data much more quickly from only a few orientations of the crystal. The crystal may then be translated so that a fresh portion is irradiated. As many as 20 Laue photographs may be recorded from a phosphorylase crystal 3 mm long.

The broad effective spectrum (0.2–2.5 Å) and the high intensity of the white X-radiation generated on the SRS wiggler magnet[6] allows the recording of Laue diffraction photographs on the millisecond time scale. Using polychromatic X rays and a stationary crystal, a large number of lattice planes diffract simultaneously as the Bragg condition is satisfied for each of these planes by at least one wavelength of the spectrum (Fig. 3b). The diffracting position of the lattice planes is determined by their orientation, spacing and the wavelength range applied; the wider the range the greater the number of planes in diffracting position. Thus, many reflections can be recorded in a short time with a single exposure. With crystals of high symmetry, a high

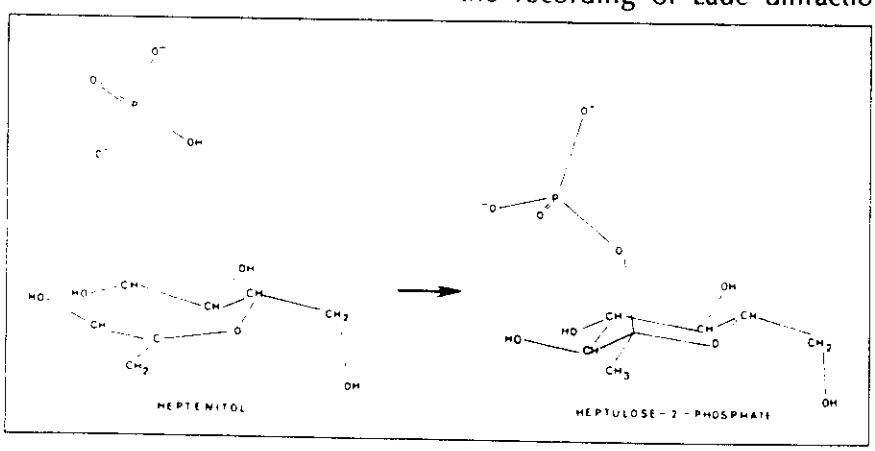

FIGURE 6

The phosphorylase catalysed heptenitol → heptulose 2-phosphate reaction

proportion of the unique data set may be recorded on a single photograph. With crystals of lower symmetry, a few more photographs with different crystal orientations may be required. Using the high intensity white X-radiation of synchrotron sources to record Laue photographs, data rates well in excess of 100000 reflections per second can be achieved. This is due to the high intensity of the source and the large number of reciprocal lattice points that occupy diffracting positions simultaneously.

There are two ways of extracting information from Laue photographs of protein crystals. The difference methods are designed to analyse structural changes relative to a known starting structure[24] whereas wavelength normalization techniques are being developed to extract structural information without the knowledge of a starting 'native' structure[25–27]. With proteins, the difference method was the first to produce interpretable electron-density maps on the binding of a ligand to the enzyme phosphorylase b (Ref. 24). With this method, a sequence of (nearly) identical Laue data sets are taken before, during and after the initiation of the reaction. Data sets in the sequence are scaled to the starting (native) Laue data set to compensate for factors such as variations in exposure times, beam decay and radiation damage. The advantages of this method are that wavelength and position-dependent corrections to the intensities are not needed.

Case study: binding of oligosaccharides to phosphorylase b

Previous experiments with monochromatic radiation had established the binding site for the oligosaccharide, maltoheptaose (mol.wt 1152), at the surface glycogen storage site of phosphorylase b (Ref. 17). Comparative studies with the Laue method were undertaken in order to test the feasibility of the technique. In the Laue experiments[24], data sets of three exposures (1 s each) were taken from the same crystal at different angular settings before, during and after the addition of ligand. The intermediate data set indicated a transient disorder in the crystal and the data could not be processed. Efforts are under way to develop methods which will enable structural information to be revealed from such photos. The comparison of the two data sets for the native and the liganded enzyme resulted in a data set that contained approximately 58% of the total number of unique reflections to 2.4 Å resolution. When restricted to the highest quality measurements (i.e. intensities greater than three standard deviations, and greater than a quarter of the mean intensity) the total number of reflections was 9029, representing 25% of the complete data set to 2.4 Å resolution. The resulting difference Fourier synthesis clearly showed the oligosaccharide-binding site on the enzyme and compared favourably with the corresponding difference Fourier synthesis calculated with the equivalent measurements from the monochromatic data set.

With the wavelength normalization technique, it is possible to extract structural information for Laue data without the knowledge of a starting native structure. The success of this approach depends on a satisfactory

treatment of wavelength-dependent effects such as incident intensity, absorption, Lorentz and polarization factors, obliquity and detector response. The determination of the so called 'wavelength normalization curve' to compensate for these effects is a crucial step in the extraction of independent structural information from Laue photographs. The first successful use of the wavelength normalization technique was in the determination of a small molecule structure by Wood *et al.* in 1982[27]. Lately the method has been used to determine the unknown structure of a small organometallic compound[28] where only microcrystals were available. With proteins, the first successful use of this technique was the localization of heavy atom sites in a crystal of xylose isomerase[26].

The detailed structural information available in the protein Laue maps calculated to date is limited by the use of only partial data. Theoretical calculations show that with a slightly different recording geometry a much greater proportion of the unique data can be recorded than with the present normal beam geometry. In principle therefore it should be possible to obtain as detailed structural information with the Laue method as with the more conventional monochromatic method. These developments are in hand.

DIFFUSION AND BINDING LIMITATIONS

With the very swift data collection times it is important to ensure that neither diffusion of ligands into the crystals nor binding of the ligand to the enzyme form the rate-limiting steps in the reaction. Diffusion times will depend on the size of the ligand and its free diffusion coefficient, the pore size in the crystal, the dimensions of the crystal, and temperature. For most protein crystals, diffusion times are in the range of seconds and minutes. Thus in many instances it will be necessary to pre-diffuse the ligand into the crystal under inactive conditions and to initiate the reaction by (say) pH jump, pressure jump, photodissociation or photo activation. The latter method appears to have considerable promise. The substrate (or enzyme) is blocked with a photoactive group that can be released rapidly to initiate the reaction. Crystallographic experiments with phosphorylase b have been performed using 'caged' phosphate compounds similar to those that have been developed in the study of ATP utilization in muscle contraction[29]. A problem arises with saturating concentrations of caged substrates. The photo-label when released (a nitroso ketone in this case) reacts with the protein, extensively modifying the nucleophilic side chains of the enzyme. This, in our experiment, may have lead to an inhibition of the enzyme. An alternative route that may alleviate this problem would be to cage the enzyme. Glycogen phosphorylase contains the essential cofactor, pyridoxal phosphate, which plays an obligatory role in catalysis through its phosphate group. Caged pyridoxal phosphate has been synthesized and kinetic, reconstruction and crystallization studies are under way. Many other approaches have been taken to photolabel enzymes including the synthesis of photolabile inhibitors for thrombin and other serine proteinases[30].

TOWARDS A PICOSECOND TIME RESOLUTION

The pulsed nature of the synchrotron radiation offers the possibility for stroboscopic experiments with time resolution in the picosecond range. In the Daresbury storage ring, the circulating electron bunches (160 of them) produce a short (120 ps) and intense burst of X rays whenever they pass by the window of the experimental station. Each pulse is followed by a pause of 2 ns. The length of the pause can be altered to some extent: In the so called 'single bunch' mode, there is only one electron bunch (120 ps) circulating in the whole storage ring with a pulse separation of about 320 ns. Other storage rings have different time structures (see, for example, Ref. 9). Let us consider a photoexcitable crystal which returns to the ground state before the next X-ray pulse arrives at the crystal. If we use a high intensity pulsed light source (a laser or the storage ring itself) to excite the sample crystal with the same frequency but with a fixed phase shift relative to the phase and frequency of the X rays of the storage ring, then we have everything in our hands to perform a stroboscopic experiment and to record a structure which has a lifetime in the time range set by the length, phase and frequency of the light and X-ray pulses. First, the exciter light pulse hits the crystal followed by the analyser X-ray pulse. Every X-ray photon arriving at the crystal and, consequently, at the detector will then report on a structure whose age is determined by the phase shift between the exciter light and the analyser X-ray pulses. A single X-ray pulse is usually not sufficient to produce a strong enough diffraction image at the detector (film) but the process can be repeated as many times as necessary to build up a diffraction picture (seconds, minutes). This picture will contain information on a structure that is only a few hundred picoseconds old. To record another picture at another time after excitation, the phase shift has to be changed and the whole procedure repeated. A system of mechanical beam choppers may extend the time range for crystals with longer relaxation times.

In a stroboscopic experiment at the SRS a crystal will have to survive 500 million excitations during a one second long exposure. With high-energy accelerators used in today's physics and available for tomorrow's synchrotron radiation experiments it may be possible to record a complete Laue pattern with a single X-ray pulse from a single electron bunch. This, in fact, would mean an overall exposure time of 10–100 ps and could lead to a new era in structural chemistry.

CONCLUSIONS

With existing technology a variety of methods is available for the three-dimensional study of transient structures: (1) Collection of a sequence of complete monochromatic data sets if the lifetime of the intermediate is longer than about 30 min. (2) Collection of a sequence of Laue photographs if the lifetime of the intermediate is longer than about 3 s. (3) Collection of streaked Laue photographs if the lifetime is of the order of 0.1 s. (The film is translated so that each diffraction spot is drawn into a streak in which the intensity at a particular position corresponds

to a particular time interval. This saves the time needed to change the film.) (4) Stroboscopic experiments utilizing the pulsed nature of the synchrotron radiation for intermediates with lifetimes of a few hundred picoseconds (the distance light travels in a picosecond is 0.3 mm).

Fast data collection methods have only recently become accessible to the crystallographer. Developments in milliseconds and sub-millisecond data collection methods are of vital importance, offering a route to the dissection and detailed understanding of molecular events associated with catalysis, ligand binding and structural transitions in crystals. Equally important developments are needed at the software side to enable mixtures of structural states to be analysed and in the biochemistry and chemistry for the design of suitable substrates and ligands.

Acknowledgements

This work was supported by the Medical Research Council and the Science and Engineering Research Council. We thank our colleagues N. G. Oikonomakos, P. J. McLaughlin and K. Varvill for their contributions to the phosphorylase work and D. R. Trentham for collaboration with the caged phosphates. We also wish to show our appreciation to the staff of the Daresbury Laboratory for the facilities and service and to P. A. Machin, J. W. Campbell, T. J. Greenough, I. J. Cliftron, S. Zurek, S. Gover, J. R. Helliwell, R. C. Liddington and M. Elder for their contributions to the Laue work.

References

1 Phillips, D. C. (1967) *Proc. Natl Acad. Sci. USA* 57, 484–495
2 Alber, T., Petsko, G. A. and Tsernoglou, D. (1976) *Nature* 263, 297–300
3 Walter, J., Steigemann, W., Singh, T. P., Bartunik, H. D., Bode, W. and Huber, R. (1982) *Acta Crystallogr. Sect B* 38, 1462–1472
4 Fink, A. L. and Petsko, G. A. (1981) *Adv. Enzymol.* 52, 177–246
5 Makinen, M. and Fink, A. L. (1977) *Annu. Rev. Biophys. Bioeng.* 6, 301–342
6 Greaves, G. N., Bennett, R., Duke, P. J., Holt, R. and Suller, V. P. (1983) *Nucl. Instrum. Methods* 208, 139–142
7 Pool, M. W., Munro, I. H., Taylor, D. G. and Walker, R. P. (1983) *Nucl. Instrum. Methods Phys. Res.* 208, 143–145
8 Helliwell, J. R. (1985) *J. Mol. Struct.* 130, 63–91
9 Mills, D. M. (1984) *Physics Today*, April 1984
10 Huxley, H. E., Faruqi, A. R., Bordas, J., Koch, M. H. J. and Milch, J. R. (1980) *Nature* 284, 140–143
11 Kress, M., Huxley, H. E. and Faruqi, A. R. (1986) *J. Mol. Biol.* 188, 325–342
12 Mandelkow, E. M., Harmsen, A., Mandelkow, E. and Bordas, J. (1980) *Nature* 287, 595–596
13 Caffrey, M. (1985) *Biochemistry* 24, 4826–4844
14 Kasvinsky, P. J. and Madsen, N. B. (1976) *J. Biol. Chem.* 251, 6852–6859
15 McLaughlin, P. J., Stuart, D. I., Klein, H. W., Oikonomakos, N. G. and Johnson, L. N. (1984) *Biochemistry* 23, 5862–5873
16 Hajdu, J., Acharya, K. R., Stuart, D. I., McLaughlin, P. J., Barford, D., Klein, H. W., Oikonomakos, N. G. and Johnson, L. N. (1987) *EMBO J.* 6, 539–546
17 Johnson, L. N., Hajdu, J., Acharya, K. R., Stuart, D. I., McLaughlin, P. J., Oikonomakos, N. G. and Barford D. (1989) in *Allosteric Enzymes* (Herve, G., ed.), pp. 81–127, CRC Press
18 Hehre, E. J., Brewer, C. F., Uchiyama, T., Schlesselman, P. and Lehmann, J. (1980) *Biochemistry* 19, 3557–3564
19 Klein, H. W., Im, M. J., Palm, D. and Helmreich, E. J. M. (1984) *Biochemistry* 23, 5853–5861

20 Klein, H. W., Im, M-J. and Palm, D. (1986) *Eur. J. Biochem.* 157, 107–114
21 Wyckoff, H. W., Doscher, M., Tsernoglou, D., Inagami, T., Johnson, L. N., Hardman, K. D., Allewell, N. N., Kelly, D. M. and Richards, F. M. (1967) *J. Mol. Biol.* 27, 5372–5382
22 Hajdu, J., McLaughlin, P. J., Halliwell, J. R., Sheldon, J. and Thompson, A. W. (1986) *J. Appl. Crystallogr.* 18 528–532
23 Moffat, K., Szebenyi, D. M. E. and Bilderback, D. H. (1984) *Science* 223, 1423–1425
24 Hadju, J., Machin, P. A., Campbell, J. W., Greenough, T. J., Clifton, I. J., Zurek, S., Gover, S., Johnson, L. N. and Elder, M. (1987) *Nature* 329, 178–181
25 Campbell, J., Clifton, I., Machin, P. A., Zurek, S., Helliwell, J. R., Habash, J., Hajdu, J. and Harding, M. M. (1987) in *Biophysics and Synchrotron Radiation Research* (Bianconi, A. and Congiu Castellano, A., eds), pp. 52–60, Springer-Verlag
26 Farber, G. K., Machin, P. A., Almo, S., Petsko, G. A. and Hajdu, J. (1988) *Proc. Natl Acad. Sci. USA* 85, 112–115
27 Wood, I. G., Thompson, P. and Matthewman, J. C. (1983) *Acta Crystallogr.* B39, 543–547
28 Harding, M. M., Maginn, S. J., Campbell, J. W., Clifton, I. and Machin, P. A. (1988) *Acta Crystallogr., Sect. B* 44, 142–146
29 Hibberd, M. G., Dantzig, J. A., Trentham, D. R. and Goldman, T. E. (1985) *Science* 228, 1317–1319
30 Turner, A. D., Pizzo, S. V., Rozakis, G. and Porter, N. A. *J. Am. Chem. Soc.* (in press)
31 Blundell, T. L. and Johnson, L. N. (1976) *Protein Crystallography*, Academic Press

J. Hajdu, K. R. Acharya, D. I. Stuart, D. Barford and L. N. Johnson are at the Laboratory of Molecular Biophysics, Oxford University, Oxford OX1 3QU, UK.

Time-resolved macromolecular crystallography

Emil F. Pai

University of Toronto, Toronto, Ontario, Canada

The number of research projects in the field of time-resolved macromolecular crystallography is still very limited. Although there has been constant progress in monitoring enzymatic reactions in crystals by applying diffraction methods to determine the accompanying structural changes, it is still mostly the suitability of the system that decides success or failure. On the other hand, there is promise of time resolution in the nano- to picosecond range, and ongoing exciting research in cryocrystallography, reaction initiation, and diagnostic observations of reactants should enable us to devise tailor-made approaches to solving more demanding problems.

Current Opinion in Structural Biology 1992, 2:821–827

Introduction

Conventional crystallography has been tremendously successful in determining the three-dimensional structures of hundreds of enzymes, very often including their respective substrate, inhibitor or product complexes. In some fortunate cases, it has even been possible to stabilize true reaction intermediates in the crystalline state. The techniques used have included, for example, cryoenzymology [1], chemical tricks such as pH shifts [2] or the choice of slow substrates [3], and less reactive mutants [4,5]. All of these methods slow down the reaction rates, such that the time it takes for substrates to diffuse into a crystal becomes short compared with the decay time of the intermediates of interest. This results in a high and stable concentration of these intermediate complexes in the crystal, which makes them accessible to monochromatic X-ray diffraction analyses.

In their quest to bring the time scale of data collection closer to that of enzymatic reactions, crystallographers rediscovered the Laue diffraction technique [6,7]. The simultaneous use of a broad spectrum of X-rays (practical considerations restrict the range to ~0.2–2.5 Å) made it possible to keep the crystal stationary during data collection. A few diffraction pictures taken at different orientations of the crystal can result in useful data sets. The exact number depends on the symmetry of the space group; in the case of a cubic crystal, one single exposure can be sufficient. When applied in combination with the 'parasitic' use of synchrotron radiation [8,9,10•], this technique in principle allows diffraction experiments in the subsecond time range. Major problems associated with the use of the Laue technique are the strict requirement for extremely well ordered crystals, the need to synchronize the large number of molecules in a given crystal, and the lack of low-resolution reflections in the diffraction pattern [11].

Several excellent reviews on the subject of time-resolved macromolecular crystallography have appeared in recent years [12–15]. This short report will therefore concentrate on the progress that has since been achieved in developing the methodology, in realizing the many problems associated with this line of scientific work, but also in understanding the enzymatic reactions under study. A meeting addressing these topics took place in January 1992, providing a snapshot of the present status of the field. Its proceedings have been published [16••] and reviewed in a condensed but very concise form [17].

Methodology

Diffraction technique

At present, the method of choice for recording diffraction patterns of intermediate reaction states in a crystal is still the Laue technique. In a quantitative analysis of Laue diffraction patterns recorded from the radiation emitted from a single bunch of electrons traversing an undulator, Szebenyi *et al.* [18] showed that data obtained in a 100 ps exposure are of useful quality. These results indicate that crystallography is feasible at the fast border of the time range in which processes of biological interest take place. The same group described an ultrafast mechanical shutter which can open and close in microseconds [19]. Using the bremsstrahlung of a sealed-tube X-ray source, Brooks and Moffat [20] obtained precise structure amplitudes from Laue patterns of a lysozyme crystal, opening the door for in-house Laue diffraction experiments. Because of the long exposure times needed, the use of sealed-tube or even rotating anode sources, however, should be restricted to testing and evaluation purposes.

Imaging plates [21,22] have replaced film as the medium for measuring diffraction intensities. They are faster, more

Abbreviations

Boc—tert. butyl oxycarbonyl; **Me**—methyl.

 ISSN 0959-440X

sensitive in recording weak reflections, and their response is linear over five to six orders of magnitude. The read-out times, however, for all constructions presently in use are long in comparison with the actual time spent for data collection. Charge-coupled devices hold some promise for being able to combine high count-rate capabilities, good spatial resolution, and relatively fast read-out. Basic tests of the performance of such a device applying synchrotron radiation have been reported [23]. In order to overcome the problem of spatially overlapping reflections, Helliwell [24,25] has suggested the use of a so-called 'toast-rack' detector. Several layers of film or imaging plates are placed parallel to each other, but spaced apart, thereby allowing the shorter and more penetrating wavelength reflections to be separated.

In parallel with technical and design improvements, theoretical and computational approaches in analyzing some of the problems of Laue diffraction have been reported [26,27]. The optimization of data-collection strategies [28] and improvements in the handling of data reduction, e.g. through the analysis of gnomonic projections [29,30], have also been considered recently.

Reaction initiation

Although there are still many problems associated with the crystallographic part of time-resolved macromolecular crystallography, with most systems, the major obstacles now seem to be chemical in nature. For most reactions in the crystalline state, jumps in temperature, pressure or pH [31] might be used to start the reaction. Very often, however, only photochemical activation is fast enough for efficient synchronization of the reaction [32,33]. In their contribution to the London meeting, Trentham and colleagues [34] described those caging groups that are currently available. Most of the caged compounds in use today rely on the 1-(2-nitrophenyl)ethyl group for protection. 3,5 Dinitrophenyl and 3',5'-dimethoxybenzoin esters also show promise, but although they possess sufficient quantum yields and their kinetics of photoactivation are reasonably fast, there is certainly still much room for improvement. An interesting twist to the caging approach has been described by Ringe *et al.* [35]. Instead of protecting the substrate against attack by the enzyme, these workers developed the strategy of blocking the catalyst itself through the covalent attachment of a photoreversible component to crucial active-site groups.

The intense light pulses needed to achieve fast conversion of caged compounds into substrates are usually produced using flash lamps or lasers. The actual wavelength and the amount of energy with which the crystal is irradiated have to be chosen very carefully to prevent overheating and the generation of heat gradients. These effects could lead to streaking diffraction patterns and the loss of the time window that is the most interesting one in terms of reaction monitoring. Moffat and coworkers [36•] have performed careful analyses of these problems.

Reaction monitoring

As Laue data sets usually do not provide true atomic resolution, making it impossible in most cases to directly identify the chemical nature of the molecule(s) bound to the protein, it is imperative to investigate carefully the kinetics of the catalyzed reaction, in solution as well as in the crystalline state, before starting time-resolved diffraction work. Knowledge of the different rates of transformation of substrate into intermediates and finally into products should guide the design of the experiment. If the reaction rates are slow, one might be able to devise rather crude experimental procedures (such as chromatographic analysis of the ligands after dissolving the crystals [37,38]) which will nevertheless yield the information needed.

If the intermediates of a reaction under study give rise to distinct spectra, monitoring light absorption is certainly the method of choice for following the course of the reaction. Mounting crystals so that they are suspended in a free-standing thin film is a procedure which not only makes it easier to handle sensitive crystals but is also well suited to low-temperature crystallography and optical monitoring of the crystals [39]. Microspectrophotometer systems with time resolutions in the millisecond range and set up for use on a synchrotron beam-line have been described [36•,40], as have broader and more fundamental studies of deconvoluting the spectral contributions of distinct reaction intermediates [41,42•]. These latter results are especially encouraging if one's favourite enzyme follows a reaction scheme which does not allow for the build-up of a defined protein-intermediate complex.

Projects

Elastase

A conventional study employing monochromatic X-rays confirmed the presence of an acyl intermediate at 244 K when elastase crystals were soaked in a cryoprotectant that contained the tripeptide Boc-Pro-Ala-Ala-OMe (Boc, tert. butyl oxycarbonyl; Me, methyl). On the basis of these results and combining scanning-Laue techniques [43] and cryoenzymology, Bartunik *et al.* [44] recorded the diffraction patterns of this complex as a function of slow increases in temperature. Although the data obtained have still to be analyzed in detail, they did demonstrate a dramatic change in the diffraction pattern at ~255 K indicative of the generation of disorder and probably connected to the completion of the reaction.

Cytochrome c peroxidase

A crystal of cytochrome *c* peroxidase was mounted in a flow cell and reacted with hydrogen peroxide (I Andersson and J Hajdu, personal communication). The reaction intermediate, compound I, was successfully produced by this procedure. Under the conditions employed, the half-life of compound I was ~20 min. Using the Laue technique, a data set was obtained within 10 s (described in

[17]). In data reduction, the difference Laue approach was taken [45]. The difference electron-density map showed interpretable features related to the trapped oxy-intermediate of the reaction.

Glycogen phosphorylase b

Heptenitol is a poor substrate of the highly regulated, pyridoxal-phosphate-dependent enzyme glycogen phosphorylase. In one of the first 'time-resolved' studies of enzyme activity, diffusion of this small substrate was used as a trigger to start the reaction [46]. Fast monochromatic diffraction on a synchrotron station resulted in several snapshots of the reaction pathway, with the first structural result obtained ~1 h after initiation [46].

Following up on these earlier experiments and trying to fill in more time points during the first hour of reaction, the use of 3,5-dinitrophenylphosphate as a caged substrate was attempted [47•]. Control experiments established that sufficient amounts of phosphate could be released by illuminating the presoaked crystal with several 1 ms flashes from a xenon flash lamp. A microspectrophotometer was used to monitor the concentration of free phosphate, and diffraction data were collected in the Laue mode [47•].

Unfortunately, the resulting electron-density maps indicated that no chemical reaction had occurred over the 1 h period. In addition, no phosphate ion could be detected at the attacking position. The Laue experiment had been conducted under conditions slightly different from those of the monochromatic control runs. The authors propose that this led to reduced liberation of phosphate and, taken together with the rather low affinity of glycogen phosphorylase b for phosphate, prevented successful initiation of phosphorylation.

In the same report, Duke *et al.* [47•] thoroughly discussed the influence of the missing low-resolution data on the quality of the electron-density maps calculated from such systematically truncated data sets. In a footnote, they reported that they have used a new intensity-integration protocol to yield much improved results.

ras p21

Time-resolved work on the oncogene product H-ras p21 is a perfect example of how the choice of the right system can dramatically improve one's chances of succeeding in a difficult field of research. p21 is a very slow enzyme, which makes it much easier to deal with all the technical difficulties surrounding time-resolved diffraction studies.

The protein was crystallized as a 1:1 complex with a photosensitive precursor of its substrate GTP [37]. The caged GTP used in the crystallization was a racemic mixture of the *R*- and *S*-diastereoisomers. It was nevertheless surprising to find the caged GTP molecule next to but clearly removed from what inhibitor studies had identified as the nucleotide-binding site [48]. Photolysis led to the generation of the Michaelis–Menten complex, p21·GTP, the structure of which was elucidated with the help of the Laue diffraction technique [5]. Now, GTP was found to be bound at the correct site. After generation of the catalytically competent complex, the hydrolysis reaction proceeded in the crystal with the same rate constants that had been determined in solution leading to the product complex p21·GDP [37].

In their report on extended studies of this system, Scheidig *et al.* [49•] described dramatic improvements in resolution of the diffraction patterns when pure stereoisomers of caged GTP were used in crystallization trials. In this case, the nucleotides were also bound at the same place as the inhibitors, consistent with kinetic and NMR results. The studies, however, were still handicapped by the fact that only a small number of the crystals of the cellular p21 protein had mosaicity (a measure of the sharpness of reflections) low enough to permit successful Laue data collection. It should be mentioned that the same crystals were used to collect monochromatic data sets of 1.0 Å resolution at the Photon Factory in Japan (EF Pai *et al.*, unpublished data). When the investigators switched to the non-transforming Gly12Pro mutant, whose three-dimensional structure (with the exception of the additional atoms contributed by the proline residue at position 12) can be superimposed on the cellular protein [4], most of the crystals gave satisfactory Laue patterns. Several time points after photolysis were investigated and preliminary results indicated that one can watch the movement of parts of the 'effector' loop when GTP is hydrolyzed to GDP. In particular, Tyr32 performs a nice swing from hydrogen bonding intramolecularly to another tyrosine to its position in the high-resolution inhibitor complex, where it interacts with the γ-phosphate of a neighbouring molecule (A Scheidig, personal communication).

Chymotrypsin

Ringe and coworkers [35•] also used the caging strategy to prevent untimely reactions. They, however, targeted the catalyst itself instead of possible substrates [35]. On the basis of careful characterizations of the crystal structures of caged chymotrypsins [50], which had been obtained through reaction with suicide substrates (photoreversible cinnamate compounds), photolysis and deacylation behaviour of the complexes were studied in kinetic and crystallographic terms [51]. The crystals were mounted in a flow cell. It was shown that 10 and 30 min, respectively, of continuous illumination with the focused beam from a mercury arc lamp were sufficient to 'uncage' the enzyme and restore the catalytically competent state.

In an elegant sequel to the latter study, crystals of γ-chymotrypsin inhibited with *trans-p*-diethylamino-*o*-hydroxy-α-methylcinnamate were irradiated with a short flash from a xenon lamp in the presence of the mechanism-based inhibitor 3-benzyl-6-chloro-2-pyrone [52•]. Through a series of single Laue exposures, it was possible to follow the reactions taking place in the crystal. Although only ~25 % of a complete data set was obtained for each time point, the electron-density maps showed the presence of covalently bound cinnamate before the light triggering, the empty binding pocket after

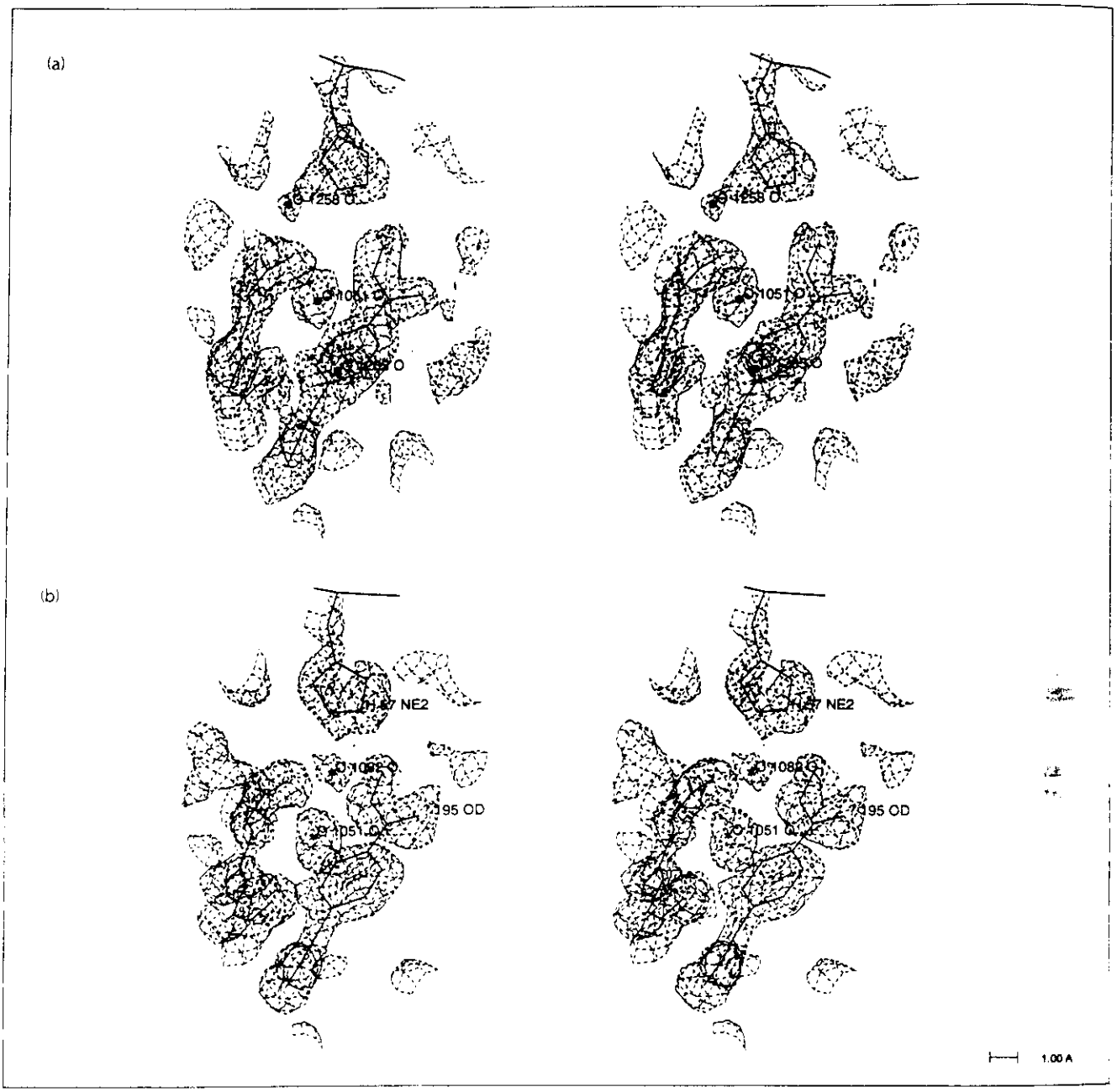

Fig. 1. Stereo pictures of the active site of bovine trypsin. The serine residue of the catalytic triad has been reacted with *p*-nitrophenyl *p*-guanidonobenzoate. The resulting intermediate is stable for days at low pH but is hydrolyzed at pH values above neutrality. (a) At pH 5.5. (b) Three minutes after raising the pH to 8.5. A water molecule (O 1082 O) is positioned for attack on the ester bond of the acyl group. The electron-density maps were calculated from Laue data (nominal resolution 1.8 Å) from coefficients $|2F_o - F_c|$ and calculated phases. The contours were drawn at 1.5σ [54••]. Published with permission [54••].

the inhibitor had been released, and the slow formation of the pyrone complex. Put one after the other, these maps constitute a still primitive but nevertheless very pleasing 'action movie' featuring a well known protein catalyst.

Trypsin

Sweet and colleagues [31] have used a variation of this approach to study the related enzyme trypsin. At pH 5.5, the acyl-intermediate (guanidinobenzoyl)trypsin, generated during the trypsin-catalyzed cleavage of *p*-nitrophenyl-*p*-guanidinobenzoate, is stable such that it can be analyzed by spectroscopic and X-ray diffraction methods [53]. If the pH is raised to ~8.5, however, deacylation proceeds with a half-life of ~1 h at room temperature and the catalytic cycle is closed.

A pH jump was used to start the reaction and Laue diffraction data were recorded in order to probe the steps in the deacylation of (guanidinobenzoyl)trypsin [54••]. The unusual stability of trypsin crystals, even in the white beam of a synchrotron beam-line, allowed the collec-

tion of several highly redundant data sets to a resolution of 1.8 Å from a single crystal. The electron-density maps obtained are of exceptional quality, testifying to the importance and comfort of complete high-resolution data sets. Induced by the change in pH, a water molecule can be seen in the electron-density map calculated from data collected 3 min after the pH shift. this water is in a position to attack the acyl group of the transiently stable intermediate (Fig. 1) [54••].

Photoactive yellow protein

This 14 kD photoreceptor protein from *Ectothiorhodospira halophila* undergoes a photocycle upon illumination which is similar to that of rhodopsin. The kinetics for this cycle reveal a series of spectrally distinct intermediates. Their decays follow first-order kinetics and the rate constants are quite different. Therefore, there are times when the crystal is made up of homogenous populations of molecules. As this protein has a built-in light-sensitive trigger with the high quantum yield of 0.64, this system avoids the problems associated with chemical conversion, diffusion or change of parameters such as pH and temperature. So far, the conditions for starting the photocycle by bleaching the chromophore, methods for the stabilization of intermediates, and the characterization of the related diffraction patterns have been described [36•]. This system is suitable for studies in quite different time ranges and promises exciting results in the near future.

Conclusions

Time-resolved macromolecular crystallography, once regarded as a contradiction in itself, has proven to be a successful merger of two complementary techniques. Studies on carbonic anhydrase [55] and trypsin [54••] have shown that even the positions of water molecules can be traced using this technique.

The advent of third-generation synchrotrons with even higher brilliance will open up new avenues of research. One example is the renewed interest in the use of Weissenberg cameras placed on monochromatic beam-lines [56]. With improvements in detector technology, it might well be possible to record monochromatic diffraction patterns in a time range presently reserved for Laue techniques [57], thereby elegantly avoiding all the problems connected with these.

In combination with cryotechniques [58], it should be possible to lengthen the time intervals available for probing specific intermediates. T-jump techniques used within a temperature range in which enzymes show a dynamical transition from a catalytically competent state to one in which they are inactive might feature usefully in experiments aimed at very short-lived intermediates [59••]. In addition to studies involving enzyme activity, one should not forget that conformational changes are also worth investigating [60]. For most of the problems connected with the diffraction part of the studies discussed above, we can at least think of possible solutions. For solutions to the problem of starting a reaction in the crystal and keeping it reasonably synchronized, it will be necessary to enlist the help of very good chemists.

References and recommended reading

Papers of particular interest, published within the annual period of review, have been highlighted as:

- • of special interest
- •• of outstanding interest

1. ALBER T, PETSKO GA, TSERNOGLOU D: **Crystal Structure of Elastase–Substrate Complex at −55 °C.** *Nature* 1976, 263:297–300.

2. PAI EF, SCHULZ GE: **The Catalytic Mechanism of Glutathione Reductase as Derived from X-ray Diffraction Analyses of Reaction Intermediates.** *J Biol Chem* 1983, 258:1752–1757.

3. HAJDU J, ACHARYA KR, STUART DI, MCLAUGHLIN PJ, BARFORD D, KLEIN H, JOHNSON LN: **Time-resolved Structural Studies on Catalysis in the Crystal with Glycogen Phosphorylase b.** *Biochem Soc Trans* 1986, 14:538–546.

4. KRENGEL U, SCHLICHTING I, SCHERER A, SCHUMANN R, FRECH M, JOHN J, KABSCH W, PAI EF, WITTINGHOFER A: **Three-dimensional Structures of H-ras p21 Mutants: Molecular Basis for their Inability to Function as Signal Switch Molecules.** *Cell* 1990, 62:539–548.

5. SCHLICHTING I, ALMO SC, RAPP G, WILSON K, PETRATOS K, LENTFER A, WITTINGHOFER A, KABSCH W, PAI EF, PETSKO GA, GOODY RS: **Time-resolved X-ray Crystallographic Study of the Conformational Change in Ha-ras p21 Protein on GTP Hydrolysis.** *Nature* 1990, 345:309–315.

6. FRIEDRICH W, KNIPPING P, VON LAUE M: **Interferenzerscheinung bei Röntgenstrahlung.** *Sitzungsber Math Phys Klasse Kgl Bayer Akad Wissensch*, München 1912, 303–322.

7. AMOROS JL, BUERGER MJ, CANUT DE AMOROS M: *The Laue Method.* New York: Academic Press; 1975.

8. ROSENBAUM G, HOLMES KC, WITZ J: **Synchroton Radiation as a Source for X-ray Diffraction.** *Nature* 1971, 230:434–437.

9. HELLIWELL JR, HABASH J, CRUICKSHANK DWJ, HARDING MM, GREENHOUGH TJ, CAMPBELL JW, CLIFTON IJ, ELDER M, MACHIN PA, PAPIZ MZ, ZUREK S: **The Recording and Analysis of Synchrotron X-radiation Laue Diffraction Photographs.** *J Appl Crystallogr* 1989, 22:483–497.

10. • HELLIWELL JR: *Macromolecular Crystallography with Synchrotron Radiation.* Cambridge: Cambridge University Press; 1992.

This monograph provides an up-to-date introduction to the principles of synchrotron radiation and its properties. Sources, instrumentation, and data-collection strategies are all discussed. The author describes possible applications in diffraction studies and adds appendices containing useful information for prospective users.

11. HAJDU J, ALMO SC, FARBER GK, PRATER JK, PETSKO GA, WAKATSUKI S, CLIFTON IJ, FULOP V: **On the Limitations of the Laue Method when Applied to Crystals of Macromolecules.** In *Crystallographic Computing 5: From Chemistry to Biology.* Edited by Moras D, Podjarny AD, Thierry JC. Oxford: Oxford University Press; 1991:29–49.

12. MOFFAT K, HELLIWELL JR: **The Laue Method and its Use in Time-resolved Crystallography.** *Top Curr Chem* 1989, 151:61–74.

13. HAJDU J, ACHARYA KR, STUART DI, BARFORD D, JOHNSON LN: Catalysis in Enzyme Crystals. *Trends Biochem Sci* 1988, 13:104–109.

14. MOFFAT K: **Time-resolved Macromolecular Crystallography.** *Annu Rev Biophys Biophys Chem* 1989, 18:309–332.

15. HAJDU J, JOHNSON LJ: **Progress with Laue Diffraction on Protein and Virus Crystals.** *Biochemistry* 1990, 29:1668–1678.

16. •• CRUICKSHANK DWJ, HELLIWELL JR, JOHNSON LN (EDS): **Time-resolved Macromolecular Crystallography.** *Phil Trans R Soc Lond [A]* 1992, 340.

This issue contains the proceedings of a Discussion Meeting on time-resolved macromolecular crystallography organized at the Royal Society in London. The papers provide the reader with an account of the present state of the field. The various authors not only present exciting results but freely discuss the problems and limitations that they encountered.

17. JOHNSON LN: **Time Resolved Protein Crystallography.** *Protein Sci* 1992, 1:in press.

18. SZEBENYI DME, BILDERBACK DH, LEGRAND A, MOFFAT K, SCHILDKAMP W, TEMPLE BS, TENG T-Y: **Quantitative Analysis of Laue Diffraction Patterns Recorded with a 120 ps Exposure from an X-ray Undulator.** *J Appl Crystallogr* 1992, 25:414–423.

19. LEGRAND AD, SCHILDKAMP W, BLANK B: **An Ultrafast Mechanical Shutter for X-rays.** *Nucl Instrum Meth Phys Res [A]* 1989, 275:442–446.

20. BROOKS I, MOFFAT K: **Laue Diffraction from Protein Crystals Using a Sealed Tube X-ray Source.** *J Appl Crystallogr* 1991, 24:146–148.

21. AMAMIYA Y, KISHIMOTO S, MATSUSHITA T, SATOW Y, ANDO M: **Imaging Plate for Time-resolved X-ray Measurements.** *Rev Sci Instrum* 1989, 60:1552–1556.

22. BILDERBACK DH, MOFFAT K, OWEN J, RUBIN B, SCHILDKAMP W, SZEBENYI D, TEMPLE BS, VOLZ K, WHITING B: **Protein Crystallographic Data Acquisition and Preliminary Analysis Using Kodak Storage Phosphor Plates.** *Nucl Instrum Methods Phys Res [A]* 1988, 271:678–687.

23. ALLINSON NM, COLAPIETRO M, HELLIWELL JR, MOON KJ, THOMPSON AW, WEISGERBER S: **Charge-coupled Imagers for Time-resolved Macromolecular Crystallography.** *Res Sci Instrum* 1992, 63:664–666.

24. HELLIWELL JR: **Macromolecular Crystallography Using Synchrotron Radiation: Progress on Station 9.5 and a Novel (Toast-rack) Detector Scheme for Laue Diffraction.** *Nucl Instr Meth Phys Res [A]* 1991, 308:260–266.

25. HELLIWELL JR: **Synchrotron X-ray Crystallography Techniques: Time-resolved Aspects of Data Collection.** *Phil Trans R Soc Lond [A]* 1992, 340:221–232.

26. CRUICKSHANK DWJ, HELLIWELL JR, MOFFAT K: **Angular Distribution of Reflections in Laue Diffraction.** *Acta Crystallogr [A]* 1991, 47:352–373.

27. SHRIVE AK, CLIFTON IJ, HAJDU J, GREENHOUGH TJ: **Laue Film Integration and Deconvolution of Spatially Overlapping Reflections.** *J Appl Crystallogr* 1990, 23:169–174.

28. CLIFTON IJ, ELDER M, HAJDU J: **Experimental Strategies in Laue Crystallography.** *J Appl Crystallogr* 1991, 24:146–148.

29. CRUICKSHANK DWJ, CARR PD, HARDING MM: **Estimation of d_{min}, l_{min} and l_{max} from the Gnomonic Projections of Laue Patterns.** *J Appl Crystallogr* 1992, 25:285–293.

30. CARR PD, CRUICKSHANK DWJ, HARDING MM: **The Determination of Unit-cell Parameters from Laue Diffraction Patterns Using their Gnomonic Projections.** *J Appl Crystallogr* 1992, 25:294–308.

31. SINGER PT, CARTY RP, BERMAN LE, SCHLICHTING I, STOCK A, SMALÅS A, CAI Z, MANGEL WF, JONES KW, SWEET RM: **Laue Diffraction as a Tool in Dynamic Studies: Hydrolysis of a Transiently Stable Intermediate in Catalysis by Trypsin.** *Phil Trans R Soc Lond [A]* 1992, 340:285–300.

32. KAPLAN JH, FORBUSH B, HOFFMAN JF: **Rapid Photolytic Release of Adenosine-5'-triphosphate from a Protected Analogue: Utilisation by the Na:K Pump of Human Red Blood Cell Ghosts.** *Biochemistry* 1978, 17:1929–1935.

33. MCCRAY JA, TRENTHAM DR: **Properties and Uses of Photoreactive Caged Compounds.** *Annu Rev Biophys Biophys Chem* 1989, 18:239–270.

34. CORRIE JET, KATAYAMA Y, REID GP, ANSON M, TRENTHAM DR: **The Development and Application of Photosensitive Caged Compounds to Aid Time-resolved Structure Determination of Macromolecules.** *Phil Trans R Soc Lond [A]* 1992, 340:233–244.

35. RINGE D, STODDARD BL, BRUHNKE J, KOENIGS P, PORTER N: **Can Laue Catch Maxwell? Observation of a Short-lived Species by Laue X-ray Crystallography.** *Phil Trans R Soc Lond [A]* 1992, 340:273–284.

36. • MOFFAT K, CHEN Y, NG K, MCREE D, GETZOFF ED: **Time-resolved Crystallography: Principles, Problems and Practice.** *Phil Trans R Soc Lond [A]* 1992, 340:175–190.

This report discusses the problems involved in time-resolved macromolecular crystallography from a practical point of view. Special attention is given to the heating effects of the radiation, X-rays and laser light used to trigger photoreactions. The authors also describe those factors responsible for the deposition of too much light energy in the crystal, which in turn leads to increased mosaicity and the prevention of data collection. Ways of controlling these processes are described. In the second part of this report, preliminary results of time-resolved studies on the photoactive yellow protein from the halophilic bacterium *E. halophila* are reported.

37. SCHLICHTING I, RAPP G, JOHN J, WITTINGHOFER A, PAI EF, GOODY RS: **Biochemical and Crystallographic Characterization of a Complex of c-Ha-ras p21 and Caged GTP with Flash Photolysis.** *Proc Natl Acad Sci USA* 1989, 86:7687–7690.

38. HOWELL PL, WARREN C, AMATAYAKUL-CHANTLER S, PETSKO GA, HAJDU J: **Activity of Crystalline Turkey Egg-white Lysozyme.** *Proteins* 1992, 12:91–99.

39. TENG T-Y: **Mounting of Crystals for Macromolecular Crystallography in a Free-standing Thin Film.** *J Appl Crystallogr* 1990, 23:387–391.

40. HADFIELD A, HAJDU J: **Use of a Spectrophotometer to Monitor Reactions in the Crystal During a Kinetic Laue Crystallographic Experiment.** In *Proceedings of the Second European Conference on Progress in X-ray Synchrotron Radiation Research.* Edited by Balerna A, Bernieri E, Mobilio S. Societa Italiana di Fisica; 1990; 25:449–452.

41. MOZZARELLI A, RIVETTI C, ROSSI GL, HENRY ER, EATON WA: **Crystals of Haemoglobin with the T Quarternary Structure Bind Oxygen Non-cooperatively with No Bohr Effect.** *Nature* 1991, 351:416–419.

42. • ROSSI GL, MOZZARELLI A, PERACCIU A, RIVETTI C: **Time Course of Chemical and Structural Events in Protein Crystals Measured by Microspectrophotometry.** *Phil Trans R Soc Lond [A]* 1992, 340:191–207.

Report on the encouraging results from a multitude of spectroscopic studies on enzymatic reactions in crystals performed in the Rossi laboratory. The authors show, for example, that it is possible to calculate the ratios of the concentrations of several reaction intermediates present in a given crystal at the same time from knowledge of their respective spectral characteristics.

43. BARTUNIK HD, BARTSCH HH, HUANG Q: **Accuracy in Laue X-ray Diffraction Analysis of Protein Structures.** *Acta Crystallogr [A]* 1992, 48:180–188.

44. BARTUNIK HD, BARTUNIK LJ, VIEHMANN H: **Time-resolved X-ray Diffraction Studies of Enzymes Under Cryoconditions.** *Phil Trans R Soc Lond [A]* 1992, 340:209–220.

45. HAJDU J, MACHIN PA, CAMPBEL JW, GREENHOUGH TJ, CLIFTON IJ, ZUREK VS, GOVER S, JOHNSON LN, ELDER M: **Millisecond X-ray**

Diffraction and the First Electron Density Map from Laue Photographs of a Protein Crystal. *Nature* 1987, 329:115–116.

46. HAJDU J, ACHARYA KR, STUART DI, MCLAUGHLIN PJ, BARFORD D, OIKONOMAKOS NG, KLEIN H, JOHNSON LN: **Catalysis in the Crystal: Synchrotron Radiation Studies with Glycogen Phosphorylase b.** *EMBO J* 1987, 6:539–546.

47. • DUKE EMH, HADFIELD A, WALTERS S, WAKATSUKI S, BRYAN RR, JOHNSON LJ: **Time-resolved Diffraction Studies on Glycogen Phosphorylase b.** *Phil Trans R Soc Lond [A]* 1992, 340:245–261.

The authors describe their experience with time-resolved Laue crystallography on the large protein glycogen phosphorylase b. They compare the Laue results to those of monochromatic checks. A thorough discussion of the effects of missing most or all of the low-resolution data is given, as well as possible ways of overcoming this problem.

48. PAI EF, KRENGEL U, PETSKO GA, GOODY RS, KABSCH W, WITTINGHOFER A: **Refined Crystal Structure of the Triphosphate Conformation of H-ras p21 at 1.35 Å Resolution: Implications for the Mechanism of GTP Hydrolysis.** *EMBO J* 1990, 9:2351–2359.

49. • SCHEIDIG A, PAI EF, SCHLICHTING I, CORRIE JET, REID GP, WITTINGHOFER A, GOODY RS: **Time-resolved Crystallography on H-ras p21.** *Phil Trans R Soc Lond [A]* 1992, 340:263–272.

An update on the project of describing the conformational changes that take place in the protein p21 during and as a result of the hydrolysis of the GTP nucleotide at its active site. Of special interest are the different binding modes of the nucleotide found in two independent studies, emphasizing the importance of small differences in reaction conditions.

50. STODDARD BL, BRUHNKE J, PORTER N, RINGE D, PETSKO GA: **Structure and Activity of Two Photoreversible Cinnamates Bound to Chymotrypsin.** *Biochemistry* 1990, 29:4871–4879.

51. STODDARD BL, BRUHNKE J, KOENIGS P, PORTER N, RINGE D, PETSKO GA: **Photolysis and Deacylation of Inhibited Chymotrypsin.** *Biochemistry* 1990, 29:8042–8051.

52. • STODDARD BL, KOENIGS P, PORTER N, PETRATOS K, PETSKO GA, RINGE D: **Observation of the Light-triggered Binding of Pyrone to Chymotrypsin by Laue X-ray Crystallography.** *Proc Natl Acad Sci USA* 1991, 88:5503–5507.

A beautifully designed study of the two reactions that proceed one after the other in a crystal of chymotrypsin. Removal of the caging cinnamate group from the enzyme active site, initiated by photolysis, is followed by the slow modification of the chymotrypsin molecules by the mechanism-based inhibitor 3-benzyl-6-chloro-2-pyrone.

53. MANGEL WF, SINGER PT, CYR DM, UMLAND TC, TOLEDO DL, STROUD RM, PFLUGRATH JW, SWEET RM: **Structure of an Acyl-enzyme Intermediate During Catalysis: (Guanidinobenzoyl)trypsin.** *Biochemistry* 1990, 29:8351–8357.

54. •• SINGER PT, SMALÅS A, CARTY RP, MANGEL WF, SWEET RM: **The Hydrolytic Water Molecule in Trypsin, Revealed by Time-resolved Laue Crystallography.** *Science* 1992, in press.

A pH jump is used to probe the reaction steps of the deacylation of the transiently stable intermediate guanidinobenzoyl-trypsin. At low pH, the covalent bond is very stable. When the pH is raised to 8.5, the half life of the covalent adduct drops to ~1 h. Trypsin crystals are unusually resistant to radiation damage, even in the white beam of a synchrotron. This allows Sweet and colleagues to collect diffraction data of high redundancy which, together with the application of careful scaling procedures, results in remarkably clean electron-density maps. At a nominal resolution of 1.8 Å, they are of sufficient quality to show subtle features, such as a water molecule ready to attack the covalent intermediate.

55. LILJAS A, CARLSSON A, HAKANSSON K, LINDAHL M, SVENSSON SA, WEHNERT A: **Laue and Monochromatic Crystallography on Carbonic Anhydrase.** *Phil Trans R Soc Lond [A]* 1992, 34:301–309.

56. SAKABE N: **A Focussing Weissenberg Camera with Multi-Layer-line Screens for Macromolecular Crystallography.** *J Appl Crystallogr* 1983, 16:542–547.

57. ANDERSSON I, CLIFTON IJ, FÜLÖP V, HAJDU J: **High Speed High Resolution Data Collection on Spinach Rubisco Using a Weissenberg Camera at the Photon Factory.** In *Crystallographic Computing 5: From Chemistry to Biology.* Edited by Moras D, Podjarny AD, Thierry JC. Oxford: Oxford University Press; 1991:20–28.

58. WATENPAUGH K: **Macromolecular Crystallography at Cryogenic Temperatures.** *Curr Opin Struct Biol* 1991, 1:1012–1015.

59. •• RASMUSSEN BF, STOCK AM, RINGE D, PETSKO GA: **Crystalline Ribonuclease A Loses Function Below the Dynamical Transition at 220 K.** *Nature* 1992, 357:423–424.

An elegant series of experiments proves that there is a minimal temperature below which the ribonuclease molecules in a crystal are not able to bind substrates. Raising the temperature by only ~10 K reversibly establishes catalytical competence.

60. REYNOLDS CD, STOWELL B, JOSHI KK, HARDING MM, MAGINN SJ, DODSON GG: **Preliminary Study of a Phase Transformation in Insulin Crystals Using Synchrotron-radiation Laue Diffraction.** *Acta Crystallogr [B]* 1988, 44:512–515.

EF Pai, Departments of Biochemistry and Molecular and Medical Genetics, University of Toronto, Medical Sciences Building, 1 King's College Circle, Toronto, Ontario, M5S 1A8, Canada.